Trajectory Planning for Collision Avoidance in Urban Scenarios

Zur Erlangung des akademischen Grades
Doktor der Ingenieurwissenschaften
der Fakultät für Maschinenbau
Karlsruher Institut für Technologie (KIT)

genehmigte
Dissertation
von

M.Sc. Jens Ferdinand

Tag der mündlichen Prüfung:	25. Juni 2018
Referent:	Prof. Dr.-Ing. Christoph Stiller
Korreferent:	Prof. Dr.-Ing. Marcus Geimer

Vorwort

Die vorliegende Arbeit entstand während meiner Zeit als Doktorand bei der Opel Automobile GmbH, Abteilung Electrical Systems, Advanced Technology, Active Safety & Controls - Advanced Technology, in Rüsselsheim.

Mein besonderer Dank gilt Prof. Dr.-Ing. C. Stiller, Leiter des Instituts für Mess- und Regelungstechnik (MRT) des Karlsruher Institut für Technologie (KIT), für die Betreuung dieser Arbeit. Vielen Dank für das mir entgegengebrachte Vertrauen und die gewährten Freiheiten bei der Bearbeitung und Gestaltung dieses Projekts. Ebenso möchte mich bei Herrn Prof. Dr.-Ing M. Geimer, Leiter des Teilinstituts Mobile Arbeitsmaschinen am Institut für Fahrzeugsystemtechnik des KIT, für die Übernahme des Koreferates bedanken. Des Weiteren bedanke ich mich bei meinen Kollegen der Opel Automobile GmbH für ihre Hilfsbereitschaft und das durchgehend gute Arbeitsklima. Insbesondere bedanke ich mich bei Frank Bonarens und Norbert Simm, für die intensiven Diskussionen und die stetige Reflexion der Thematik. Dr. Johannes Huth und Dr. Stefan Berger danke ich für die sorgfältige und kritische Durchsicht des Manuskripts.

Abschließend möchte ich mich bei meiner Familie sowie meinen Freunden für die stetige Unterstützung bedanken. Sie gaben mir den notwendigen Rückhalt, um dieses Projekt zum Abschluss zu bringen.

Mainz, im Oktober 2017 *Jens Ferdinand*

This Thesis was conducted in the research project "UR:BAN Urbaner Raum: Benutzergerechte Assistenzsysteme und Netzmanagement", funded by the German Federal Ministry of Economics and Energy (BMWi) in the framework of the third traffic research program of the German government.

Abstract

The increasing density of urban traffic gives rise to more complex and critical traffic situations which needs to be approached systematically. As a contribution, the present work focuses on trajectory planning methods that enable an automated evasive maneuver to avoid a collision with a single critical dynamic obstacle within bounded environments.

Trajectory planning as functional component of an Advanced Driver Assistance System (ADAS) is located in the functional chain between environment perception and actuator control. Automated evasive maneuvers require a specific methodology for trajectory planning. Optimal trajectories shall satisfy the requirements of dynamic integrity, avoidance of collisions and optimal utilization of the available maneuver space. Furthermore, with respect to functional safety, a general goal is to determine the latest possible moment for the execution of the collision avoidance maneuver. In addition, the method shall support an efficient implementation on a production-type Electronic Control Unit (ECU).

To meet these challenges, the present work focuses on trajectory planning methods that consider a combined utilization of braking and steering. The trajectory planning task is formulated as an optimization problem which is approached in three different ways. First, optimal trajectory planning in consideration of a dynamic vehicle model is investigated. This approach comprises sufficiently precise modeling of the vehicle dynamics and shall be considered as a benchmark. The second approach shall approximate the

behavior of vehicle dynamics by suitable parametric trajectories. The third approach extends the second one by introducing heuristic sampling thus is suitable for online optimization and computational efficient for the application in a test vehicle.

In the first step, the potential of the three proposed approaches is verified in a simulative environment. In the following step, the third approach as a functional component of an ADAS for collision avoidance is integrated into a test vehicle to verify the real-time capability and practicability. It is demonstrated that the proposed method is practical for an application in an ADAS.

Keywords: Collision avoidance, Trajectory planning, Risk assessment, Optimization

Kurzfassung

Die zunehmende Verkehrsdichte in urbanen Ballungsgebieten führt zur Häufung von unübersichtlichen und kritischen Verkehrssituationen. Um dieser Entwicklung gerecht zu werden, behandelt diese Arbeit Ansätze zur Trajektorienplanung, die ein automatisiertes Ausweichen mit einem einzelnen kritischen dynamischen Hindernis in beschränkter Umgebung ermöglichten.

Als Komponente eines Fahrerassistenzsystems befindet sich die Trajektorienplanung in der Funktionskette zwischen Umfeldwahrnehmung und Aktorikregelung. Automatisiertes Ausweichen erfordert eine besondere Methodik zur Trajektorienplanung, um die spezifischen Anforderungen dieser Aufgabe zu bewerkstelligen. Die optimale Trajektorie muss die Kriterien Fahrbarkeit, Kollisionsvermeidung und optimale Nutzung des begrenzt zur Verfügung stehenden Manöverraums berücksichtigen. Des Weiteren ist es aus Sicht der funktionalen Sicherheit ein zentrales Ziel, den spätest möglichen Auslösezeitpunkt für die Kollisionsvermeidung zu bestimmen. Zusätzlich muss das Verfahren eine recheneffiziente Implementierung in einem seriennahen Steuergerät unterstützen.

Um diese Aufgabe zu bewältigen, werden hierzu in dieser Arbeit Ansätze zur Trajektorienplanung behandelt, die eine Kopplung von Längs- und Querdynamik erlaubt. Die Aufgabe der Trajektorienplanung wird als ein Optimierungsproblem formuliert; von diesem ausgehend werden drei Varianten abgeleitet: Die erste Variante betrachtet die Problemstellung der

optimale Trajektorienplanung unter Berücksichtigung eines dynamischen Fahrzeugmodells. Diese Variante verfügt über eine hinreichend genaue Abbildung der Fahrzeugdynamik und soll zur generellen Betrachtung und Bewertung des Verfahrens dienen. Die zweite Variante soll durch eine geeignete Parametrierung der Trajektorien das Verhalten des Fahrzeugmodells approximieren. Die dritte Variante erweitert die Zweite durch einen heuristischen Ansatz zur zeitlichen Abtastung. Dadurch ist diese Variante zur Onlineoptimierung geeignet und folglich ausreichend recheneffizient für die Anwendung im Fahrzeug.

Das Potenzial der drei vorgestellten Verfahren wird im ersten Schritt simulativ nachgewiesen und im darauffolgenden Schritt wird das dritte Verfahren in einem Versuchsträger zum Nachweis der Echtzeitfähigkeit implementiert. Es wird gezeigt, dass die Ansätze für die Anwendung in Fahrerassistenzsystemen geeignet sind.

Schlagworte: Kollisionsvermeidung, Trajektorienplanung, Risikobewertung, Optimierung

Contents

Notation and Symbols

Acronym

ADAS	**A**dvanced **D**river **A**ssistance **S**ystem
CAN	**C**ontroller **A**rea **N**etwork
COG	**C**enter **O**f **G**ravity
ECU	**E**lectronic **C**ontrol **U**nit
IMU	**I**nertial **M**easurement **U**nit
MPC	**M**odel **P**redictive **C**ontrol
P-Planner	**P**olynomial **T**rajectory **P**lanner
QP	**Q**uadratic **P**rogram
rP-Planner	**r**educed **P**olynomial Trajectory **P**lanner
ST-Planner	**S**ingle-**T**rack Model Trajectory **P**lanner
SQP	**S**equential **Q**uadratic **P**rogram

General Notation

Mathematical symbols within this work are defined in there corresponding context. The generation of the symbols follows the general rules defined below.

Scalars	Italic lower case	a, b, c, σ, λ
Vectors	Bold Italic lower case	$\boldsymbol{a}$, $\boldsymbol{b}$, $\boldsymbol{c}$, $\boldsymbol{\sigma}$, $\boldsymbol{\lambda}$
Matrices	Bold Italic upper case	$\boldsymbol{A}$, $\boldsymbol{B}$, $\boldsymbol{C}$
Constants	Roman case	a, A, b, B
Sets	Calligraphic upper case	$\mathcal{A}$, $\mathcal{B}$, $\mathcal{C}$

ABS Anti-lock Braking System

ADAS Advanced Driver Assistance System

AEB Automatic Emergency Braking

CAN Controller Area Network

CIB Collision Imminent Braking

CV Constant Velocity

CA Constant Acceleration

CTRA Constant Turnrate and Acceleration

CT Constant Turnrate

COG Center of Gravity

ECU Electronic Control Unit

ESP Electronic Stability Program

GIDAS German In-Depth Accident Study

IMU Inertial Measurement Unit

MPC Model Predictive Control

NMPC Nonlinear Model Predictive Control

P-Planner Polynomial Trajectory Planner

QP Quadratic Program

rP-Planner reduced Polynomial Trajectory Planner

ST-Planner Single-Track Model Trajectory Planner

SQP Sequential Quadratic Program

1 Introduction

1.1 Relevance of trajectories for Collision Avoidance

In accordance to the Federal Statistical Office of Germany [68], $2.40\,\mathrm{million}$ car accidents were recorded by the police in 2014. The amount of accidents with personal injuries has increased by $3.90\,\%$ to $302\,435$ compared to 2013. Most accidents with personal injuries occurred within built-up areas with $69.60\,\%$ (see Fig. 1.1). Among these, accidents caused by turning into a road or by crossing it had the highest rate of personal injuries where the latter also had the highest fatality rate (Table 1.1). Urban traffic situations with opponents moving in transversal directions obviously cause greatest difficulties to all involved road users. Addressing urban traffic situations with opponents moving in transversal directions provides a high potential for the improvement of road safety.

Addressing these accident types, intensive research activities for enhanced Advanced Driver Assistance System (ADAS) are conducted within the industry [80, 79, 29, 9, 62, 63]. Besides assistance functions alerting the driver, collision mitigation systems already implemented in series production assist the driver to avoid an imminent collision. Strategies with varying characteristics are applied. Several pursue an alerting strategy where the driver is alerted before the imminent collision occurs. The alerting strategy comprises of visual alerts, haptic alerts or optical alert or any combination of these methods. Others extend the alerting strategy by an active interven-

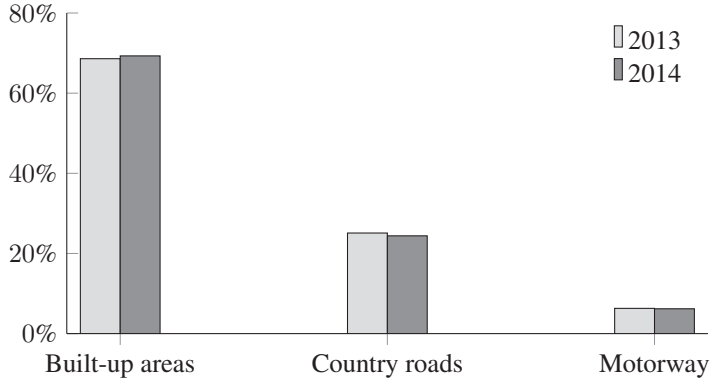

Figure 1.1: Accidents with personal injuries by location of accident for year 2013 and 2014 [68]

tion. These systems either avoid or at least reduce the imminent collision by an active braking intervention. Future systems will be able to brake earlier or even steer for a limited period without any driver activation.

A significant contribution to these evolutionary steps are the enhancements and refinements of environment perception systems and improved scene interpretation [11, 41, 52, 33]. These are the fundamental prerequisite for automated collision avoidance maneuvers. Especially maneuver planning or trajectory planning benefits from these developments. Traffic scenarios that do not change rapidly over time and are observable for a sufficient time period do not necessarily require complex maneuver planning.

These situations can be handled with relative simple methods which mostly do not require a trajectory. However, new challenges arise when time critical scenarios will be addressed, that require a combination of longitudinal and lateral intervention – especially in the field of trajectory planning. Those critical scenarios are often within dynamic environments with suddenly ap-

Type of accident	Personal injuries / %	Fatalities / %
Driving accident	10.90	20.00
Accident caused by turning off the road	16.30	10.70
Accident caused by turning into a road or by crossing it	26.30	16.90
Accident caused by crossing the road	7.10	26.80
Accident involving stationary vehicles	4.50	1.60
Accident between vehicles moving along in carriageway	21.60	8.00
Other accident	13.30	16.00

Table 1.1: Accidents within urban area by type of accident [68]

pearing obstacles where a highly dynamic intervention is indispensable. Collisions in such time critical traffic situations can be handled by either a highly dynamic braking or steering intervention. Beyond that, the combination of braking and steering enables more general maneuvers covering a broader variety of relevant traffic scenarios. For example, suddenly appearing obstacles in scenarios with limited maneuver space can be meet, which is highly relevant for urban traffic situation.

The present work will focus on trajectory planning methods addressing those time critical scenarios, that typically emerge in urban areas. One of the most challenging aspects of trajectory planning for an application within urban areas that needs to be addressed are narrow roads. Here, the consideration of the drivable area is inevitable with a clear distinction between road and pavement or roadside. Further challenges are the feasibility and

the dynamic integrity of the planned maneuvers. To ensure accurate and predictable maneuver planning, the vehicle physics and limitations must be considered to guarantee a realistic and drivable evasive trajectory. A system which takes the latter aspect into account can help to reduce traffic accidents and associated injuries.

1.2 Objectives

The aim of the present thesis is to develop methods for the planning of collision avoidance trajectories. The developed methods shall contribute to the reduction of accidents within urban areas. Collision avoidance trajectories will be developed with the following objectives:

- The objective is to develop trajectory planning methods for collision avoidance in given scenarios. The focus shall be on the usage within an Advanced Driver Assistance System for passenger cars in urban traffic scenarios. Variations of single-object scenarios in typical urban traffic environment shall be considered.
- The method shall provide trajectories that enable the execution of an evasive maneuver at the optimal moment, where optimal is defined later. Situations shall be detected where no collision-free trajectory can be found.
- The method shall consider the kinematic and dynamic characteristics of the underlying vehicle dynamics. Moreover, physical limits of the brake and steering actuators shall be considered.
- The developed method shall consider the available maneuver space and arbitrary objects, i.e., vehicles, pedestrians, or bicycles. Without limiting the generality of the proposed method, the availability of a complete and correct environment representation is assumed.

- The trajectory planning algorithm shall be proven on the basis of a prototypical implementation in an experimental vehicle. The developed method shall be integrated into an Advanced Driver Assistance System for collision avoidance. The system performance shall be evaluated with the focus on practical benefit and applicability. Any type of driver interference shall be neglected.

1.3 Outline

The structure of this Thesis is as follows:

Chapter 2: *Fundamentals*

Chapter 2 provides prerequisites and fundamentals for the planning of collision avoidance trajectories. First, a general definition of trajectories is given and the relevance of trajectories in a collision avoidance context is discussed. Second, trajectory planning as an embedded component of an ADAS is discussed. Third, an overview of related work on trajectory planning methods is given. Fourth, the most suitable method with best coverage of the requirements for trajectory planning of collision avoidance maneuver is selected. Finally, a dynamic vehicle model and actuator-specific parameters are presented.

Chapter 3: *Optimal Collision Avoidance*

Chapter 3 introduces the methodology for optimal trajectory planning of collision avoidance maneuvers. Necessary conditions, criteria and requirements for trajectory planning of collision avoidance maneuvers are presented and discussed. A general mathematical formulation of the trajectory planning problem is provided.

Chapter 4: *Optimal Collision Avoidance Approaches*

Three specific trajectory planning approaches based on the optimal trajectory planning methodology of Chapter 3 are introduced. The

first approach considers a dynamic vehicle model. The second one considers a parameterized approximation of the trajectories. The third approach modifies the parameterized approach by adding a sampling heuristic, which reduces the computational complexity. Further, relevant assessment criteria and a catalog of characteristic use-cases are introduced that shall facilitate the performance evaluation of the optimal trajectory planning approaches.

Chapter 5: *Simulation results*

The developed trajectory planning approaches are assessed in a simulation-based analysis. Analysis shall evaluate the performance of the approaches and verify the compliance with the set of requirements.

Chapter 6: *Vehicle test results*

The developed approaches are integrated into an ADAS for collision avoidance and implemented in a test vehicle. The applicability and robustness of the proposed approaches are verified by vehicle tests.

Chapter 7: *Conclusion and Outlook*

Chapter 7 finalizes this thesis with conclusion and outlook. The research questions answered within this thesis are summarized and potentials for further work are discussed.

2 Fundamentals

This chapter aims to explain the fundamentals that are prerequisites for the planning of collision avoidance maneuvers with trajectories. First, trajectory planning as an embedded part of an Advanced Driver Assistance System (ADAS) is discussed. Second, a definition of a trajectory is provided and the relevance of trajectories for maneuver planning in a collision avoidance context is given. Third, an overview of related work on trajectory planning methods is given. Fourth, the most promising method for the planning of collision avoidance trajectories is selected. Last, a dynamic vehicle model is discussed and actuator-specific parameters are presented.

2.1 Trajectory planning in the context of Advanced Driver Assistance System (ADAS)

The system architecture of ADAS which affects driving dynamics may be broken down to four main tasks: environment perception, ego-state estimation, trajectory planning and execution. The environment perception task collects and evaluates all captured sensor information of the environment. The available sensor information comprises of static and dynamic environment information. The quality and availability of the sensor information highly depends on the applied onboard sensor set and its configuration. Static environment information is, e.g., the lane markings of ego and adjacent lanes or the drivable area, which may be bounded by curbstones or parked cars on the road side. Dynamic environment information are moving obstacles that are in the surroundings of the ego-vehicle, like vehicles, pedestri-

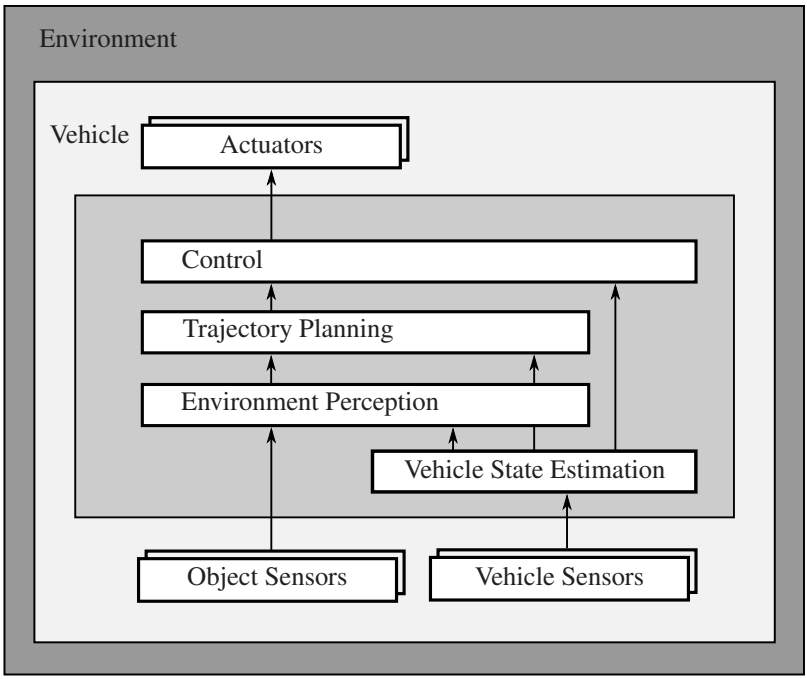

Figure 2.1: System architecture of an ADAS for collision avoidance

ans, or bicycles. Together with the ego-state estimation task, which computes the current state of the ego-vehicle, the collected data can be formed into a scenery representation of the actual traffic situation. This scenery is the basic information for the trajectory planner. The trajectory planning task computes the desired trajectory that shall be performed by the vehicle. In consideration of the scenery, a trajectory is planned that prevents a collision with dynamic obstacles and the surroundings, leading to pass safely. The trajectory execution comprises a low-level controller which is designed to ensure proper following of the trajectory. The integration of the subsystem trajectory planning into the system architecture of an ADAS is shown in

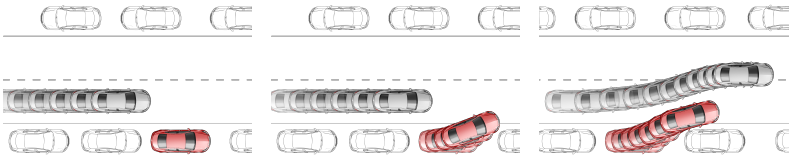

(a) (b) (c)

Figure 2.2: Critical urban traffic situation

Fig. 2.1. A practical implementation of an ADAS for collision avoidance will be presented in Chapter 6.

2.2 Trajectories for collision avoidance maneuver

Maneuver planning is the act of finding a path from an initial state to a goal state. If this path has an additional time-dependency it is called a trajectory. In control theory, a trajectory is an ordered, time-variant set of states of a dynamic system. It can be defined accordingly in a discrete manner:

> **Definition 2.1.** Let $k \in \mathbb{N}$ be a discrete point in time, representing an arbitrary starting point of a trajectory. Let $i \in I$ with $I = [0 \dots \mathrm{H}] \subset \mathbb{N}$, an equidistantly sampled sequence of H samples and $\boldsymbol{u}(i|k) \in \mathbb{R}^{n_\mathrm{u}}$, an excitation vector of a discretized dynamic system. Then, the trajectory is

$$\boldsymbol{T}(k) = [\boldsymbol{u}(0|k), \dots, \boldsymbol{u}(\mathrm{H}|k)] \qquad \mathbb{R}^{n_\mathrm{u}} \times I \to \mathbb{R}^{n_\mathrm{T}} \tag{2.1}$$

With the definition of a trajectory, it can be clarified why trajectories are required for the planning of collision avoidance maneuvers. In critical situations, the geometrical path without its temporal information is insufficient

for the avoidance of time-critical situations. Especially in dynamic environments with time variant conditions, it is indispensable to consider the temporal condition in addition to the spatial conditions. For those situations, a trajectory provides the information when to steer in which direction and when to brake with which intensity.

For better understanding of the concepts being described in the next sections, the following characteristic use case shall be explained representing an urban traffic situation, see Fig. 2.2. The gray vehicle travels along a street with vehicles parking aside the road (a). The red vehicle parking on the right roadside enters the lane and blocks the lane in front of the gray vehicle (b). To prevent a collision, the gray vehicle has to perform an evasive maneuver as illustrated in (c).

2.3 Related Work

The following section gives an overview of selected trajectory planning methods for vehicle motion planning. Trajectory planning methods discussed in the literature can be widely subdivided into two general groups. First, there are methods using an optimization scheme, which are mostly applying the principles of optimal control theory or model predictive control theory. Second, there are non-optimization based methods which mostly provide an analytic function to express the trajectory.

Trajectories represented in an analytic expression are intensively studied. Various ideal lane change trajectories in analytical expression are compared subject to various performance measures in [64]. Circular Arcs, 5th and 7th order polynomial [69], Ramp Sinusoid [16], Spirals, Acceleration Profile [66, 13], and Bezier-Spline type trajectories are considered. As a result of the analysis in [64], the 5th order polynomial trajectories prove as best representation for steering only lane change trajectories. Sigmoid functions are

considered for evasive steering trajectories in active collision avoidance system [30]. The trajectories are represented in a parametrized fashion, which is beneficial for an effective calculation. However, these sigmoid function type trajectories are limited to straight road scenarios and to steer-only maneuvers. Moshchuk et al. [46] introduce steering-only evasive trajectories composing of circular arcs and parabola functions. A quadratic lane model is considered as end condition, which enables the application in conditions with arbitrary road geometries. Moreover, lateral jerk limits are considered. Schmidt [57] studies on latest possible evasive trajectories to avoid a collision with a single obstacle. Taking Kamm's friction cycle [34] into account as a dynamic limitation, latest possible evasive trajectories in analytic expression are derived. The trajectories are capable to evade the obstacle but a steer-back cannot be performed. The practicability of the trajectory in analytic expression is discussed. A parameterized optimization problem is proposed where the maneuver length is to be minimized, that recovers the limitation imposed by the analytic approach. The trajectories are parameterized by a sequence of equidistant samples, maneuver duration and angle of the absolute acceleration within the Kamm's friction cycle. A kinematic motion model with anisotropic acceleration behavior is considered. The optimal trajectory of the acceleration angle is further approximated by an arc tangent function. Specific actuator constraints and road geometries are neglected.

The advantage of trajectories in an analytical expression is the capability of an efficient calculation. However, the methods are generally limited to restricted conditions. The coverages of arbitrary conditions can hardly be achieved with these method. Most of the approaches are capable of steering only trajectories or provide trajectories that just avoid a collision with an obstacle without considering additional constraints like available maneuver space.

Among the group of optimization methods, there are methods that consider state lattices [51, 83] or consider a sampling strategy for trajectory planning [39, 40, 54]. Others apply the method of artificial potential fields [31, 50, 44, 5] to the trajectory planning task.

The method of artificial potential field generates a gradient field of the surrounding. The idea originates from robot motion planning. The vehicle is guided through the gradient field considering attraction forces and repulsion forces acting on the vehicle. Repulsion forces push the vehicle away from obstacles in descending direction across the field. A drawback of this method is the risk of terminating in a local minimum instead of the global optimum [44, 50]. Also, the detection of an imminent collision is hard to realize. The separation of obstacles highly depends on the design of the artificial potential field. If the gradients at boundaries of the obstacles are considered too shallow, obstacles could be interpreted as a single obstacle even though the gap between those obstacles is wide enough for safe passing of the ego-vehicle.

Another trajectory planning method based on the principle of optimization is Model Predictive Control (MPC). It forms a subgroup of optimal control, which is a finite-horizon optimization control scheme [10, 38]. MPC utilizes a motion model to predict future vehicle states and optimizes a set of inputs such that these predicted states satisfy constraints while a cost function is iteratively minimized. A main differentiation factor are the considered vehicle models and their complexity. The used vehicle models vary from simple ones like a point mass model, via the single-track model up to complex models like the double-track model with the further consideration of wheel dynamics, roll motion, etc. [84, 45]. Trajectory planning methods applying the principles of MPC generally implement a constant finite planning horizon, which can be interpreted as a lookahead horizon. For each iteration, the trajectory is successively optimized for the planning horizon towards a

predefined goal state subject to the dynamic model and the constraints, if constraints are applied.

Werling et al. [76] present a trajectory planner for collision avoidance with pedestrians applying a nonlinear MPC scheme [20]. The proposed cost functional defines the ratio between the clearance distance to the pedestrian and the maneuver intensity. Optimal collision avoidance trajectories are found that utilize the braking and steering capabilities of the vehicle up to their physical limits. The subsequent analysis of the simulated concept evaluation shows only small deviations comparing the planned and executed trajectories. It is claimed that the presented algorithm can reach real-time capabilities, although it is a nonlinear optimization approach. Applying MPC to trajectory planning is also addressed in [28, 25, 24].

The challenge in the MPC design is to find an appropriate duration for the planning horizon. Especially for the application of trajectory planning for collision avoidance maneuvers, the design of the planning horizon is crucial. If the planning horizon is too short, obstacles which suddenly appear could be missed. If the planning horizon is too long, the computation of the trajectory might exceed the available computational power.

Optimization is a common method for trajectory planning which is discussed in numerous studies. Trajectory planning is formulated as a constrained or unconstrained optimization problem. A popular approach is to generate an array of trajectories, which generates a subset of solutions [75, 27, 26]. By this approach, the set of all possible solutions is reduced. The optimal trajectory which minimizes a cost functional is sought out of the subset. The design of the cost functional is chosen depending on the required application of the trajectory. Others apply a direct optimization approach. The trajectories are directly optimized for given optimization criteria. The trajectories may vary by their representation and expression.

Common representations are kinematic vehicle models [81, 82] or single-track model [61, 60, 43].

A parameterized expression of the trajectories is also often applied. The trajectories are approximated using a parameterized function where polynomials, spirals [36] or spline functions [37] are used. In [65], 5th order polynomial trajectories are compared with a direct trajectory optimization approach for a lane change maneuver . Further, the trajectory is optimized for a constant finite maneuver duration and a nonlinear single-track model is considered as a constraint. Two test scenarios, one for a comfortable lane change and one for an evasive maneuver, are proposed for comparison. The optimal trajectory shows lower absolute lateral acceleration compared to the 5th order polynomial trajectory. In contrast to the 5th order polynomial trajectory, yaw rate and lateral acceleration for the optimized trajectory are nonzero. This phenomenon is explained by the absence of terminal constraints defining the optimal trajectory. The author's perspective is to prefer the optimized maneuver over the 5th degree polynomial for evasive maneuvers, which is justified by the lower absolute acceleration. In collision avoidance scenarios, comfortable maneuver characteristics are questionable.

Different sets of constraints are applied to optimal trajectory planning , which depend on the application of the intended trajectory. Besides the collision avoidance with obstacles the drivable corridor is considered by several authors [82, 82, 77, 37]. Also different approaches for the planning horizon are applied. Similar to the MPC-based methods, a typical approach is to use a predefined planning horizon. A fixed planning horizon or maneuver duration is typically applied to trajectories that are intended for the use in automated systems [82, 75, 25]. In those applications, the trajectories are consecutively planned for the purpose of vehicle guidance. Trajectories for the use in an ADAS have different requirements - specially for collision avoidance maneuvers. Here, trajectories are required to avoid the critical

situation. Consequently, only relatively small maneuver durations are considered in contrast to an automated driving scenario where the maneuver duration is theoretically infinite. In typical collision avoidance scenarios, a maneuver duration is required that enables the collision avoidance maneuver and the transition between the automated maneuver and the handover to the driver.

A variety of research activities are conducted that focus on the investigation of trajectory planning. Various different approaches and methods are analyzed. However, it is remarkable that the main research focus is on the characteristic design of trajectories. In the context of trajectory planning, the moment when a trajectory shall be executed is investigated with minor significance. Hillenbrand et al. [23] for example, examines maneuver execution strategies from a scene representation perspective. The discussion of the maneuver execution is mostly separated from the trajectory planning. This disconnect between trajectory planning and decision shall be resolved. Consequently, a specific need is the jointly trajectory planning together with the trajectory execution, which shall be investigated. These aspects should be jointly considered in the trajectory planning.

2.4 Method selection

The selection of the applied method for trajectory planning of collision avoidance maneuvers is discussed in this section. An appropriate method shall be selected by a study of the requirements. First, the set of essential requirements for the planning of collision avoidance maneuvers shall be derived. Thereafter, the most appropriate method for this work will be selected based on the requirements.

Collision avoidance systems designed for urban traffic scenarios have specific requirements. The design of collision avoidance maneuvers demands

specific criteria building up the foundation for the subsequently introduced trajectory planning. Collision avoidance maneuvers shall avoid imminent collisions and react to suddenly changing situations. To avoid imminent collisions, all feasible corrective actions shall be applied without the limitations of any comfort requirements. After the critical situation has been cleared, the maneuver shall enable a safe passage. In consequence, collision avoidance maneuvers shall have the following essential properties.

- A collision with a dynamic obstacle and the environment shall be avoided
- The maneuvers shall satisfy the vehicle physics and limitations
- A safe passage shall be enabled after the imminent collision has been avoided
- The moment when the maneuver has to be executed shall be known

Finding evasive trajectories which satisfy all those properties is a challenging task. The reaction to suddenly changing situations is essential for collision avoidance. To enable a reactive intervention, a successive trajectory planning and evaluation, whether a collision is avoidable or not, is required. It is crucial to determine the moment when the evasive trajectory has to be executed. Planning of evasive trajectories without consideration of the appropriate moment of the maneuver execution could potentially lead to increased accident severity.

The compelling character of an evasive maneuver induces the necessity to exploit the full potential of the vehicle dynamics. Utilizing the entire dynamic capabilities of a vehicle requires the consideration of combined steering and braking in the trajectory design. The theoretical foundation for collision avoidance trajectories combining braking and steering is provided by [57]. The combination of longitudinal and lateral motion additionally

increases the complexity. This is mainly induced by the nonlinear coupling of the lateral and longitudinal vehicle dynamics [45, 59, 84]. To ensure the dynamic integrity and a predictable planning of the trajectories, dynamic limitations of the vehicle shall be considered. This also requires the consideration of specific actuator limitations. Disregarding the specific actuator characteristics could potentially lead to an overestimation of the vehicle dynamics and an underestimation of the criticality of the scene.

In structured environments such as urban roads, a bounded drivable area is typical. The drivable area can be structurally restricted or obstructed by parked vehicles on the roadside. The boundary of this area needs to be considered in the design of evasive trajectories. Facilitating the highest flexibility of coverable scenarios, arbitrary road geometries are required, too. Depending on the available drivable area, it is to be evaluated whether an evasive maneuver is feasible or not. In the latter case, it shall be evaluated if at least a braking maneuver is feasible.

Besides the influencing environmental factors, a most general solution to the trajectory planning problem for collision avoidance maneuvers shall be provided. It enables the adaption to a broad variety of possible scenarios. To address this, a variable length and duration of the trajectories is additionally required.

In append to the discussed requirements, the trajectory planning shall be integrated into an ADAS for collision avoidance. Its practicability and performance shall be proven on the basis of a prototypical implementation in an experimental vehicle. Therefore, the method shall allow a real-time capable implementation.

With the introduced set of requirements, the appropriate method for trajectory planning of collision avoidance maneuvers can be selected. An

Requirements	Analytical	MPC	Optimization
Maneuver execution time	-	○	+
Vehicle Dynamics	○	+	+
Braking	○	+	+
Steering	○	+	+
Actuator limitations	○	+	+
Road Geometry	○	+	+
Road boundaries	○	+	+
Variable end position	-	○	+
Variable end time	-	○	+
Real-time capable	+	○	○

Table 2.1: Scorecard for the selection of applied trajectory planning method

overview of trajectory planning methods is presented in the previous section. Considering the risks and disadvantages of artificial potential fields, this method shall not be considered any further. The remaining methods are assessed for how well they can cope with the requirements. The results of the assessment are collected in Table 2.1. As one outcome of the assessment, trajectory planning methods relying on the principles of optimization show clear advantages over using the other methods. A challenging aspect for optimal trajectory planning is to ensure the real-time capability which also holds for the MPC. The analytic trajectories are fast in computation but are overruled in all other items by the others. Optimal trajectory planning

enables a variable design of the maneuver end position and time.

Summarizing the requirement analysis, the winning method is optimal trajectory planning. In comparison to the other discussed methods, optimal trajectory planning attains most of the requirements. The advantage of applying the principles of optimization to trajectory planning is the straightforward incorporation of constrains. Input, output and states can be considered, which inaugurates the integration of road boundaries, actuator and dynamic limitations. In consequence, the focus of this work is set to optimal trajectory planning. The challenge of real-time implementation will be further considered in this work.

2.5 Optimal trajectory planning

Corresponding to the discussion in the previous section, this work will focus on the method of optimization for optimal trajectory planning of collision avoidance maneuvers. As a prerequisite for the definition of the optimal trajectory planning problem, a general nonlinear optimization problem with nonlinear constraints is discussed in the subsequent section. In the context of optimization, optimality is associated to a cost function to be minimized or maximized subject to a set of constraints. The constrained solution is a subset of the unconstrained optimal solution. Corresponding to trajectory planning, the constraints may comprise of geometric or physical limitations. For example, the drivable area can be bounded or the vehicle dynamic is limited.

The general nonlinear trajectory optimization problem is:

Definition 2.2. Let $\boldsymbol{x}(i|k) \in \mathbb{R}^{n_x}$ be a state vector, $\boldsymbol{u}(i|k) \in \mathbb{R}^{n_u}$ be an excitation vector and $\Delta\boldsymbol{t}(i|k) \in \mathbb{R}$ be a sequence of sampling rates. Further, let $k \in \mathbb{N}$ be a discrete point in time, representing an arbitrary starting point of a trajectory, $i \in I$ with $I = [0 \dots \mathrm{H}] \subset \mathbb{N}$ be an equidistantly sampled sequence of H samples.

The optimization problem is defined as:

$$\begin{aligned} &\min_{\boldsymbol{T}} \boldsymbol{J}(\boldsymbol{T}(k)) \\ &\text{subject to} \quad \boldsymbol{x}(i+1|k) = \boldsymbol{f}(\boldsymbol{x}(i|k), \boldsymbol{u}(i|k), \Delta\boldsymbol{t}(i|k)) \\ &\qquad\qquad \boldsymbol{x}(i|k) \in \mathcal{X} \subset \mathbb{R}^{n_x} \\ &\qquad\qquad \boldsymbol{u}(i|k) \in \mathcal{U} \subset \mathbb{R}^{n_u} \\ &\qquad\qquad \forall i \in I \end{aligned} \tag{2.2}$$

with the functions $\boldsymbol{f} : \mathbb{R}^{n_x} \times \mathbb{R}^{n_u} \times \mathbb{R} \to \mathbb{R}^{n_x}$; $\boldsymbol{J} : \mathbb{R}^{n_T} \to \mathbb{R}$

The cost function $\boldsymbol{J}$ is defined as a function of the trajectory $\boldsymbol{T}(k)$, which is to be optimized subject to the constraints. The nonlinear state constraints and excitation constraints are collected in the constraint sets $\mathcal{X}$ and $\mathcal{U}$, respectively.

Except for a limited number of nonlinear optimization problems, in general, nonlinear optimization problems must be solved numerically. The necessity of solving the nonlinear optimization problem has given rise to a wide range of numerical methods. Amongst those Sequential Quadratic Program (SQP) is a frequently used method. SQP is a numerical solver for a general nonlinear optimization problem with nonlinear constraints. The problem is approximated with a Quadratic Program (QP) which is then solved for every iteration. Other methods use a linear approximation of the nonlinear opti-

mization problem, which is iteratively solved applying the Newton method [53]. The implementation and numerical solution of nonlinear solvers may be referenced to the appropriate literature [7, 21, 3, 6, 53, 48].

2.6 Vehicle modeling

The single-track model is introduced in this section. The single-track model considers the forces acting on the vehicle's front and rear wheel. More complex models like the double track model [72], which considers the roll motion as well, are not considered in this work. Previous authors have shown that the single-track model is an adequate dynamic model with the required depth of detail for evasive maneuvers up to the vehicle's dynamic bounds [43]. The single-track model is a simplified nonlinear model of the vehicle dynamics. In this section, the nonlinear equations of vehicle motion are derived. For the further use in an optimization algorithm, the set of nonlinear equations is discretized.Assuming the vehicle mass distribution coincides with the Center of Gravity (COG) that lies within the horizontal

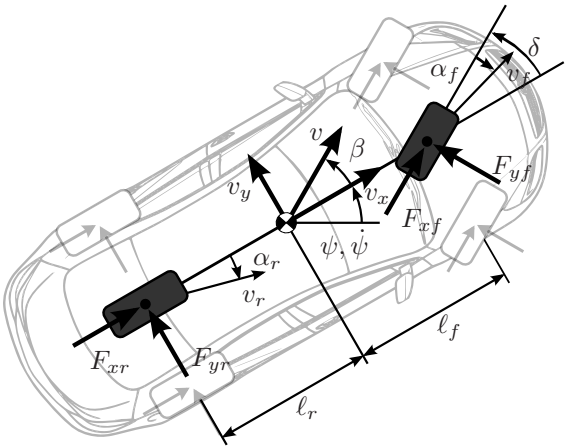

Figure 2.3: Single track model with relevant quantities

road level, roll moments causing dynamic wheel loads can be neglected. Therefore, wheel forces on the respective axis can be combined in a single wheel centered on the longitudinal axis of the vehicle according to Fig. 2.3 [72, 71, 45, 59].

Here δ is the steering angle of the front wheel. α_f and α_r are the front and rear slip angles, v_f and v_r are the front wheel and rear wheel velocities, respectively. The longitudinal and lateral wheel forces of the front and rear axis are $F_{x\mathrm{f}}, F_{y\mathrm{f}}, F_{x\mathrm{r}}$ and $F_{y\mathrm{r}}$. The angle ψ is the heading or yaw angle of the vehicle with respect to the COG. The heading or yaw angle rate is $\dot{\psi}$. The absolute vehicle velocity v related to the COG can be further subdivided into a longitudinal and lateral velocity component v_x and v_y, acting under the side slip angle β. The distances of the front and rear wheel to the COG ℓ_f and ℓ_r, respectively.

In the following, the dynamic equations of the nonlinear single-track model are derived. Followed by the discretization of the single-track model for the use in an optimization algorithm. Applying the principle of conservation of linear momentum on the chassis yields

$$\begin{aligned} F_{x\mathrm{f}}\cos(\delta) - F_{y\mathrm{f}}\sin(\delta) + F_{x\mathrm{r}} &= m(\dot{v}_x - v_y\dot{\psi}) \\ F_{x\mathrm{f}}\sin(\delta) + F_{y\mathrm{f}}\cos(\delta) + F_{y\mathrm{r}} &= m(\dot{v}_y + v_x\dot{\psi}), \end{aligned} \tag{2.3}$$

with the vehicle mass m acting on the COG.

The lateral forces action on the wheels are considered as a linear tire model yielding

$$\begin{aligned} F_{y\mathrm{f}} &= -c_\mathrm{f}\alpha_\mathrm{f} \\ F_{y\mathrm{r}} &= -c_\mathrm{r}\alpha_\mathrm{r} \end{aligned} \tag{2.4}$$

with constant corner stiffness c_f, c_r an the wheel slip angle α_f, α_r for the front and rear tire, respectively [59].

$$\begin{aligned}\alpha_\mathrm{f} &= \tan^{-1}\left(\frac{v_y + \ell_\mathrm{f}\dot{\psi}}{v_x}\right) - \delta \\ \alpha_\mathrm{r} &= \tan^{-1}\left(\frac{v_y - \ell_\mathrm{r}\dot{\psi}}{v_x}\right).\end{aligned} \tag{2.5}$$

The longitudinal forces of the front and rear wheel are modeled by the relation of the brake force acting on the vehicles COG

$$\begin{aligned}F_{x\mathrm{f}} &= -\frac{2}{3}F_\mathrm{B} \\ F_{x\mathrm{r}} &= -\frac{1}{3}F_\mathrm{B}\end{aligned} \tag{2.6}$$

where the brake force distribution of front and rear axis is considered in relation of $\frac{2}{3}$ on the front axis and $\frac{1}{3}$ on the rear axis. The brake force acting on the COG yields

$$F_\mathrm{B} = m(a_x + \dot{a}_x t) \tag{2.7}$$

with the longitudinal acceleration a_x and jerk $\dot{a}_x$. Applying the principle of conservation of the angular momentum yields

$$\ell_\mathrm{f}\left(F_{x\mathrm{f}}\sin(\delta) + F_{y\mathrm{f}}\cos(\delta)\right) - \ell_\mathrm{r}F_{y\mathrm{r}} = I_z\ddot{\psi} \tag{2.8}$$

with the angular yaw acceleration $\ddot{\psi}$ and the moment of inertia around the mass center I_z. Now the equations of motion can be transfered into the state space form:

$$\dot{\boldsymbol{x}} = \boldsymbol{f}(\boldsymbol{x}, \boldsymbol{u}, \boldsymbol{t}) \tag{2.9}$$

The state vector is

$$\boldsymbol{x} = [s_x, s_y, v_x, v_y, a_x, a_y, \psi, \dot{\psi}, \beta, \delta]^\mathsf{T}. \tag{2.10}$$

With the states s_x and s_y, the longitudinal and lateral position, v_x and v_y, the longitudinal and lateral velocity, a_x and a_y, the longitudinal and lateral acceleration. Further, ψ and $\dot{\psi}$ are the yaw angle and yaw angle rate, β is the slip angle and δ is the steering angle, acting on the vehicle' front wheel. The excitation vector is

$$\boldsymbol{u} = [\dot{a}_x, \dot{\delta}]^\mathsf{T} \tag{2.11}$$

along with the longitudinal jerk $\dot{a}_x$ and the steering angle rate $\dot{\delta}$.As a whole, Eqs. (2.9) – (2.11) reads

$$\underbrace{\begin{bmatrix} \dot{s}_x \\ \dot{s}_y \\ \dot{v}_x \\ \dot{v}_y \\ \dot{a}_x \\ \dot{a}_y \\ \dot{\psi} \\ \ddot{\psi} \\ \dot{\beta} \\ \dot{\delta} \end{bmatrix}}_{\dot{\boldsymbol{x}}} = \underbrace{\begin{bmatrix} v\cos(\psi+\beta) \\ v\sin(\psi+\beta) \\ \frac{F_{x\mathrm{f}}\cos(\delta) - F_{y\mathrm{f}}\sin(\delta) + F_{x\mathrm{r}}}{m} + v_y\dot{\psi} \\ \frac{F_{x\mathrm{f}}\sin(\delta) + F_{y\mathrm{f}}\cos(\delta) + F_{y\mathrm{r}}}{m} - v_x\dot{\psi} \\ \dot{a}_x \\ 0 \\ \dot{\psi} \\ \frac{\ell_\mathrm{f}(F_{x\mathrm{f}}\sin(\delta) + F_{y\mathrm{f}}\cos(\delta)) - \ell_\mathrm{r}F_{y\mathrm{r}}}{I_z} \\ 0 \\ \dot{\delta} \end{bmatrix}}_{\boldsymbol{f}(\boldsymbol{x},\boldsymbol{u},\boldsymbol{t})} \tag{2.12}$$

with the auxiliary functions

$$\begin{aligned} v &= \sqrt{v_x^2 + v_y^2} \\ a &= \sqrt{a_x^2 + a_y^2} \\ \beta &= \tan^{-1}\left(\frac{v_y}{v_x}\right). \end{aligned} \tag{2.13}$$

Where v and a are the absolute velocity and acceleration, respectively. β is the slip angel acting on the COG.

The set of differential equations is discretized using the Euler Forward Integration method [73], yielding:

$$\boldsymbol{x}(i+1|k) = \boldsymbol{x}(i|k) + \Delta\boldsymbol{t}(i|k)\boldsymbol{f}(\boldsymbol{x}(i|k), \boldsymbol{u}(i|k), \Delta\boldsymbol{t}(i|k)) \tag{2.14}$$

with the sequence of sampling rates $\Delta\boldsymbol{t}(i|k)$. Applying Eq. (2.14) to Eq. (2.12) yields to the discretized nonlinear single-track model. With Eq. (2.15), the single-track model is fully defined.

2.7 Actuator representation

Time is a critical resource in the context of trajectory planning of collision avoidance maneuvers. An underestimation of a critical situation can lead to drastic results for all participants. Therefore, it is required to identify the key factors that have a significant impact to the timing of a trajectory. Besides the previously discussed vehicle dynamics, the specific actuators are amongst the number of key factors. The performance and capabilities of the actuators significantly influence the timing of the trajectory. For a predictable and reliable trajectory planning, it is inevitable to consider these effects. The time delays induced by the actuators need special consideration in the design of the trajectory. Actuator performance limits in combination

$$\begin{bmatrix} s_x \\ s_y \\ v_x \\ v_y \\ a_x \\ a_y \\ \psi \\ \dot{\psi} \\ \beta \\ \delta \end{bmatrix} (i+1|k) = \begin{bmatrix} s_x(i|k) + v(i|k)\Delta t(i|k)\cos(\psi(i|k) + \beta(i|k)) \\ s_y(i|k) + v(i|k)\Delta t(i|k)\sin(\psi(i|k) + \beta(i|k)) \\ v_x(i|k) + \left(\frac{F_{xf}\cos(\delta(i|k)) - F_{yf}\sin(\delta(i|k)) + F_{xr}}{m} + v_y(i|k)\dot{\psi}(i|k)\right)\Delta t(i|k) \\ v_y(i|k) + \left(\frac{F_{xf}\sin(\delta(i|k)) + F_{yf}\cos(\delta(i|k)) + F_{yr}}{m} - v_x(i|k)\dot{\psi}(i|k)\right)\Delta t(i|k) \\ a_x(i|k) + \dot{a}_x(i|k)\Delta t(i|k) - \dot{\psi}(i|k)v_y(i|k) \\ \dot{\psi}(i|k)v_x(i|k) \\ \psi(i|k) + \dot{\psi}(i|k)\Delta t(i|k) \\ \dot{\psi}(i|k) + \left(\frac{\ell_f(F_{xf}\sin(\delta) + F_{yf}\cos(\delta)) - \ell_r F_{yr}}{I_z}\right)\Delta t(i|k) \\ \tan^{-1}\left(\frac{v_y(i|k)}{v_x(i|k)}\right) \\ \delta(i|k) + \dot{\delta}(i|k)\Delta t(i|k) \end{bmatrix} \tag{2.15}$$

with the auxiliary functions

$$\begin{aligned} v(i|k) &= \sqrt{v_x^2(i|k) + v_y^2(i|k)} \\ a(i|k) &= \sqrt{a_x^2(i|k) + a_y^2(i|k)} \end{aligned} \tag{2.16}$$

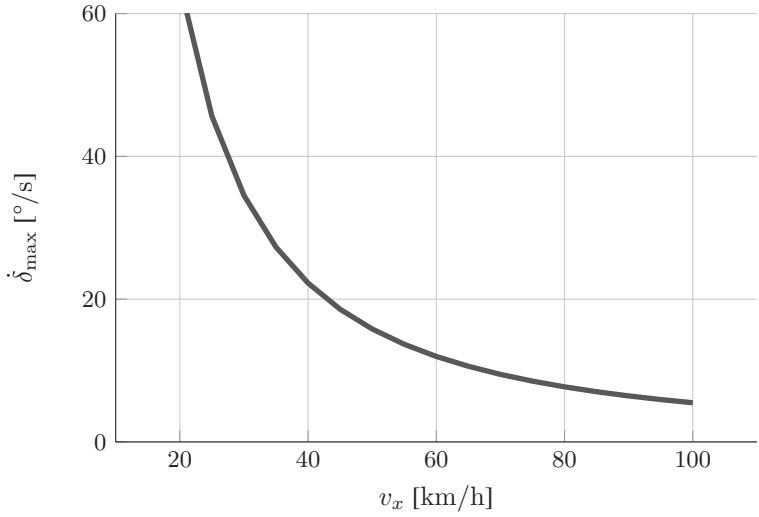

Figure 2.4: Characteristic curve of the steering rate $\dot{\delta}_{\max}$ and the longitudinal velocity v_x

with the vehicle dynamics determine the overall capabilities of the maneuver. The faster the actuators can change the vehicle's acceleration the more reactive a maneuver can be designed. However, considering ideal actuators without limitations leads to a temporal misinterpretation.

This section covers the actuator specific limitations. The integration of the actuator limitations into the trajectory planning is discussed in a later section. The significant measures of the actuators are their maximum control values, i.e., the maximum steering angle and the corresponding rate limits for a steering actuator. For a brake actuator the significant measures are, i.e., the maximum brake acceleration and the corresponding rate limit. To achieve a design that is independent of the specific actuator technology and its dynamic model, the influences and reactions of the actuators on the vehicle's COG are considered. In general, the acceleration build-up rates

acting on the COG are of interest. Incorporating the actuator dynamics into the vehicle dynamic model is done by constraining the model's control values. For the single-track model Eq. (2.11), e.g, this will be achieved by introducing dynamic constraints (See Section 3.5.2).

For the required prototypical implementation in a test vehicle, the actuator limitations are determined by vehicle tests. The tests are conducted as follows: For a variation of the longitudinal vehicle speed in a range of $20\,\mathrm{km/h}$ to $100\,\mathrm{km/h}$, a step is applied to the actuator. The tests are conduced separately for the steering and for the brake.

Brake Parameterization

For the variation of the vehicle speed, a maximum deceleration step of $a_x = -9.81\,\mathrm{m/s^2}$ is applied to the brake controller. The longitudinal acceleration in the COG are measured and analyzed. The maximum acceleration build-up, the jerk, is independent of the velocity. For the test vehicle, the maximum longitudinal jerk of $\dot{a}_x^{\max} = 20\,\mathrm{m/s^3}$ is observed.

Steering Parameterization

For a variation of the vehicle speed, a maximum steer step of $6\,\mathrm{Nm}$ is applied to the steering controller. Also for the steering, the lateral jerk is independent of the velocity. For the test vehicle, a maximum lateral jerk of $\dot{a}_y^{\max} = 15\,\mathrm{m/s^3}$ is observed. The maximum steering rate $\dot{\delta}_{\max}$, opposed to the braking rate, highly depends on the velocity. Fig. 2.4 shows the characteristic curve of the steering rate $\dot{\delta}_{\max}$ the longitudinal velocity v_x. The characteristic curve is implemented as a lookup table.

3 Optimal Collision Avoidance

A general approach for the planning of optimal collision avoidance trajectories is presented in this chapter considering traffic scenarios with a single critical dynamic obstacle ahead. The approach shall consider a bounded drivable area and limitations of the vehicle dynamics and actuators.

The crucial factors for the planning of collision avoidance trajectories are the timing and intensity of braking and steering activation. The interdependencies of braking and steering intervention [45] are considered by the proposed design. Also the vehicle dynamics and realistic limitations, including actuators, are considered aiming to provide dynamically feasible trajectories. Besides necessary dynamic considerations ensuring the dynamic integrity of the trajectory, the moment in time when the maneuver, described by the trajectory, has to be executed needs special attention. This moment is a crucial point and distinguishes whether or not an imminent collision is avoidable. Determining this moment represents a key parameter for the execution strategy of an Advanced Driver Assistance System (ADAS) for automated collision avoidance.

The structure of this chapter is as follows: the methodology for optimal trajectory planning of collision avoidance maneuvers is developed. Necessary conditions, criteria and requirements for trajectory planning of collision avoidance maneuvers are presented and discussed. A general mathematical formulation of the trajectory planning problem is derived.

3.1 Structural definition of the optimization problem

To satisfy the requirements introduced in Section 2.4, trajectory planning is formulated as a nonlinear optimization problem. Optimal trajectory planning is considered as previously discussed in Section 2.5. A general mathematical formulation of optimal trajectory planning for collision avoidance is given. On the basis of Definition 2.2, optimal trajectory planning is defined with adaptations to the necessary requirements.

Definition 3.1. Let $k \in \mathbb{N}$ be a discrete time, representing an arbitrary starting point of the trajectory. Let $i \in I$ with $I = [0 \dots \mathrm{H}] \subset \mathbb{N}$ be a sampled sequence of H samples. Further, let $\boldsymbol{x}(i|k) \in \mathbb{R}^{n_x}$ be a state vector, $\boldsymbol{u}(i|k) \in \mathbb{R}^{n_u}$ an excitation vector, and $\Delta\boldsymbol{t}(i|k) \in \mathbb{R}$ a sequence of sampling rates. Let $\boldsymbol{z}(k)$ be an augmented trajectory with

$$\boldsymbol{z}(k) = [\boldsymbol{T}(k), \boldsymbol{p}(k)] \qquad \mathbb{R}^{n_T} \times \mathbb{R}^{n_p} \to \mathbb{R}^{nZ} \tag{3.1}$$

where $\boldsymbol{T}(k) \in \mathbb{R}^{n_T}$ is a trajectory according to Definition 2.1 and $\boldsymbol{p}(k) \in \mathbb{R}^{n_p}$ is a parameter vector, which is specified in the further course of this section. The nonlinear optimization problem in general expression is:

$$\begin{aligned} &\min_{\boldsymbol{z}} \boldsymbol{J}(\boldsymbol{z}(k)) \\ &\text{subject to} \quad \boldsymbol{x}(i+1|k) = \boldsymbol{f}(\boldsymbol{x}(i|k), \boldsymbol{u}(i|k), \Delta\boldsymbol{t}(i|k)) \\ &\qquad\qquad \boldsymbol{x}(i|k) \in \mathcal{X} \subset \mathbb{R}^{n_x} \\ &\qquad\qquad \boldsymbol{u}(i|k) \in \mathcal{U} \subset \mathbb{R}^{n_u} \\ &\qquad\qquad \boldsymbol{x}(0|k) = \boldsymbol{x}(k) \\ &\qquad\qquad \forall i \in I \end{aligned} \tag{3.2}$$

With the functions $\boldsymbol{f} : \mathbb{R}^{n_x} \times \mathbb{R}^{n_u} \times \mathbb{R} \to \mathbb{R}^{n_x}$, $\boldsymbol{J} : \mathbb{R}^{n_z} \to \mathbb{R}$

The cost function $\boldsymbol{J}$ is defined as a function of the augmented trajectory $\boldsymbol{z}(k)$. The trajectory $\boldsymbol{z}(k)$ is sought which yields minimal cost in $\boldsymbol{J}$ subject to the set of constraints. The state and excitation vectors are constrained to satisfy the requirements of the collision avoidance maneuver. The state and excitation constraints are collected in the constrained sets $\mathcal{X}$ and $\mathcal{U}$, respectively. A detailed definition of the constraints is given in the next sections. Function $\boldsymbol{f}$ represents a general discretized functional description of an arbitrary dynamic model mimicking the vehicle dynamics. This can be a single-track model as recapped in Section 2.6 for example or any other expression.

The general mathematical formulation of optimal trajectory planning according to Definition 3.1 shall serve as the fundamental for the following sections, finalizing a comprehensive formulation of a collision avoidance problem. The remaining open items are described in the following sections.

3.2 Optimality criteria and cost function

Optimality criteria for collision avoidance maneuvers are discussed. Initially, it shall be clarified what optimal collision avoidance maneuvers are and which criteria are decisive. Based on this, a mathematic expression of the cost function $\boldsymbol{J}$ is deduced. The criteria and the cost function were already partially covered in [17] and [18] and shall be readdressed and discussed in detail.

To clarify the optimality criteria for collision avoidance maneuvers, the initial step is to identify the sufficient conditions which guarantees the absence of collision. This condition holds if a maneuver is capable to avoid the imminent collision with a dynamic obstacle and the environment, while satisfying the physical characteristics and limitations of the vehicle. Ensuring the adherence of the sufficient condition shall be attained by the set of

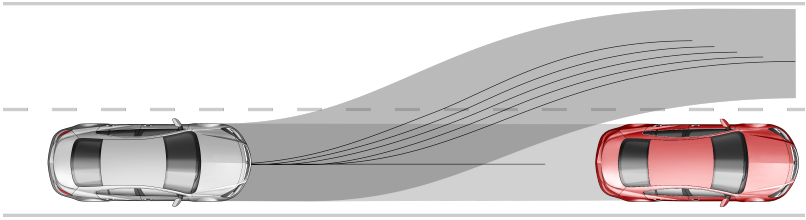

Figure 3.1: Closed band comprising the set of collision-free trajectories

constraints, which are introduced in a later section. Trajectories that satisfy the sufficient condition are collected in an extensive set of collision-free trajectories.

A representative scenery with the corresponding band comprising the set of all collision-free trajectories is shown in Fig. 3.1. The ego-vehicle travels along a road towards an obstacle blocking the ego-vehicle's lane. The adjacent lane is unoccupied. A variety of possible trajectories exists that ensure a safe passage of the obstacle. The possible collision avoidance maneuvers are grouped into two classes, which are also called homotopy class as discussed in [2] for example. There are either evasive maneuvers to the left, collected in the gray area, or braking maneuvers with the intention to stop in front of the obstacle, collected in the light gray area. The challenge is to identify which trajectory in the set is optimal. This example shows the necessity of additional criteria to specify the optimality of collision avoidance trajectories.

A suitable optimality criterion can be obtained by considering the temporal behavior of collision avoidance trajectories. A trajectory is not considered to be optimal, if another trajectory exists that prevents the imminent collision at a later time. The moment of the last possible evasive maneuver is consequently highly relevant. This complies with the works of [78] and [57].

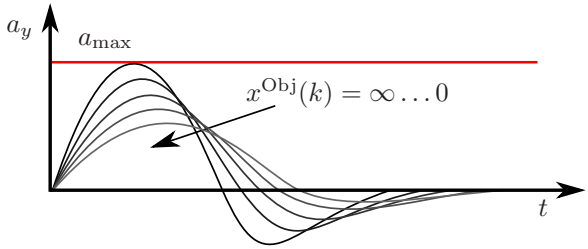

Figure 3.2: Lateral acceleration trajectories for decreasing distance to critical obstacle

Collision avoidance maneuvers comprising a steering intervention enables a maneuver execution at a later time compared to a brake-only intervention under certain conditions (vehicle speed) [78]. A combined braking and steering intervention has the potential to further extend the time compared to a pure steering intervention [56]. These findings were conducted assuming a maximum utilization of the absolute acceleration. Vehicle specific limitations like actuator limits or tire dynamics and environmental limitations were not considered.

The relevance of utilizing the last possible evasive maneuver as an optimality criterion shall be supported by the following example: The ego-vehicle is approaching a stationary obstacle which blocks the ego-vehicle's lane, comparable to the situation in Fig. 3.1. An evasive maneuver to the adjacent lane is feasible. The assumption is that a pure braking intervention would be too late to avoid the imminent collision. While the ego-vehicle is approaching the obstacle, the necessary lateral acceleration trajectories are successively evaluated. It is assumed that the trajectories are planned prior to an instantaneous execution. Fig. 3.2 shows the corresponding acceleration trajectories. While the ego-vehicle is approaching the critical obstacle, the longitudinal distance to the obstacle $x^{\mathrm{Obj}}(k)$ decreases for each instance k. With decreasing distance, the magnitudes of the lateral acceleration trajectories

increase until the limit is reached. The moment when the acceleration limit is reached determines the last possible evasive maneuver. After this specific moment, no further collision-free trajectory can be found while approaching the obstacle without violation of the main constraint, which is the absence of collision. With regards to the constraints, reaching the limits of at least one constraint is not a direct requirement for an evasive trajectory. This is rather a consequence or a characteristic of a last possible maneuver, which can be classified as an extremal maneuver [57]. The example shown in Fig. 3.2 also highlights the importance of the trigger condition. Arbitrary execution of a collision avoidance maneuver is not the favorable strategy which is highlighted by the acceleration trajectories where most are hardly at the limit. This contradicts the characteristics of a highly dynamic maneuver. Instead, the moment when the acceleration limit is reached, which indicates the moment of the last possible execution, shall be desired. Consequently, successively trajectory planning prior to the execution of evasive trajectories and determining the trigger time shall be a decoupled process.

Motivated by the subsequent discussion, the optimality criteria for evasive trajectories are clarified. Optimal trajectories are identified by their temporal characteristics. Looking at the chronological sequence, the moment of the latest possible maneuver specifies the optimal moment for the trajectory execution. After this point is exceeded no further collision-free trajectory exists while converging further to the critical object. Not only the moment of the last possible evasive maneuver is crucial but also the chronological sequence to this moment. While observing and interpreting a scenery, it is a huge benefit to comprehend how much time is left until an intervention is urgently needed. Concluding from the criteria, the period to the execution of that trajectory shall be known at every instance.

The period to the execution of the last possible evasive trajectory shall be further refereed to *Time to Last Maneuver Execution* t_{TLME} . The time-

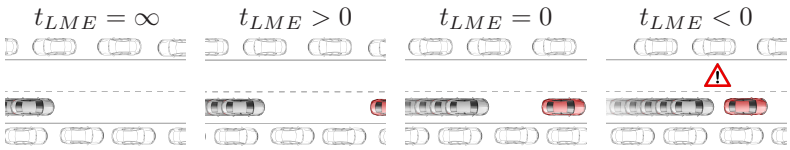

Figure 3.3: Relevant events for t_{TLME}

related reference of t_{TLME} is shown in Fig. 3.3 for relevant events. The ego-vehicle travels along a street and the driving corridor is scanned for any obstructions. At the absence of any obstacle, t_{TLME} is infinite, referring to sequence (a). This event specifies a uncritical situation where no evasive maneuver is necessary. In sequence (b), an obstacle appears in the driving corridor that blocks the ego-vehicle's lane. The relative longitudinal distance to the obstacle is sufficiently large. An immediate intervention at this stage is not necessary. Therefore, t_{TLME} is greater than zero and the intervention can be postponed until t_{TLME} reaches zero. The ego-vehicle approaches the obstacle without any noticeable reactions until t_{TLME} is zero, shown in sequence (c). This moment identifies the moment for the last possible collision-free trajectory execution. After this spatiotemporal point is exceeded, a collision with the obstacle is inevitable. This corresponds to sequence (d).

To define the required cost function $\boldsymbol{J}$, the discussed time to last maneuver execution t_{TLME} provides an appropriate temporal measure.

$$\boldsymbol{J}(\boldsymbol{z}(k)) = -t_{\mathrm{TLME}} \tag{3.3}$$

Defining the cost function according to Eq. (3.3) ensures the demanded criteria. The cost function is defined to maximize t_{TLME}. Since the cost function $\boldsymbol{J}$ is a function of the augmented trajectory $\boldsymbol{z}(k)$ for the given

situation k, it is highly depending on both the individual situation and the trajectory itself. Maximizing t_{TLME} indirectly provides the optimal triggering time while the last possible evasive trajectory is sought, subject to the constraints. Another advantage of this approach is the capability to assess the criticality of the scenery by evaluating the duration to optimal trigger time, which is the value of the maximized t_{TLME} . Depending on t_{TLME} , the criticality of the present situation can be interpreted. Values of t_{TLME} greater zero can be interpreted as less critical whereas t_{TLME} close to zero or zero are highly critical and should trigger a rapid intervention. Values below zero can preemptively identify situations where a collision is not avoidable.

A mechanical analogon for the proposal can be found in moulding processes where a machined workpiece, e.g., a rod, is pressed into the mold and is remolded. The analogon to t_{TLME} is the applied pressure to the rod. The physical properties of the workpiece, e.g., Young's modulus, are the analogon to the vehicle physics. The mould cavity is the analogon to the constraints.

3.3 Trajectory sampling

An appropriate approach for the sampling of collision avoidance trajectories shall be introduced. The applied trajectory sampling approach was already introduced in [18] and is described in this section.

Trajectory planning concepts designed for automated systems consider a successive trajectory re-planning with a fixed planning horizon. A typical example for such an approach is the concept of Model Predictive Control theory. Typically, trajectories are planned for a predefined planning horizon [19, 24, 27], where the trajectory is sampled with a fixed step size of H steps. The advantage of the fixed step size is the a priori determined trajectory duration and, hence, reduces the complexity of the problem.

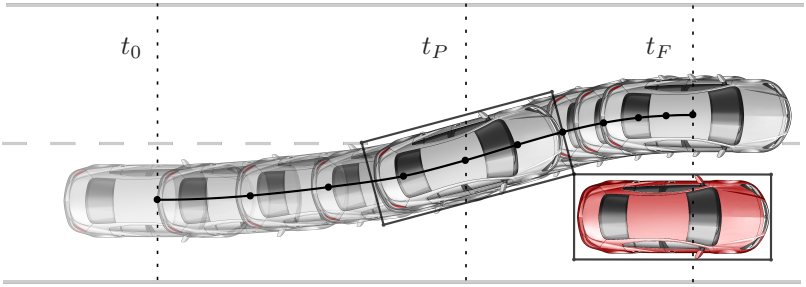

Figure 3.4: Relevant events for trajectory sampling

However, applying a fixed trajectory duration to trajectories that are intended for collision avoidance could be insufficient. If the fixed planning horizon is too short, a holistic calculation of the trajectory cannot be ensured in a single planning step. Additionally, the avoidance of a road departure after a successful evasion cannot be ensured. On the other hand, if the fixed planning horizon is too long, computational complexity and sampling size increase with the risk of exceeding the maximum allowable computation time. In consequence, for the specific application of collision avoidance, the trajectory for the entire evasive maneuver shall be planned in a single planning step.

Prior to the discussion of the trajectory sampling approach, the distinctive events of evasive trajectories are introduced. The relevant points are shown for an exemplary evasive trajectory in Fig. 3.4. Three relevant events are identified. The start and the end of the trajectory are t_0 and t_F. The most important time of evasive trajectories is the time when the ego-vehicle's front vertex and the obstacle's rear vertex coincide. For an evasion to the left, the relevant vertices are the front-right for the ego-vehicle and the rear-left for the obstacle. An evasion to the right is analog, respectively.This specific point determines whether or not a collision occurs between the two

opponents. This temporal point will be further referred to *Passing Time* t_P. The time, related to the stylized ego-vehicle front-right vertex, when the ego-vehicle firstly coincides with the rear corner of the obstacle. Determining t_P and t_F highly depends on the situation and is required to be individually determined for every trajectory. This implies t_P and t_F to be evaluated jointly with the trajectory during the optimization process.

Next, the proposed sampling approach is discussed which shall provide a holistic description of evasive trajectories. Evasive trajectories shall comprise a fixed sequence of H samples in total. This sequence is split into two sub intervals. The first interval begins at the start of the maneuver, t_0, and ends at t_P. This interval is sampled with N samples. The subsequent interval starts at t_P, terminates at the end of the evasive maneuver, t_F, and is sampled with $\mathrm{M} = \mathrm{H} - \mathrm{N}$ samples. The split into two maneuver sequences enables more flexibility in the trajectory design and supports an individual adaption to the specific needs for the two maneuver intervals.

The proposed sampling approach enables an optimal passing time, t_P, and an optimal maneuver duration, t_F, for each individual situation. Further, the restriction to two representative times diminishes the computational complexity by its inherent definition of the temporal sequence. These two subintervals facilitate the definition of applicable time vectors for the planned evasive trajectory of the actual planning step k. A discrete time prediction vector $\boldsymbol{t}(i|k)$ and a sequence of sampling rates $\Delta\boldsymbol{t}(i|k)$ are defined. For the first interval the discrete time vector and the sequence of sampling rates are

$$\boldsymbol{t}(i|k) = 0 \qquad \forall i = 0 \tag{3.4}$$

$$\boldsymbol{t}(i|k) = \frac{t_\mathrm{P}}{\mathrm{N}} \cdot i \qquad \forall i = 1, \ldots, \mathrm{N} \tag{3.5}$$

$$\Delta \boldsymbol{t}(i|k) = \frac{t_\mathrm{P}}{\mathrm{N}} \qquad \forall i = 0, 1, \ldots, \mathrm{N} \tag{3.6}$$

with $\mathrm{N}+1$ samples from maneuver start until passing the object t_P. The second intervals of the discrete time vector and the sequence of sampling rates with M samples for the time period after passing the obstacle t_P until the end of the maneuver t_F are

$$\boldsymbol{t}(i|k) = t_\mathrm{P} + \frac{t_\mathrm{F} - t_\mathrm{P}}{\mathrm{M}} \cdot (i - \mathrm{N}) \qquad \forall i = \mathrm{N}+1, \ldots, \mathrm{N}+\mathrm{M} \tag{3.7}$$

$$\Delta \boldsymbol{t}(i|k) = \frac{t_\mathrm{F} - t_\mathrm{P}}{\mathrm{M}} \qquad \forall i = \mathrm{N}+1, \ldots, \mathrm{N}+\mathrm{M}. \tag{3.8}$$

With Eqs. (3.4) – (3.8), the discrete time vector and sequence of sampling rates for optimal evasive trajectories are holistically described.

The temporal complexity of the algorithm $\mathcal{O}(\log(\mathrm{H}))$ with $\mathrm{H} = \mathrm{N} + \mathrm{M}$ was verified by a complexity analysis of the algorithm where the optimal solution converges for a total number of $\mathrm{H} = 20$ samples.

3.4 Trajectory definition

The trajectory shall be defined in this section. Considering the structure of the augmented trajectory for each instance k, which is

$$\boldsymbol{z}(k) = [\boldsymbol{T}(k), \boldsymbol{p}(k)] \qquad \mathbb{R}^{n_T} \times \mathbb{R}^{n_p} \rightarrow \mathbb{R}^{n_Z}. \tag{3.9}$$

The Trajectory is defined by the sequence of the excitation vector yielding

$$\boldsymbol{T}(k) = [\boldsymbol{u}(0|k), \ldots, \boldsymbol{u}(\mathrm{H}|k)] \qquad \mathbb{R}^{n_{\boldsymbol{u}}} \times I \rightarrow \mathbb{R}^{n_\mathrm{T}}. \tag{3.10}$$

The parameter vector $\boldsymbol{p}(k)$ is defined according to

$$\boldsymbol{p}(k) = [t_\mathrm{TLME}, t_\mathrm{P}, t_\mathrm{F}] \tag{3.11}$$

with the relevant times of the trajectory. It comprises the time to last maneuver execution t_{TLME}, the optimal passing time t_{P} and the trajectory duration t_{F}.

The definition of the trajectory $\boldsymbol{T}(k)$ and the parameter vector $\boldsymbol{p}(k)$ yields the augmented trajectory

$$\boldsymbol{z}(k) = [\boldsymbol{u}(0|k), \ldots, \boldsymbol{u}(\mathrm{H}|k), t_{\mathrm{TLME}}, t_{\mathrm{P}}, t_{\mathrm{F}}]. \tag{3.12}$$

Applying the sequence of the excitation vector $\boldsymbol{u}(k)$ and the reconstructed time vector $\Delta\boldsymbol{t}(k)$ to the dynamic function $\boldsymbol{f}$ yields the state vector sequence:

$$\boldsymbol{x}(k) = [\boldsymbol{x}(0|k), \ldots, \boldsymbol{x}(\mathrm{H}|k)] \qquad \mathbb{R}^{n_{\boldsymbol{x}}} \times I \to \mathbb{R}^{n_{\mathrm{T}}}. \tag{3.13}$$

Depending on the applied dynamic model $\boldsymbol{f}$, the state vector $\boldsymbol{x}(k)$ and excitation vector $\boldsymbol{u}(k)$ may vary in their components. In general, the state vector shall comprise of the longitudinal and lateral position s_x and s_y, velocity v_x and v_y, and acceleration a_x and a_y. Further, the excitation vector $\boldsymbol{u}(k)$ shall comprise of two components that enables a manipulation of the lateral and longitudinal vehicle motion.

3.5 Constraints

In addition to the cost function, a set of constraints is required to generate collision avoidance trajectories. The constraints are subdivided into geometric and dynamic constraints and final conditions. Geometric constraints shall ensure the absence of collisions and shall prevent a departure off the road. Dynamic constraints shall ensure the integrity of the vehicle dynamics and limitations. Final conditions shall ensure a proper handover after the trajectory was terminated.

Edge ι	FL	FR	RL	RR
${}^{\mathrm{C}}\boldsymbol{p}_{\iota} = \begin{bmatrix} {}^{\mathrm{C}}x_{\iota} \\ {}^{\mathrm{C}}y_{\iota} \end{bmatrix}$	$\begin{bmatrix} a \\ \frac{w}{2} \end{bmatrix}$	$\begin{bmatrix} a \\ -\frac{w}{2} \end{bmatrix}$	$\begin{bmatrix} -b \\ \frac{w}{2} \end{bmatrix}$	$\begin{bmatrix} -b \\ -\frac{w}{2} \end{bmatrix}$

Table 3.1: Edges of the vehicle's contour which are the front-left, front-right, rear-left and rear-right vertices related to the COG

3.5.1 Geometric constraints

Geometric constraints are essential to the definition of collision avoidance trajectories. The surroundings of the ego-vehicle needs special attention, especially in the presence of dynamic obstacles and restrictions to the drivable area. While moving on public roads, especially in urban areas, arbitrary road geometries and road limitations, e.g., pavements, verges or parked vehicles on the roadside, shall be considered. In the presence of critical obstacles, e.g. vehicles or pedestrians, their geometry as well as the ego-vehicle's geometry shall be considered. All together require a representation in a convenient form to derive mathematical expressions of the necessary geometries.

Vehicle shape approximation

The shape of a vehicle is approximated by a rectangle that encloses the vehicle's expansion as illustrated in Fig. 3.5. All quantities are further related to the vehicle's Center of Gravity (COG), which is assumed as fixed rotation center. Dynamic variations of its position caused by braking and turning movements are neglected. The length from the COG to the stylized vehicle front is called a, b is the length from the COG to the stylized vehicle rear, and w is the maximum vehicle width, respectively. The four corresponding vertices of the stylized vehicle shape are summarized in Table 3.1, where ${}^{\mathrm{C}}\boldsymbol{p}_{\iota}$ is a generalized vertex vector of the vehicle contour with ${}^{\mathrm{C}}x_{\iota}$ and ${}^{\mathrm{C}}y_{\iota}$ being the coordinates related to the vehicle's COG. The four vertices are

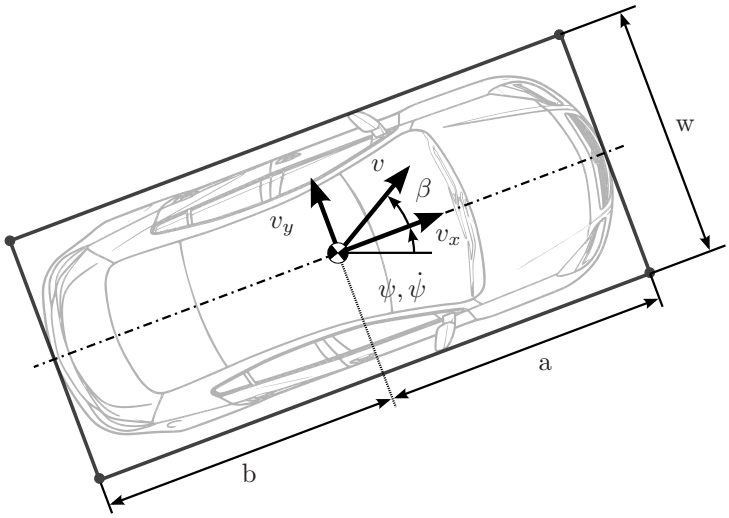

Figure 3.5: Stylized vehicle contour

listed with the equivalent vertex labels $\iota = \mathrm{FL}, \mathrm{FR}, \mathrm{RL}, \mathrm{RR}$, which are the front-left, front-right, rear-left, and rear-right vertices, respectively[28].

For the further application, the vertex vectors ${}^{\mathrm{C}}\boldsymbol{p}_{\iota}$ are required in global coordinates. Therefore, a transformation matrix $\boldsymbol{T}_{\mathrm{z}}$ is defined that transforms the vehicle vertex vectors, related to COG, into vertices relative to global coordinates. The vectors are rotated around the vehicle's z-axis, with the COG as center of rotation, with the vehicle's yaw angle ψ and the slip angle β. The transformation matrix is defined as:

$$\boldsymbol{T}_{\mathrm{z}}(\psi+\beta) = \begin{bmatrix} \cos(\psi+\beta) & -\sin(\psi+\beta) \\ \sin(\psi+\beta) & \cos(\psi+\beta) \end{bmatrix} \tag{3.14}$$

Multiplying the transformation matrix with the vertex vector in vehicle related coordinates

$$^{\mathrm{G}}\boldsymbol{p}_{\iota} = \boldsymbol{T}_{\mathrm{z}}(\psi + \beta)\,^{\mathrm{C}}\boldsymbol{p}_{\iota} \tag{3.15}$$

yields the global vertex-vector

$$^{\mathrm{G}}\boldsymbol{p}_{\iota} = [^{\mathrm{G}}x_{\iota}, {}^{\mathrm{G}}y_{\iota}]^{\mathsf{T}} \qquad \iota = \mathrm{FL}, \mathrm{FR}, \mathrm{RL}, \mathrm{RR} \tag{3.16}$$

with $^{\mathrm{G}}x_{\iota}$ and $^{\mathrm{G}}y_{\iota}$ in global coordinates, respectively.

The vehicle envelope caused by slip angle changes requires special considerations if the applied dynamic model does not provide a valid slip angle information. To cover those limitations, the vehicle envelope is approximated by adding an extra safety margin to the vehicle width w due to the unknown direction and value of the induced slip angle related rotation. The safety margin is approximated assuming a maximum slip angle $\beta^{*}_{\max}$, which is in the range of $-6°, \ldots, 6°$. Rotating the vehicle in both directions by $\beta^{*}_{\max}$ reveals a larger envelope, as shown in Fig. 3.6. The obtained envelope determines the new width of the vehicle contour w^{*}. It is obtained by rotating the diagonal vertices front-left and rear-right in positive direction. The rotated vertices are

$$^{\mathrm{C}}\boldsymbol{p}^{*}_{\iota} = \boldsymbol{T}_{\mathrm{z}}(\beta^{*}_{\max})\,^{\mathrm{C}}\boldsymbol{p}_{\iota}, \qquad \iota = \mathrm{FL}, \mathrm{RR} \tag{3.17}$$

with the coordinates

$$^{\mathrm{C}}\boldsymbol{p}^{*}_{\iota} = [^{\mathrm{C}}x^{*}_{\iota}, {}^{\mathrm{C}}y^{*}_{\iota}]^{\mathsf{T}} \tag{3.18}$$

The new width substituting w in Table 3.1 is

$$\mathrm{w}^{*} = \max(^{\mathrm{C}}y_{\mathrm{FL}}, {}^{\mathrm{C}}y_{\mathrm{RR}}) \tag{3.19}$$

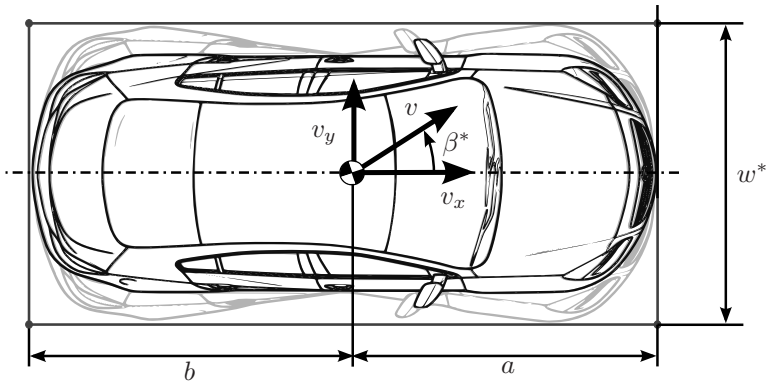

Figure 3.6: Vehicle contour with approximated slip angle β

Environment information

Reliable data of the environment are a prerequisite for trajectory planning. Especially for collision avoidance trajectories, data related to the critical obstacle are highly relevant. These shall comprise at least the obstacle's relative position and velocity. Additionally, data of the drivable area is required. It shall be assumed that the necessary environmental information is available.

For each trajectory planning step k, the relevant environmental information are continuously collected in the environment vector

$$\boldsymbol{e}(k) = [\boldsymbol{e}_{\mathrm{Obj}}(k), \boldsymbol{e}_{\mathrm{Road}}(k)]^{\mathsf{T}}. \tag{3.20}$$

The current information of the critical obstacle ahead is collected in

$$\boldsymbol{e}_{\mathrm{Obj}}(k) = [x^{\mathrm{Obj}}(k), y^{\mathrm{Obj}}(k), v_x^{\mathrm{Obj}}(k), w^{\mathrm{Obj}}(k)]^{\mathsf{T}} \tag{3.21}$$

with the coordinates of the critical obstacle relative to the ego-vehicle, the longitudinal distance $x^{\mathrm{Obj}}(k)$ and the lateral coordinate $y^{\mathrm{Obj}}(k)$. The relative longitudinal velocity of the obstacle is denoted as $v_x^{\mathrm{Obj}}(k)$. The width of the obstacle is $w^{\mathrm{Obj}}(k)$. The parameterized data of the drivable area for the planning step k are collected in

$$\boldsymbol{e}_{\mathrm{Road}}(k) \tag{3.22}$$

Collision avoidance with a single obstacle

The successful planning of evasive maneuvers starts with the understanding of the spatial constellation of the potential accident opponents. Assessing the necessary geometric conditions that lead to a safe passage of an obstacle are investigated. The spatio-temporal point, when and where the two potential opponents pass each other, is crucial whether or not a collision occurs. Fig. 3.7 shows a general exemplary situation where the gray ego-vehicle passes the red vehicle to the left. The vehicle contours are approximated by rectangles as presented in Section 3.5.1. The critical point is at the location where the ego-vehicle's stylized front-right corner coincides with the opponent's stylized rear-left corner. This point can be interpreted as a vir-

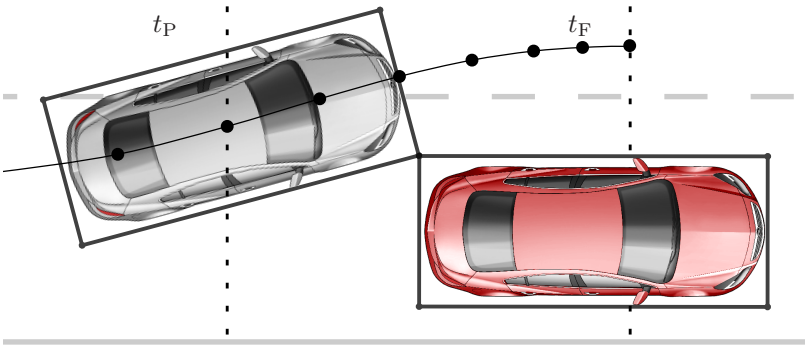

Figure 3.7: Relevant geometric points of the ego-vehicle and obstacle

tual point of first contact. The critical time related to that spatial point is referred to as the passing time t_{P}, which is referenced to the ego-vehicle's COG. The transformation of the ego-vehicle's approximated contour coordinates to COG related coordinates is defined in Eq. (3.15), where the contour approximation reveals an additional safety margin. Consequently, the coincidence of both opponents at the passing time can be considered as the smallest point to point distance where a collision-free passage is still possible. A feasible condition to define geometric constraints for collision avoidance trajectories is obtained by considering the coincident point as a critical and crucial point. Nonetheless, more conditions are required to ensure the absence of collisions while the ego-vehicle is passing the opponent's rear corner, especially while the ego-vehicle's side-face is next to the critical point. The necessary conditions for a collision-free passing of the opponent's rear corner shall be clarified in detail.

As a consequence of the expected high lateral acceleration during evasive maneuvers, the slip angle can reach a significant magnitude, which would induce a side drift of the ego-vehicle, hence an increased envelope. To ensure the absence of collision, the minimal distance of the ego-vehicle's contour to the opponent's rear corner needs to be at least equal or greater than zero while the ego-vehicle's side-face is next to the critical point.

Another condition that needs to be considered is how to proceed after the ego-vehicle has passed the critical point. In principle, there are two possible options. The first option is a return to the ego-vehicle's initial lane. For the second option, the ego-vehicle may keeps its current lateral displacement while adjusting its orientation parallel to the road. In this work, option two is favorable, keeping the lateral displacement during the maneuver.

In consequence, the following conditions are required to extract geometric constraints to avoid the collision with a single obstacle. First, the coincident

point shall be considered. Second, the minimal distance of the ego-vehicle's contour to the opponent's rear corner shall be at least equal or greater than zero. And third, the lateral offset of the ego-vehicle after the opponent is passed shall be greater or equal than the lateral coordinate of the critical point. With these considerations, geometric constraints can be defined ensuring a collision-free maneuver.

Starting with the first condition when the front-right corner of the ego-vehicle and the rear-left corner of the opponent coincide. The geometric constraint covering an evasion to the left is described hereafter.

$$\begin{aligned} s_x(\mathrm{N}|k) + {}^{\mathrm{G}}x_{\mathrm{FR}}(\mathrm{N}|k) = x^{\mathrm{Obj}}(k) &+ v_x^{\mathrm{Obj}}\,(t_{\mathrm{TLME}} - t_{\mathrm{P}}) \\ &- v_x(0|k) \cdot t_{\mathrm{TLME}} \\ s_y(\mathrm{N}|k) + {}^{\mathrm{G}}y_{\mathrm{FR}}(\mathrm{N}|k) = y^{\mathrm{Obj}}(k) &+ 0.5 w^{\mathrm{Obj}}(k) \end{aligned} \tag{3.23}$$

The left hand side of Eq. (3.23) defines the spatio-temporal coincident point of the trajectory for the actual planning step k. This point is reflecting the global coordinate of the ego-vehicle's front-right corner at that point. The passing time t_{P} is expressed by sample N as defined in Section 3.3. With the longitudinal and lateral coordinate of the trajectory, $s_x(\mathrm{N}|k) + {}^{\mathrm{G}}x_{\mathrm{FR}}(\mathrm{N}|k)$ and $s_y(\mathrm{N}|k) + {}^{\mathrm{G}}y_{\mathrm{FR}}(\mathrm{N}|k)$ reflect the ego-vehicle's front-right corner related to the vehicle's COG. The right side of Eq. (3.23) defines the coordinates of the opponent's rear-left corner related to the ego-vehicle's COG for the actual planning step k with the longitudinal and lateral coordinates of the opponent's rear-left corner,

$$x^{\mathrm{Obj}}(k) + v_x^{\mathrm{Obj}}\,(t_{\mathrm{TLME}} - t_{\mathrm{P}}) - v_x(0|k) \cdot t_{\mathrm{TLME}} \quad \text{and}$$
$$y^{\mathrm{Obj}}(k) + 0.5 w^{\mathrm{Obj}}(k).$$

Where $v_x(k)^{\mathrm{Obj}}$ is the opponents longitudinal velocity and $v_x(0|k)$ is the ego-vehicle's initial longitudinal velocity.

Depending on the value of the optimized solution of t_{TLME} , it can be interpreted differently as described below.

$t_{\mathrm{TLME}} > 0$	The maneuver execution can be postponed, additional time reserve is available for the current situation.
$t_{\mathrm{TLME}} = 0$	An immediate trajectory execution is required, no additional time reserve is available for the current situation.
$t_{\mathrm{TLME}} < 0$	For the current situation, no feasible trajectory can be found that avoids the imminent collision.

Subsequent to the geometric constraint for the first condition, the geometric constraint for the second condition will be discussed in the next section. The distance of the ego-vehicle's contour to the opponent's rear corner is interpreted by the geometrical problem of finding the minimal distance between a line and a point [74, 49]. In this analogon, the side of the ego-vehicle is interpreted as the line and the opponent's rear corner is interpreted as the point. Let the line be specified by the two contour points of the ego-vehicle lying on it, with the corresponding position vectors for the rear-right corner ${}^{\mathrm{G}}\boldsymbol{p}_{\mathrm{RR}}(i|k)$ and for the front-right corner ${}^{\mathrm{G}}\boldsymbol{p}_{\mathrm{FR}}(i|k)$. These vectors define the i^{th} trajectory sample of the two corners for the k^{th} trajectory. The position vector of the opponent's rear-left corner is

$$\boldsymbol{q}_{\mathrm{Obj}}(k) = [x^{\mathrm{Obj}}(k), y^{\mathrm{Obj}}(k)]^{\mathsf{T}} \tag{3.24}$$

Applying the formula for the distance of a point to a line, the minimal distance becomes:

$$d_{\mathrm{e2o}}(i|k) =$$

$$\frac{|\left({}^{\mathrm{G}}\boldsymbol{p}_{\mathrm{FR}}(i|k) - {}^{\mathrm{G}}\boldsymbol{p}_{\mathrm{RR}}(i|k)\right) \times \left({}^{\mathrm{G}}\boldsymbol{p}_{\mathrm{RR}}(i|k) - \boldsymbol{q}_{\mathrm{Obj}}(k)\right)|}{|{}^{\mathrm{G}}\boldsymbol{p}_{\mathrm{FR}}(i|k) - {}^{\mathrm{G}}\boldsymbol{p}_{\mathrm{RR}}(i|k)|} \tag{3.25}$$

Where $d_{\mathrm{e2o}}(i|k)$ is the trajectory of the minimal distance for the k^{th} measurement. Eq. (3.25) enables the formulation of a geometric constraint for the second and third collision avoidance condition. Ensuring a collision-free passing of the opponent, the distance to the critical point is required to be greater than or equal to zero. Further, to ensure no collision until the maneuver is finished, the lateral displacement is kept up to the end of the trajectory. The geometric constraint is

$$d_{\mathrm{e2o}}(i|k) \geq 0, \quad \forall i = \mathrm{N} \ldots \mathrm{H} \tag{3.26}$$

Road Boundaries

The consideration of boundaries of the drivable area is essential for collision avoidance, especially within narrow roads typical for urban areas. A collision with road boundaries or a road departure shall be avoided. Lane markings do not represent the physical limit of the drivable area. Within urban areas, lane markings are untypical on one-way streets or in residential areas. In contrast, e.g., pavement boarders or physical boarders, like parking vehicles on the roadside, are highly relevant obstacles. A suitable expression of the road boundaries and the road geometry shall be defined. This shall lead to the definition of geometric constraints for arbitrary road geometries that keep the ego-vehicle within the drivable area.

A common geometrical road model is a parameterized approximation of the road clothoid as a third-degree polynomial function [42, 67, 22]. This compact notation is also reasonable for the curved road boundaries. The

lateral road boundary with related quantities is shown in Fig. 3.8. The polynomial expression for the lateral road boundary is defined as

$$d_j(k) = c_{0,j}(k) + c_{1,j}(k)x + c_{2,j}(k)x^2 + c_{3,j}(k)x^3 \quad j = \mathrm{L}, \mathrm{R} \tag{3.27}$$

Where $d_j(k)$ denotes the left or right road boundary at planning step k. The polynomial coefficients $c_{0,j}(k), c_{1,j}(k), c_{2,j}(k), c_{3,j}(k)$ of the current planning step k are collected in

$$\boldsymbol{e}_{\mathrm{Road}}(k) = [c_{0,j}(k), c_{1,j}(k), c_{2,j}(k), c_{3,j}(k)]^{\mathsf{T}} \quad j = \mathrm{L}, \mathrm{R} \tag{3.28}$$

with the corresponding coefficients $c_{0\ldots3,j}(k)$ of the left and right side of the drivable area. Here, $c_{0,j}(k)$ denotes the lateral offset of the road boundary to the ego-vehicle's longitudinal axis, $c_{1,j}(k)$ denotes the angle between the ego-vehicle's longitudinal axis and the road boundary's tangent in the initial point $x = 0$, and $c_{2,j}(k)$ and $c_{3,j}(k)$ denote the curvature and curvature rate

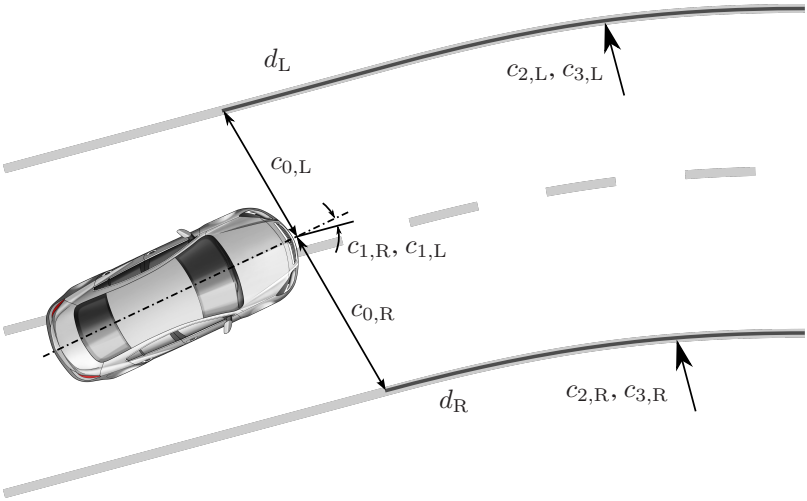

Figure 3.8: Road boundary and related quantities

of the road boundary, respectively. Index $j = \mathrm{L}, \mathrm{R}$ denotes left or right road boundary related to the ego-vehicle. x denotes a longitudinal distance ahead of the ego-vehicle.

Differentiating Eq. (3.27) with respect to the longitudinal distance x leads to

$$\frac{\partial}{\partial x} d_j(k) = \varphi_j(k) = c_{1,j}(k) + 2 \cdot c_{2,j}(k)x + 3 \cdot c_{3,j}(k)x^2 \tag{3.29}$$

with the heading angle of the road boundary $\varphi_j(k)$. The curvature of the lateral road boundary is obtained by differentiating Eq. (3.27) twice with respect to the longitudinal distance x, obtaining

$$\frac{\partial^2}{\partial x^2} d_j(k) = 2 \cdot c_{2,j}(k) + 6 \cdot c_{3,j}(k)x \tag{3.30}$$

To formulate the constraints, the representation of the road boundaries needs to be modified. The longitudinal distance x of Eq. (3.27) is substituted by the sequence of the trajectory's longitudinal positions

$$s_x(0|k), \ldots, s_x(\mathrm{H}|k). \tag{3.31}$$

The sequence of lateral road boundaries is

$$d_j(0|k), \ldots, d_j(\mathrm{H}|k) \quad j = \mathrm{L}, \mathrm{R} \tag{3.32}$$

The road boundary that shall avoid a road departure are defined as geometric constraints

$$\begin{aligned} s_y(i|k) + \max\left({}^{\mathrm{G}}y_{\mathrm{FL}}(i|k), {}^{\mathrm{G}}y_{\mathrm{RL}}(i|k)\right) &\leq d_L(i|k) \\ s_y(i|k) + \min\left({}^{\mathrm{G}}y_{\mathrm{FR}}(i|k), {}^{\mathrm{G}}y_{\mathrm{RR}}(i|k)\right) &\geq d_R(i|k) \end{aligned} \tag{3.33}$$

with the sequence of the lateral road boundaries, Eq. (3.32), the approximation of the vehicle shape, Eq. (3.16), and the sequence of the lateral position of the evasive trajectory

$$s_y(0|k), \ldots, s_y(\mathrm{H}|k) \tag{3.34}$$

leading to 2H inequality constraints. Applying the min and max functions to Eq. (3.33) ensures the selection of the nearest vertex of the ego-vehicle contour to the road boundary. The critical vertex of the ego-vehicle and the opponent are the front-left and the rear-right, respectively.

In summary, the geometric constraints are collected in the set of geometric constraints, $\mathcal{X}_g$, Eq. (3.32). For an evasion to the right direction, the same constraints can be applied analogously to the conditions for an evasion to the left.

$$
\mathcal{X}_g = \left\{ \boldsymbol{x} \in \mathbb{R}^{n_x} \;\middle|\; \begin{array}{ll}
s_y(i|k) + \max\left({}^{\mathrm{G}}y_{\mathrm{FL}}(i|k),\, {}^{\mathrm{G}}y_{\mathrm{RL}}(i|k)\right) \leq d_L(i|k) & \forall i = 0 \ldots \mathrm{H} \\
s_y(i|k) + \min\left({}^{\mathrm{G}}y_{\mathrm{FR}}(i|k),\, {}^{\mathrm{G}}y_{\mathrm{RR}}(i|k)\right) \geq d_R(i|k) & \forall i = 0 \ldots \mathrm{H} \\
d_{\mathrm{e2o}}(i|k) \geq 0 & \forall i = \mathrm{N} \ldots \mathrm{H} \\
s_x(\mathrm{N}|k) + {}^{\mathrm{G}}x_{\mathrm{FR}}(\mathrm{N}|k) = x^{\mathrm{Obj}}(k) \;\; + v_x^{\mathrm{Obj}}\left(t_{\mathrm{TLME}} - t_{\mathrm{P}}\right) & \\
\qquad\qquad\qquad\qquad\qquad\qquad - v_x(0|k) \cdot t_{\mathrm{TLME}} & \\
s_y(\mathrm{N}|k) + {}^{\mathrm{G}}y_{\mathrm{FR}}(\mathrm{N}|k) = y^{\mathrm{Obj}}(k) &
\end{array} \right. \tag{3.32}
$$

3.5.2 Dynamic constraints

This section covers the dynamic constraints required for the planning of evasive trajectories. Dynamic constraints ensure the integrity of the required dynamic limitations of the vehicle and, thus, ensure the driveability of the planned trajectory. Incorporating the limitations is highly relevant, especially in the planing of collision avoidance trajectories. The utilized trajectories are intended to be as late as possible, which induces a highly dynamic maneuver. The vehicle's dynamic limitations are mainly influenced by the interaction of the contact points between the road surface and the wheels [45]. For a practical implementation, considering the influence of actuator limitations is absolutely essential for the planning of collision avoidance trajectories. Considering only the friction circle as constraint is probably insufficient. Utilizing a last possible maneuver induces rapid directional changes, hence, the state transition within the friction circle is highly relevant. The vehicle's capability for rapid directional changes are given by the dynamics of the braking and steering actuators. Thus, actuator limitations are considered.

In the following, the considered dynamic constraints are defined and clarified. The vehicle's absolute acceleration is constrained by the friction circle [34], which was already proposed for a trajectory planning context [56, 57, 82]. It is given as

$$\|\boldsymbol{a}\| \leq \mathrm{a}_{\max} \tag{3.33}$$

where $\mathrm{a}_{\max}$ is the maximum allowed absolute acceleration, which is typically in a range of $7\,\mathrm{m/s^2}$ to $9.81\,\mathrm{m/s^2}$.

$$\|\boldsymbol{a}\| = \sqrt{a_x^2 + a_y^2} \tag{3.34}$$

is the absolute acceleration calculated for longitudinal acceleration a_x and lateral acceleration a_y. The vehicle's curvature κ [4] is considered as constraint where the curvature is given as

$$\kappa = \frac{v_x a_y - v_y a_x}{(v_x^2 + v_y^2)^{\frac{3}{2}}} \tag{3.35}$$

where v_x, a_x, v_y, and a_y are the longitudinal velocity and acceleration and the lateral velocity and acceleration, respectively, yielding the inequality constraint for the vehicle's curvature

$$|\kappa| \leq \kappa_{\max} \tag{3.36}$$

with the maximum curvature bound $\kappa_{\max}$. Constraining the vehicle's curvature is also considered by [82]. The dynamics of the steering actuator is constrained with respect to steering angle and steering angular rate, similar to [23, 76]. The steering angle is constrained by

$$|\delta| \leq \delta_{\max} \tag{3.37}$$

with the maximum steering angle $\delta_{\max}$. Further, the steering angular rate is defined as inequality constraint that yields

$$|\dot{\delta}| \leq \dot{\delta}_{\max} \tag{3.38}$$

with the maximum steering angular rate $\dot{\delta}_{\max}$. The parameterization of the specific actuator limitations shall be done according to the experimentally evaluated limitations (see Section 2.7).

Vehicle specific dynamic models, e.g., the single-track model (Section 2.6), ensure a direct interface to the actuators. The single-track model enables a direct limitation of the steering angle and the brake actuator. More general dynamic models which do not consider a direct actuator interface, actuator

limits are constrained by jerk limitations. Constraining the lateral motion with this approach was previously proposed by [46]. Formulating the actuator constraints in terms of jerk limitations for the lateral and longitudinal jerk $\dot{a}_y$ and $\dot{a}_x$.

$$\begin{aligned} |\dot{a}_x| &\leq \dot{a}_{x,\max} \\ |\dot{a}_y| &\leq \dot{a}_{y,\max} \end{aligned} \tag{3.39}$$

Summing up, the dynamic constraints are collected in the set of dynamic constraints $\mathcal{X}_d$ yielding

$$\mathcal{X}_d = \left\{ \boldsymbol{x} \in \mathbb{R}^{n_x} \;\middle|\; \begin{aligned} \|\mathbf{a}\| &\leq \mathrm{a}_{\max} \\ |\kappa| &\leq \kappa_{\max} \\ |\delta| &\leq \delta_{\max} \end{aligned} \right. \tag{3.40}$$

The constraints acting on the input of the dynamic model are collected in the set of input constraints $\mathcal{U}$. For the single-track model, see Section 2.6, the brake jerk $\dot{a}_x$ and the steering angular rate $\dot{\delta}$ are collected in the set of input constraints:

$$\mathcal{U} = \left\{ \boldsymbol{u} \in \mathbb{R}^{n_u} \;\middle|\; \begin{aligned} |\dot{a}_x| &\leq \dot{\mathrm{a}}_{x,\max} \\ |\dot{\delta}| &\leq \dot{\delta}_{\max} \end{aligned} \right. \tag{3.41}$$

For a general dynamic model with no specific actuator interface, the steering angular rate is substituted by the lateral jerk. The substituted set of input constraints yields:

$$\mathcal{U}_s = \left\{ \boldsymbol{u} \in \mathbb{R}^{n_u} \;\middle|\; \begin{array}{ll} |\dot{a}_x| & \leq \dot{\mathrm{a}}_{x,\max} \\ |\dot{a}_y| & \leq \dot{\mathrm{a}}_{y,\max} \end{array} \right. \tag{3.42}$$

3.5.3 Final conditions

The final or end conditions shall specify the characteristics of the trajectory at the end of the maneuver. One objective of the final condition is to reduce the risk of a road departure as a consequence of the evasive maneuver. In this context, the final condition supports the geometric constraint, Eq. (3.33), which prevents the ego-vehicle from road departure during the evasive maneuver. Ensuring this requirement, the ego-vehicle should be oriented parallel to the road. After the critical situation is successfully avoided, the ego-vehicle is intended to return into a safe state. The safe state shall be ensured by constraining the slip angle to zero.

These final conditions are formulated as equality constraints. To orientate the ego-vehicle parallel to the road at the end of the evasive maneuver yields

$$\psi(\mathrm{H}|k) - \frac{\partial}{\partial x} d_j(k) = 0 \tag{3.43}$$

with the predicted ego-vehicle orientation at the end of the evasive trajectory $\psi(\mathrm{H}|k)$ and the current orientation of the road $\frac{\partial}{\partial x} d_j(k)$ according to Eq. (3.29).

To ensure that the vehicle reaches a safe state at the end of the evasive maneuver, the final condition for the slip angle $\beta(\mathrm{H}|k)$ is given by

$$\beta(\mathrm{H}|k) = 0 \tag{3.44}$$

The final conditions are collected in the set of constraints:

$$\mathcal{X}_f = \left\{ \boldsymbol{x} \in \mathbb{R}^{n_x} \;\middle|\; \begin{aligned} \beta(\mathrm{H}|k) &= 0 \\ \psi(\mathrm{H}|k) - \tfrac{\partial}{\partial x} d_j(k) &= 0 \end{aligned} \right. \tag{3.45}$$

The definition of the final condition completes the set of constraints necessary for the planning of collision avoidance trajectories. The set of state constraints is defined with the set of geometric constraints, the set of dynamic constraints, and the set of final conditions. It is given by

$$\mathcal{X} = \mathcal{X}_g \cap \mathcal{X}_d \cap \mathcal{X}_f \tag{3.46}$$

4 Optimal Trajectory Planning Approaches

Three specific trajectory planning approaches for optimal collision avoidance trajectories are introduced which all build upon the optimal trajectory planning concept discussed in Chapter 3. The first approach considers the integration of a dynamic vehicle model into optimal trajectory planning. It shall provide theoretical insights to trajectory planning for collision avoidance with one critical dynamic obstacle on urban roads. Furthermore, it shall serve as a benchmark for the subsequent approaches. The second approach proposes a parametric trajectory planning concept for collision avoidance trajectories. The third approach augments the second one by a heuristic sampling method to satisfy the required real-time demands for trajectory planning. The goal is to facilitate a fast trajectory planning that enables an implementation into a prototype Electronic Control Unit (ECU). This approach shall be implemented into an Advanced Driver Assistance System (ADAS) for collision avoidance and assessed in an vehicle test regarding benefit and practicability.

4.1 Model-based approach

This section covers the integration of a dynamic vehicle model into an optimal trajectory planning approach. Definition 3.1 provides the definition of optimal trajectory planning for collision avoidance comprising of functional f as constraint. The set of constraints was previously defined in Section 3.5. Functional f is considered as an arbitrary discretized functional,

which shall mimic the vehicle dynamics. To further specify this functional, the discretized single-track model, as given in Section 2.6, is considered for the proposed approach. This optimal trajectory planning approach shall be further referred to as Single-Track Model Trajectory Planner (ST-Planner).

Trajectory representation

With the functional $\boldsymbol{f}$ being defined as single-track model according to Eq. (2.15), the trajectory and its structure can be specified for the ST-Planner. The state vector of the single-track model Eq. (2.15) is

$$\boldsymbol{x} = [s_x, s_y, v_x, v_y, a_x, a_y, \psi, \dot{\psi}, \beta, \delta]^{\mathsf{T}} \tag{4.1}$$

with the trajectory states longitudinal and lateral position, s_x and s_y, longitudinal and lateral velocity v_x and v_y, and longitudinal and lateral acceleration, a_x and a_y. Further, ψ and $\dot{\psi}$ are yaw angle and yaw angle rate, β is the slip angle and δ is the steering angle, acting on the vehicle's front wheel.

The excitation vector of the single-track model is

$$\boldsymbol{u} = [\dot{a}_x, \dot{\delta}]^{\mathsf{T}} \tag{4.2}$$

with the longitudinal jerk $\dot{a}_x$ and the steering angle rate $\dot{\delta}$. The general augmented trajectory $\boldsymbol{z}(k)$ is defined according to Eq. (3.12), which comprises of trajectory $\boldsymbol{T}(k)$ (see Eq. (3.10)) and parameter vector $\boldsymbol{p}(k)$ (see Eq. (3.11)). With the excitation vector $\boldsymbol{u}$, the augmented trajectory $\boldsymbol{z}(k)$ for the ST-Planner yields

$$\boldsymbol{z}(k) = [\dot{a}_x(0|k) \dots \dot{a}_x(\mathrm{H}|k), \dot{\delta}(0|k) \dots \dot{\delta}(\mathrm{H}|k), t_{\mathrm{TLME}}, t_{\mathrm{P}}, t_{\mathrm{F}}]. \tag{4.3}$$

Consideration of the derivatives of the longitudinal acceleration and the steering angle rate results in smooth trajectories with continuous accelera-

tion and steering angle. Moreover, it enables continuity at trajectory start and trajectory end.

Applying the sequence of the excitation vector $\boldsymbol{u}(i|k)$ and the sequence of sampling rates $\Delta\boldsymbol{t}(i|k)$ to the recursive single-track functional $\boldsymbol{f}$ yields the state vector sequence:

$$\boldsymbol{x}(k) = [\boldsymbol{x}(0|k) \dots \boldsymbol{x}(\mathrm{H}|k)] \qquad \mathbb{R}^{n_{\boldsymbol{x}}} \times I \to \mathbb{R}^{n_{\mathrm{T}}}. \tag{4.4}$$

Substituting the arbitrary dynamic model $\boldsymbol{f}$ by the single-track model and the previously defined augmented trajectory $\boldsymbol{z}(k)$ in the nonlinear optimization problem, defined by Eq. (3.2), provides a holistic description of the ST-Planner. The trajectories planned by the ST-Planner will be analyzed in the next chapter and provide theoretical insights into trajectory planning for collision avoidance with single obstacles on urban roads.

4.2 Parametric trajectory planning approach

This section focuses on a suitable parameterization for collision avoidance trajectories. The previously introduced ST-Planner considers a single-track model to evaluate trajectories, which are generated applying the sequence of sampling rates $\Delta\boldsymbol{t}(i|k)$, the optimized excitation vector $\boldsymbol{u}(i|k)$, and the state vector $\boldsymbol{x}(i|k)$ to the dynamic model $\boldsymbol{f}$, and iteratively evaluated for the future trajectory sample $\boldsymbol{x}(i+1|k)$. The consideration of the single-track model provides trajectories that satisfy the dynamic integrity. A drawback of forward integration of dynamic models is the computational complexity. For each sample i, the nonlinear model has to be evaluated and the optimal sequence of excitation vectors has to be sought. Suitable parametric trajectories, which satisfy the dynamic integrity, reduce the computational complexity. However, this approximations might reduces the set of coverable use cases and lead to lower accuracy. Trajectories in various parameteri-

zations are widely discussed in literature. Common parameterizations are splines or polynomials. In [47], curvature polynomials of arbitrary degree are considered. Polynomials of degree 7 are considered in [35] for evasive trajectories. Quintic polynomials are common parametric trajectories (e.g. [77, 69]). In [75], polynomials of degree 5 are separately planned for lateral and longitudinal trajectories.

The latter approach is adopted in this work. Splitting up the trajectory into its motion components provides flexibility to the design, e.g, by allowing different polynomial degrees for lateral and longitudinal motion. Moreover, it enables a direct integration of actuator-specific properties into the trajectories. Incorporating the coupled vehicle dynamics, the vehicle curvature as a function of the lateral and longitudinal motion is considered as constraint. This approach will be referred to as Polynomial Trajectory Planner (P-Planner) in this work.

Polynomial Trajectory Planner

In this section, the general P-Planner is discussed. Parametric trajectories are defined as polynomials of arbitrary degree. Thereafter, a suitable polynomial degree for collision avoidance trajectories is determined. Finally, polynomial trajectories for lateral and longitudinal motion are integrated into the optimal trajectory planning, yielding the P-Planner.

Polynomial trajectories of arbitrary degree are defined as

Definition 4.1. Let $k \in \mathbb{N}$ be a discrete time, representing an arbitrary starting point of the trajectory, $\mathrm{L} \in \mathbb{N}$ be an arbitrary degree of a polynomial function. Let $i \in I$ with $I = [0 \dots \mathrm{H}] \subset \mathbb{N}$ be an equidistantly sampled sequence of H samples, $\boldsymbol{t}(i|k) \in \mathbb{R}$ be a sequence of time samples, and $\tilde{p}_j(k) \in \mathbb{R}$ with $j = 0, \dots, \mathrm{L}$ be the j^{th} polynomial coefficient. Further, let $\zeta(i|k)^{(q)}$ be the q^{th} derivative of the i^{th} polynomial trajec-

tory sample. The polynomial coefficients are collected in the parameter vector

$$\tilde{\boldsymbol{p}}_{\mathrm{L}}(k) = [\tilde{p}_j(k)]^{\mathsf{T}}, \quad j = 0, \ldots, \mathrm{L}. \tag{4.5}$$

Trajectories and the corresponding derivatives are defined according to the polynomial function, yielding

$$\begin{aligned}\zeta(i|k)^{(q)} = \boldsymbol{f}_{\zeta}^{(q)}(\tilde{\boldsymbol{p}}_{\mathrm{L}}(k), \boldsymbol{t}(i|k)) := \\ \sum_{j=q}^{\mathrm{L}} \prod_{p=0}^{q} (j-p)\tilde{p}_j(k)\boldsymbol{t}(i|k)^{(j-q)}, \; q = 0, \ldots, \mathrm{L}\end{aligned} \tag{4.6}$$

with the arbitrary polynomial function $\boldsymbol{f}_{\zeta}^{(q)}$ of the q^{th} derivative. With Eq. (4.6), the polynomial trajectory according to Definition 2.1 yields

$$\boldsymbol{T}_p = [\zeta(0|k)^{(q)}, \ldots, \zeta(\mathrm{N}|k)^{(q)}]. \tag{4.7}$$

The polynomial coefficients $\tilde{\boldsymbol{p}}_{\mathrm{L}}(k)$ are obtained by applying boundary conditions to Eq. (4.6) and determining the polynomial coefficients $\tilde{p}_j(k)$. For an a priori known temporal sequence $\boldsymbol{t}(i|k)$, there exists a closed solution for the applied boundary conditions problem.

In order to determine a suitable polynomial degree for the collision avoidance trajectory planner, the following requirements need to be considered. Trajectories shall be smooth and several times differentiable. To obtain polynomial trajectories that satisfy the requirements, the boundary value problem needs to be solved. Boundary conditions are given as initial and final values of the polynomial and its derivatives. The number of boundary conditions specifies the degree of the polynomial. Polynomials of degree 5, for example, are commonly used for trajectory planning. They are defined by six boundary conditions (position, velocity, and acceleration), three ini-

tial and three final values, respectively. However, polynomials of degree 5 are discontinuous in jerk at start and end [8]. In order to obtain trajectories with continuous jerk, besides boundary conditions on acceleration, velocity and position, it is also required to assign initial and final conditions to the jerk. Therefore, in overall eight boundary conditions need to be considered (four initial and four final), a seventh degree polynomial shall be applied.

Polynomial trajectories of degree 5 and 7 shall be compared briefly. boundary conditions for a characteristic collision avoidance trajectory are considered. The initial conditions for the polynomial trajectories of degree 5 and 7, with $t_0 = 0$ and $t_\mathrm{f} = 2$, are $s_x(t_0) = 0$, $v_x(t_0) = 10$, $a_x(t_0) = 0$, for the longitudinal trajectory and $s_y(t_0) = 0$, $v_y(t_0) = 0$, $a_y(t_0) = 0$, for the lateral trajectory. The final conditions are $s_x(t_\mathrm{F}) = 0$, $v_x(t_\mathrm{F}) = 5$, and $a_x(t_\mathrm{F}) = 0$, for the longitudinal trajectory and $s_y(t_\mathrm{F}) = 2$, $v_y(t_\mathrm{F}) = 0$, and $a_y(t_\mathrm{F}) = 0$, for the lateral trajectory. Additionally, for the polynomial trajectories of degree 7, the initial and final conditions for the longitudinal and lateral jerk are $\dot{a}_x(t_0) = 0$, $\dot{a}_y(t_0) = 0$, $\dot{a}_x(t_\mathrm{F}) = 0$, and $\dot{a}_y(t_\mathrm{F}) = 0$, respectively.

Fig. 4.1 shows the comparison of polynomial trajectories of degree 5 and 7. Jerk trajectories are shown in the bottom row. Polynomials of degree 5 show the discontinuity, whereas polynomials of degree 7 are continuous in jerk. Polynomials of degree 7 provide trajectories with a lower absolute jerk compared to degree 5, even though polynomials of degree 5 have minimal squared jerk [75]. However, with respect to the acceleration, degree 7 trajectories lead to higher absolute accelerations, both lateral and longitudinal, to achieve equivalent end positions. In the x-y plane the trajectories appear to be considerably similar. For equivalent boundary conditions, polynomial of degree 5 seems more reactive than polynomial of degree 7. Achieving comparable absolute acceleration levels to the degree 7, degree 5 would need less time to achieve that level. However, this reactive character of degree 5

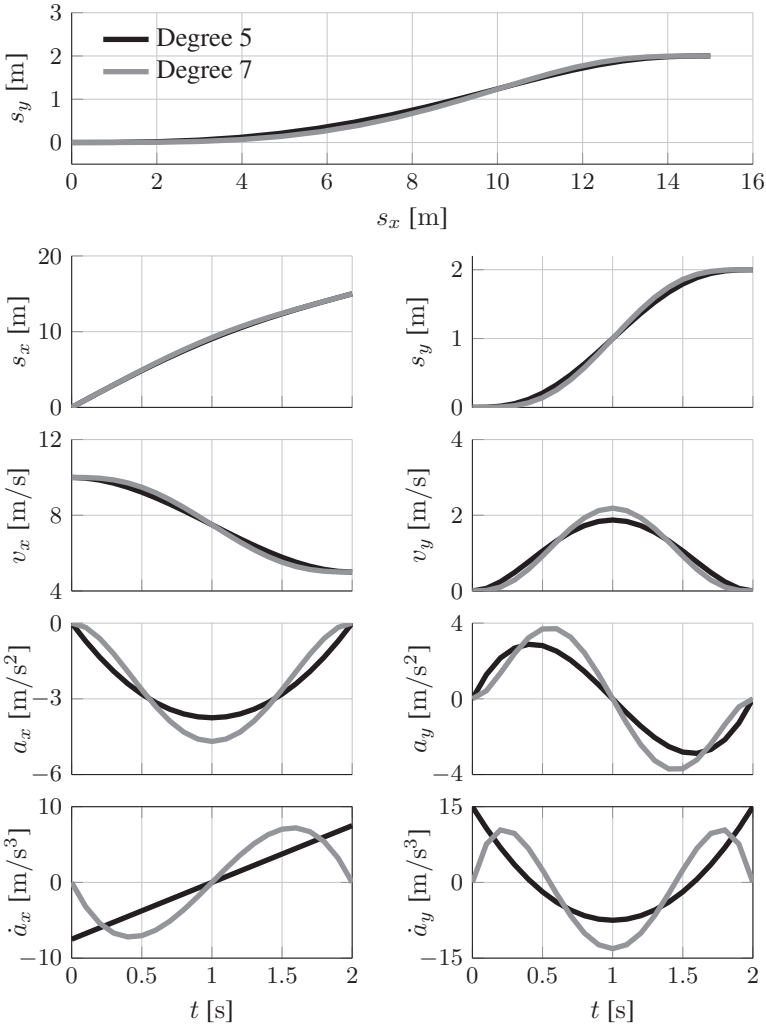

Figure 4.1: Comparison of polynomial trajectories of degree 5 and 7. The upper plot shows the trajectories in the x-y plane. The left column shows the longitudinal trajectories (from top to bottom): position, velocity, acceleration, and jerk. The right column shows the lateral trajectories, respectively.

comes at the cost of the discontinuities at start and end. Disregarding the ramp-up and down of the jerk leads to the diminished absolute acceleration and the comparable lower maneuver time if trajectories with equivalent acceleration profiles are compared.

Polynomials of degree 7 shall be considered for the planning of braking and steering trajectories. It enables direct incorporation of actuator-specific limitations. Steering jerk is equivalent to the torque rate of the power steering motor. Brake jerk is equivalent to the pressure build-up in the hydraulic system of the brake.

Optimal parametric collision avoidance trajectories are obtained applying an additional set of parameters and substituting the dynamic model in Eq. (3.2). In the next step, optimal polynomial collision avoidance trajectories shall be defined.

Definition 4.2. Let $k \in \mathbb{N}$ be a discrete time, representing an arbitrary starting point of the trajectory. Let $i \in I$ with $I = [0 \dots \mathrm{H}] \subset \mathbb{N}$ be a sampled sequence of H samples. Further, let $\boldsymbol{x}(i|k) \in \mathbb{R}^{n_x}$ be a state vector, $\boldsymbol{u}(i|k) \in \mathbb{R}^{n_u}$ an excitation vector, and $\boldsymbol{t}(i|k) \in \mathbb{R}$ a sequence of time samples. Let

$$\begin{aligned} \tilde{\boldsymbol{p}}_7^x(k) &= [\tilde{\boldsymbol{x}}_0(k), \tilde{\boldsymbol{q}}_7^x(k)] \quad \text{and} \\ \tilde{\boldsymbol{p}}_7^y(k) &= [\tilde{\boldsymbol{y}}_0(k), \tilde{\boldsymbol{q}}_7^y(k)] \end{aligned} \tag{4.8}$$

be the coefficient vector of longitudinal and lateral polynomial trajectory of degree 7. Where $\tilde{\boldsymbol{x}}_0(k)$ and $\tilde{\boldsymbol{y}}_0(k)$ are the initial values of the the longitudinal and lateral polynomials with

$$\begin{aligned} \tilde{\boldsymbol{x}}_0(k) &= [s_x(0|k), v_x(0|k), a_x(0|k), \dot{a}_x(0|k)] \quad \text{and} \\ \tilde{\boldsymbol{y}}_0(k) &= [s_y(0|k), v_y(0|k), a_y(0|k), \dot{a}_y(0|k)] \end{aligned} \tag{4.9}$$

$\tilde{\boldsymbol{q}}_7^x(k)$ and $\tilde{\boldsymbol{q}}_7^y(k)$ comprise the polynomial coefficients to be determined of the longitudinal and lateral polynomials which are

$$\begin{aligned}\tilde{\boldsymbol{q}}_7^x(k) &= [\tilde{p}_4^x(k), \tilde{p}_5^x(k), \tilde{p}_6^x(k), \tilde{p}_7^x(k)] \quad \text{and} \\ \tilde{\boldsymbol{q}}_7^y(k) &= [\tilde{p}_4^y(k), \tilde{p}_5^y(k), \tilde{p}_6^y(k), \tilde{p}_7^y(k)].\end{aligned} \tag{4.10}$$

Further, let $\tilde{\boldsymbol{z}}(k)$ be an augmented parameterized trajectory with

$$\tilde{\boldsymbol{z}}(k) = [\tilde{\boldsymbol{q}}_7^x(k), \tilde{\boldsymbol{q}}_7^y(k), \boldsymbol{p}(k)] \quad \mathbb{R}^{n_{q^x}} \times \mathbb{R}^{n_{q^y}} \times \mathbb{R}^{n_p} \to \mathbb{R}^{n_z} \tag{4.11}$$

where $\boldsymbol{p}(k) \in \mathbb{R}^{n_p}$ is the parameter vector according to Eq. (3.11). The arbitrary dynamic model, represented by the functional $\boldsymbol{f}$, is substituted by the polynomial trajectory description which is defined accordingly.

$$\underbrace{\begin{bmatrix} s_x \\ s_y \\ v_x \\ v_y \\ a_x \\ a_y \\ \psi \\ \kappa \end{bmatrix}}_{\boldsymbol{x}} (i|k) = \underbrace{\begin{bmatrix} \boldsymbol{f}_x^{(0)}(\tilde{\boldsymbol{p}}_7^x(k), \boldsymbol{t}(i|k)) \\ \boldsymbol{f}_y^{(0)}(\tilde{\boldsymbol{p}}_7^y(k), \boldsymbol{t}(i|k)) \\ \boldsymbol{f}_x^{(1)}(\tilde{\boldsymbol{p}}_7^x(k), \boldsymbol{t}(i|k)) \\ \boldsymbol{f}_y^{(1)}(\tilde{\boldsymbol{p}}_7^y(k), \boldsymbol{t}(i|k)) \\ \boldsymbol{f}_x^{(2)}(\tilde{\boldsymbol{p}}_7^x(k), \boldsymbol{t}(i|k)) \\ \boldsymbol{f}_y^{(2)}(\tilde{\boldsymbol{p}}_7^y(k), \boldsymbol{t}(i|k)) \\ \tan^{-1}\left(\frac{v_y(i|k)}{v_x(i|k)}\right) \\ \frac{v_x(i|k)a_y(i|k) - v_y(i|k)a_x(i|k)}{(v_x(i|k)^2 + v_y(i|k)^2)^{\frac{3}{2}}} \end{bmatrix}}_{\boldsymbol{f}_{\boldsymbol{x}}(\tilde{\boldsymbol{p}}_7(k), \boldsymbol{t}(i|k))} \tag{4.12}$$

with the state vector $\boldsymbol{x}$ and the functional $\boldsymbol{f_x}(\tilde{\boldsymbol{p}}_7(k), \boldsymbol{t}(i|k))$ defining the parametric trajectories. The excitation vector $\boldsymbol{u}$ is defined according to the parametric functional $\boldsymbol{f_u}(\tilde{\boldsymbol{p}}_7(k), \boldsymbol{t}(i|k))$

$$\underbrace{\begin{bmatrix} \dot{a}_x \\ \dot{a}_y \end{bmatrix}}_{\boldsymbol{u}}(i|k) = \underbrace{\begin{bmatrix} \boldsymbol{f}_x^{(3)}(\tilde{\boldsymbol{p}}_7^x(k), \boldsymbol{t}(i|k)) \\ \boldsymbol{f}_y^{(3)}(\tilde{\boldsymbol{p}}_7^y(k), \boldsymbol{t}(i|k)) \end{bmatrix}}_{\boldsymbol{f_u}(\tilde{\boldsymbol{p}}_7(k), \boldsymbol{t}(i|k))} \tag{4.13}$$

With these considerations, the P-Planner can be defined as

$$\begin{aligned} &\min_{\tilde{\boldsymbol{z}}} \boldsymbol{J}(\tilde{\boldsymbol{z}}(k)) \\ &\text{subject to} \quad \boldsymbol{x}(i|k) = \boldsymbol{f_x}(\tilde{\boldsymbol{p}}(k), \boldsymbol{t}(i|k)) \\ &\qquad\qquad \boldsymbol{u}(i|k) = \boldsymbol{f_u}(\tilde{\boldsymbol{p}}(k), \boldsymbol{t}(i|k)) \\ &\qquad\qquad \boldsymbol{x}(i|k) \in \mathcal{X} \subset \mathbb{R}^{n_x} \\ &\qquad\qquad \boldsymbol{u}(i|k) \in \mathcal{U} \subset \mathbb{R}^{n_u} \\ &\qquad\qquad \boldsymbol{x}(0|k) = \boldsymbol{x}(k) \\ &\qquad\qquad \forall i \in I \end{aligned} \tag{4.14}$$

with cost function $\boldsymbol{J} : \mathbb{R}^{n_z} \rightarrow \mathbb{R}$ and the sets of constraints $\mathcal{X}$ and $\mathcal{U}$ that are defined in Section 3.5.

The maneuver duration for a collision avoidance trajectory cannot be determined a-priori due to the wide variation of possible scenarios. Consequently, for each situation, an optimal maneuver duration is individually evaluated for each trajectory. As a result, it is required to determine the polynomial coefficients within the optimization process. The computational complexity of the optimization problem correlates with the dimensionality of the augmented trajectory $\boldsymbol{z}$ which is to be sought. Substituting the sampling-based trajectory representation, as considered in the ST-Planner

(Section 4.1), with the polynomial trajectories of degree 7 diminishes the dimensionality from $\dim(\boldsymbol{z}) = (2 \times \mathrm{H} + 3)$ to $\dim(\tilde{\boldsymbol{z}}) = (2 \times 4 + 3)$, where H is typically ≥ 20.

Considering polynomials of degree 7 as collision avoidance trajectory correlates with the expense of two times four polynomial coefficients that need to be sought. For a practical application and implementation, the longitudinal trajectory is considered as polynomial of degree 5. Reducing the polynomial degree from 7 to 5 diminishes the computational costs in additions. The necessary polynomial coefficients to be sought diminishes to two for the longitudinal trajectory, which leads to a dimensionality of $\dim(\tilde{\boldsymbol{z}}) = (4{+}2{+}3)$.

Regarding polynomial of degree 5, the parametric vector for the longitudinal trajectory becomes

$$\tilde{\boldsymbol{p}}_5^x(k) = [\tilde{\boldsymbol{x}}_0(k), \tilde{\boldsymbol{q}}_5^x(k)] \tag{4.15}$$

with

$$\begin{aligned} \tilde{\boldsymbol{x}}_0(k) &= [s_x(0|k), v_x(0|k), a_x(0|k)] \quad \text{and} \\ \tilde{\boldsymbol{q}}_5^x(k) &= [\tilde{p}_3^x(k), \tilde{p}_4^x(k), \tilde{p}_5^x(k)]. \end{aligned} \tag{4.16}$$

The parameter vector is handled analog to polynomials of degree 7 within the P-Planner.

4.3 Fast parametric trajectory planning approach

Integration of optimal trajectory planning in an ADAS for collision avoidance is a nontrivial task. Challenges arise when a nonlinear optimization problem has to be solved in real-time. Especially when the ADAS shall

be utilized on a production-type ECU with limited resources, e.g. limited computational power. Meeting real-time requirements can be approached from two sides. Either the optimization algorithm can be adapted to the optimization problem and to the target hardware. Or the problem formulation can be modified to meet real-time requirements. This work will focus on a solution that modifies the previously trajectory planning approaches to meet the real-time requirements.

The previous section covered parametric trajectories for collision avoidance. Polynomials of degree 5 and 7 are considered to parameterize the trajectories in longitudinal and lateral direction, respectively. This approach already reduced the search space of the ST-Planner from $\dim(\boldsymbol{z}) = (2 \times \mathrm{H} + 3)$ to $\dim(\tilde{\boldsymbol{z}}) = (2 \times 4 + 3)$ for the P-Planner.

A further reduction of computational complexity is achieved by considering the trajectory's sequence which is sampled by i samples. ST-Planner and P-Planner successively evaluate all constraints for the entire sampling interval, which leads to a set of nonlinear equations of dimension $\dim(\mathcal{X} + \mathcal{U}) \times \dim(I)$ to be solved, with $I = [0 \ldots \mathrm{H}] \subset \mathbb{N}$ being the sampled sequence of H samples. In order to reduce the number of required samples, a heuristic sampling approach is introduced in the next section that substitutes the equidistantly sampled time sequence $\boldsymbol{t}(k)$ of H samples in the P-Planner. This will yield to a real-time capable trajectory planner for collision avoidance which is further referred to reduced Polynomial Trajectory Planner (rP-Planner)

4.3.1 Heuristic trajectory sampling

Obtaining the relevant temporal points that are required to plan collision avoidance trajectories, symmetric properties of the polynomial trajectories are considered (Fig. 4.2). The boundary conditions are analog to those

of Section 4.2, which leads to symmetric trajectories. The left column of Fig. 4.2 shows the longitudinal polynomial trajectories of degree 5 with its motion components (position, velocity, acceleration, jerk). The right column shows the lateral polynomial trajectories of degree 7 with its motion components (position, velocity, acceleration, jerk). The relevant sampling points can be expressed in fractions of the trajectory duration t_F. With

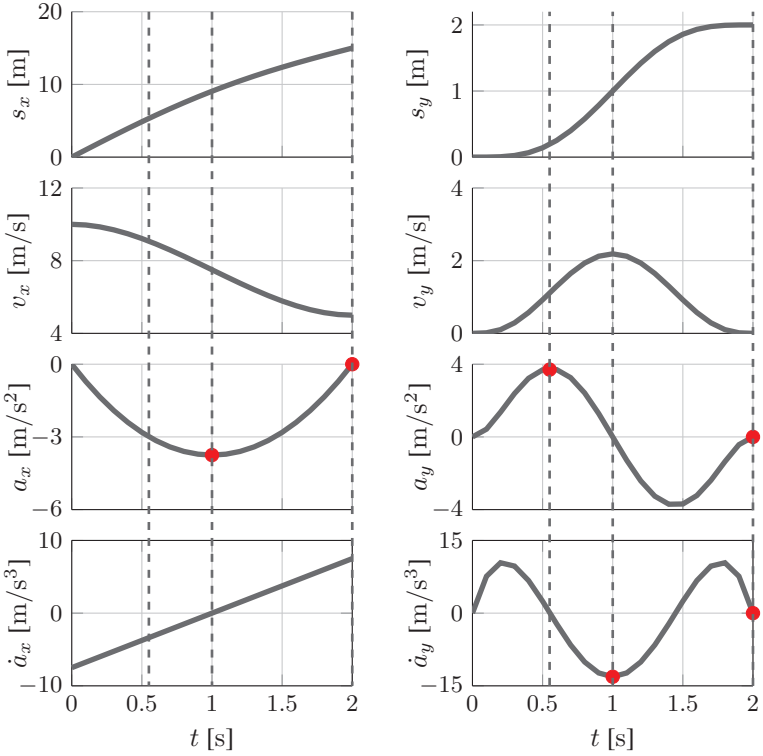

Figure 4.2: Characteristic sample points for symmetric collision avoidance trajectories. The left column shows the longitudinal polynomial trajectories of degree 5 (from top to bottom): position, velocity, acceleration, jerk. The right column shows analog the lateral polynomial trajectories of degree 7.

respect to longitudinal acceleration, one relevant point is the minimum of acceleration which is at $t = 0.5 \cdot t_\mathrm{F}$. This point is vital to determine the absolute minimum or maximum lateral jerk for evasive maneuvers to the left or to the right, respectively. The next relevant point is the maximum lateral acceleration. This point is obtained by finding the roots of the lateral jerk leading to $t = -\frac{\sqrt{5}-5}{10} \cdot t_\mathrm{F}$.

With these points and the passing time t_P(see Section 3.3), the reduced time sequence is specified as

$$\tilde{\boldsymbol{t}}(k) = [0, -\tfrac{\sqrt{5}-5}{10} \cdot t_\mathrm{F}, 0.5 \cdot t_\mathrm{F}, t_\mathrm{P}, t_\mathrm{F}]. \tag{4.17}$$

Substituting the equidistantly sampled time sequence $\boldsymbol{t}(k)$ in the P-Planner leads to the rP-Planner which is defined accordingly.

Definition 4.3. Let $k \in \mathbb{N}$ be a discrete time, representing an arbitrary starting point of the trajectory. Let $r \in I_\mathrm{r}$ with $I_\mathrm{r} = [0 \dots 4] \subset \mathbb{N}$ be a sampled sequence of 4 samples. Further, let $\boldsymbol{x}(r|k) \in \mathbb{R}^{n_x}$ be a state vector, $\boldsymbol{u}(r|k) \in \mathbb{R}^{n_u}$ an excitation vector, and $\tilde{\boldsymbol{t}}(r|k) \in \mathbb{R}$ a sequence of time samples. The rP-Planner is

$$\begin{aligned}
&\min_{\tilde{\boldsymbol{z}}} \boldsymbol{J}(\tilde{\boldsymbol{z}}(k)) \\
&\text{subject to} \quad \boldsymbol{x}(r|k) = \boldsymbol{f}_{\boldsymbol{x}}(\tilde{\boldsymbol{p}}(k), \tilde{\boldsymbol{t}}(r|k)) \\
&\qquad\qquad \boldsymbol{u}(r|k) = \boldsymbol{f}_{\boldsymbol{u}}(\tilde{\boldsymbol{p}}(k), \tilde{\boldsymbol{t}}(r|k)) \\
&\qquad\qquad \boldsymbol{x}(r|k) \in \mathcal{X} \subset \mathbb{R}^{n_x} \\
&\qquad\qquad \boldsymbol{u}(r|k) \in \mathcal{U} \subset \mathbb{R}^{n_u} \\
&\qquad\qquad \boldsymbol{x}(0|k) = \boldsymbol{x}(k) \\
&\qquad\qquad \forall r \in I_\mathrm{r}
\end{aligned} \tag{4.18}$$

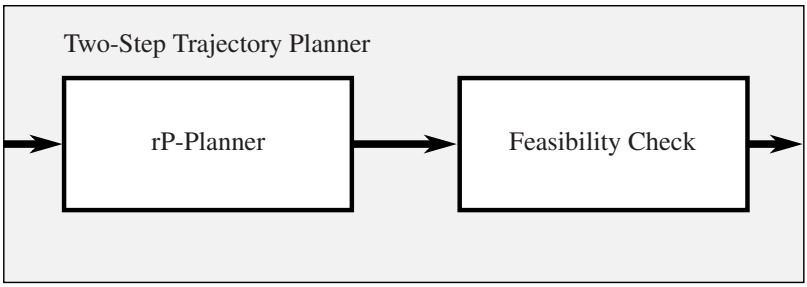

Figure 4.3: Structure of two-step trajectory planning approach comprising the rP-Planner and a feasibility check

with cost function $\boldsymbol{J} : \mathbb{R}^{n_z} \rightarrow \mathbb{R}$ and the sets of constraints $\mathcal{X}$ and $\mathcal{U}$ which are defined in Section 3.5.

Evaluating trajectories with the reduced set of samples enables online trajectory planning with high computational efficiency. However, this also imposes limitations. Assuming symmetric properties of trajectories limits the applicable use cases to straight road scenarios. Furthermore, due to the trajectory evaluation with the reduced set of samples, the solution delivers just the polynomial coefficients. A trajectory that can be used as an input to a controls algorithm needs to be generated in a second step. Trajectories have to be re-evaluated with a sufficiently higher amount of samples leading to a higher temporal resolution. Also, to evaluate the compliance of constraints for only the reduced set has a potential risk of missing constraint violation in between the sparse samples.

4.3.2 Two-step trajectory planning

To overcome the risk of missed constraints violation and to provide trajectories for controls, a tow-step trajectory planning approach is proposed. The structure of the two-step approach is shown in Fig. 4.3 It comprises of the rP-Planner followed by a feasibility check. rP-Planner provides the para-

metric trajectories which are re-evaluated in the feasibility check. First, the trajectories are evaluated for a denser set of samples $i \in I$. These trajectories are then further reviewed for compliance with the constraints. If a violation of any constraint is observed, the time to last maneuver execution, t_{TLME}, is set to a negative value. Otherwise, if the feasibility test passed, the densely sampled trajectories are provided to the vehicle controls system.

4.4 Assessment Criteria

This chapter summarizes relevant assessment criteria to evaluate the performance of the developed approaches, based on assessing the trajectories. Additionally, a catalog of characteristic use cases is introduced that is used to evaluate the performance of the proposed optimal trajectory planning approaches.

4.4.1 Performance measures

Evaluation and assessment of collision avoidance trajectories demands suitable performance measures. Besides the compliance to constraints and limitations, which is relevant for each individual trajectory, an assessment criteria to distinguish between trajectories and evaluate their specific differences is required.

Various performance measures for the comparison of ideal lane change trajectories are presented in [64]. Amongst those, one performance measure is the area between a trajectory and a straight line for one half of a single lane change maneuver. Considering this proposal as a starting point, a more specific performance measure to determine the difference of two trajectories is the area between the trajectories, as shown in Fig. 4.4. The gray area between the two distinct trajectories shows this performance measure. The smaller the area between the trajectories, the smaller the difference of the

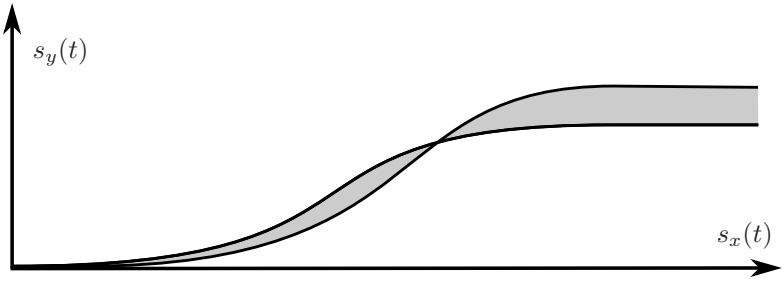

Figure 4.4: Area between two trajectories

trajectories. The performance measure is defined in terms of a relative error yielding

$$A_E = \frac{A - A_\mathrm{c}}{A_\mathrm{c}} \cdot 100\% \tag{4.19}$$

where A is the area of the desired or objective trajectory, A_c is the area of the simulated or compared trajectory, respectively. The area is defined as

$$A = \int_0^\mathrm{T} F\left(\xi_x(t), \xi_y(t)\right) dt \tag{4.20}$$

where F is a parametric trajectory with longitudinal and lateral components, $\xi_x(t)$ and $\xi_y(t)$, respectively. T is the upper limit, e.g., the maneuver duration.

Another useful performance measure is the *Mean-Absolute-Percent-Error* [1] to compare trajectory deviations.

$$\mathrm{MAPE} = \frac{1}{\mathrm{T}} \int_0^\mathrm{T} \left| \frac{y(t) - y_\mathrm{c}(t)}{y_\mathrm{c}(t)} \right| dt \cdot 100\% \tag{4.21}$$

or

$$\mathrm{MAPE} = \frac{1}{\mathrm{T}} \sum_{i=1}^{\mathrm{T}} \left| \frac{y(i) - y_{\mathrm{c}}(i)}{y_{\mathrm{c}}(i)} \right| \cdot 100\% \tag{4.22}$$

as applicable, where y is the desired or objective measure, y_{c} is the simulated or compared measure, T is the upper limit, e.g., the maneuver duration. Normalizing the argument enables the comparison of trajectories with variable properties, e.g. variable maneuver duration t_{F} and final maneuver position $s_x(t_{\mathrm{F}})$ and $s_y(t_{\mathrm{F}})$.

4.4.2 Characteristic use cases

The performance of the developed trajectory planner for collision avoidance trajectories shall be verified by three characteristic use cases.

Use case 1: The topology of the first scenario is illustrated in Fig. 4.5. The gray ego-vehicle follows the blue leading vehicle on a straight two-lane road traveling on the right lane. The road has an unoccupied adjacent lane to the left. Both vehicles, lead and ego-vehicle, are traveling with constant speed up to $70\,\mathrm{km/h}$ while keeping a safety distance within the legally required specifications (§4 S1 StVO). At a certain moment, the lead vehicle evades a suddenly appearing obstacle that blocks the lane while the ego-vehicle is still approaching the suddenly appearing obstacle. Without an intervention, a collision between the ego-vehicle and the obstacle is imminent.

Use case 2: The topology of use case 2 is analog to the first use case, shown in Fig. 4.6. Except, the blue lead-vehicle and the gray ego-vehicle are traveling on the left lane. The right adjacent lane is unoccupied. Here, the lead vehicle evades an obstacle that blocks the left lane.

Use case 3: The topology of the third scenario is illustrated in Fig. 4.7. The gray ego-vehicle is traveling on a one-way road. At a certain moment, a pedestrian steps suddenly out onto the road, out of a row of parked cars on the left pavement. The ego-vehicle approaches the sudden appearing pedestrian and a collision is imminent.

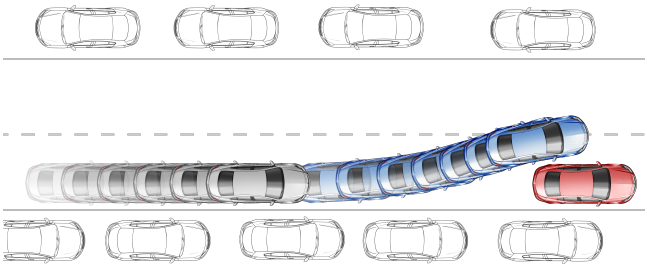

Figure 4.5: Use case 1

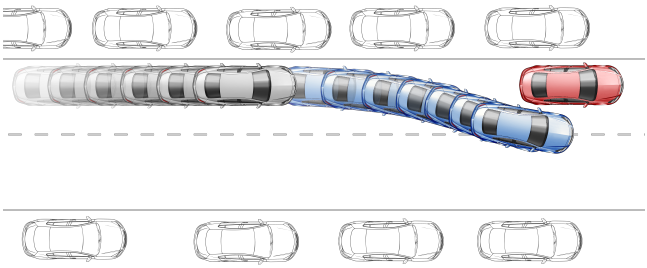

Figure 4.6: Use case 2

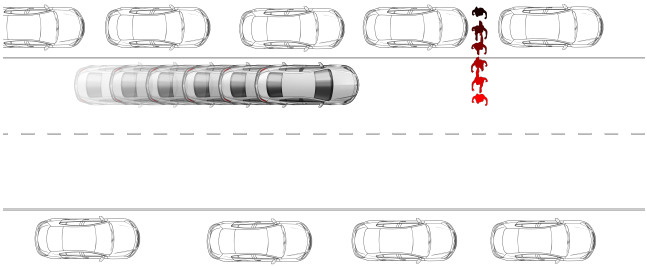

Figure 4.7: Use case 3

5 Simulation results

Optimal trajectory planning approaches discussed in Section 4 are analyzed and compared. Typical urban traffic situations are considered as test scenarios, see Fig. 5.1. The ego-vehicle travels along a straight road, which is bounded on either side, towards a stationary obstacle blocking the ego-vehicle's lane. For the traffic situation, relevant parameters defining the geometry of the scene are shown. In the following sections, the three trajectory planning approaches are evaluated based on simulations. The ST-Planner (Section 4.1) is evaluated first. Thereafter, the ST-Planner is compared with the Polynomial Trajectory Planner (P-Planner) (Section 4.2) and the reduced Polynomial Trajectory Planner (rP-Planner) (Section 4.3).

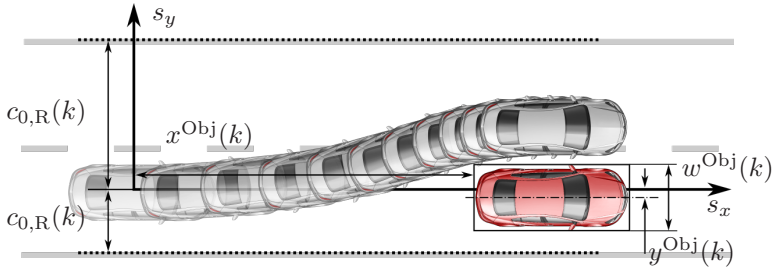

Figure 5.1: Urban traffic situation with evasive maneuver. Relevant scene parameters are left and right margin, $c_{0,\mathrm{L}}(k)$ and $c_{0,\mathrm{R}}(k)$, the obstacle's coordinate relative to the ego-vehicle with the longitudinal distance $x^{\mathrm{Obj}}(k)$, the lateral coordinate $y^{\mathrm{Obj}}(k)$, and the width of the obstacle $w^{\mathrm{Obj}}(k)$.

5.1 Single-Track Model Trajectory Planner

In the following section the ST-Planner (see Section 4.1) is evaluated and verified. The simulation and the subsequent analysis shall verify if the proposed planner provides dynamically feasible trajectories at a latest possible moment.

The ST-Planner is embedded into an Advanced Driver Assistance System (ADAS) for collision avoidance, which will be discussed in detail in Chapter 6.1. An IPG CarMaker® vehicle simulation environment is used to perform the simulations of the ADAS. The simulation environment considers a detailed multi-body vehicle model of an Opel Insignia with emulated steering and braking control unit software. Applying such simulation mod-

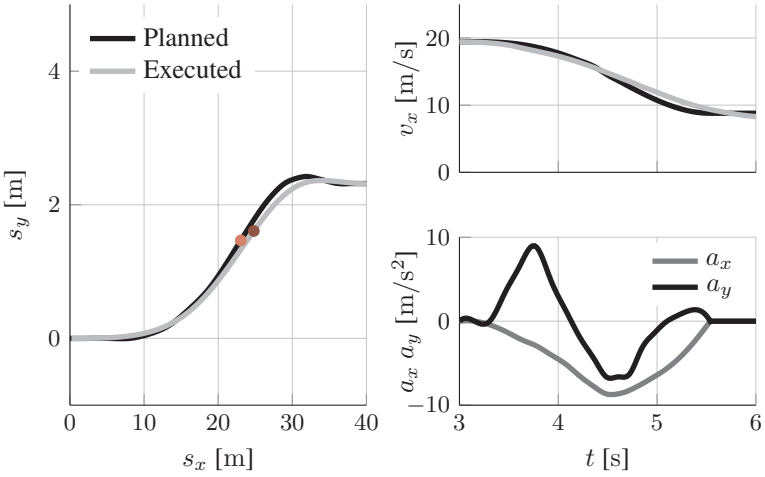

Figure 5.2: Simulated collision avoidance maneuver for $\mathrm{a}_{\max} = 9.81\,\mathrm{m/s^2}$ and $v_x(0|k) = 70\,\mathrm{km/h}$. The left figure shows the planned and executed trajectories in the x-y plane, the upper right shows the velocities over time, the lower right shows the planned lateral and longitudinal acceleration trajectories over time.

Approach	ST-Planner
$x^{\mathrm{Obj}}(k)$ [m]	$v_x(0\|k) \cdot t_{\mathrm{TTC_{ini}}}$
$y^{\mathrm{Obj}}(k)$ [m]	0.0
$w^{\mathrm{Obj}}(k)$ [m]	2.0
$v_x(0\|k)$ [km/h]	[50.0 70.0]
$t_{\mathrm{TTC_{ini}}}$ [s]	2.00
$c_{0,\mathrm{L}}(k)$ [m]	3.75
$c_{0,\mathrm{R}}(k)$ [m]	-1.50

Table 5.1: Scene parameter set evaluating the ST-Planner. The obstacle's coordinate relative to the ego-vehicle with longitudinal distance $x^{\mathrm{Obj}}(k)$, lateral coordinate $y^{\mathrm{Obj}}(k)$, and width of the obstacle $w^{\mathrm{Obj}}(k)$. Variation of initial speed $v_x(0|k)$. First detection time of the obstacle $t_{\mathrm{TTC_{ini}}}$, and left and right lateral margin, $c_{0,\mathrm{L}}(k)$ and $c_{0,\mathrm{R}}(k)$.

els with this complexity and degree of detail shall lead to reliable and robust simulation results. The goal is make the simulation match real vehicle tests as closely as possible (which will be further verified in the next chapter).

An urban traffic situation according to Fig. 5.1 is considered as test scenario. The parameters defining the scene are listed in Table 5.1. The initial ego-vehicle speed $v_x(0|k)$ is assessed in two levels. All trajectory parameters are listed in Table 5.2. To better explore the potential of the algorithm, two different absolute acceleration limits $\mathrm{a_{max}}$ are investigated. Achieving comparable test results, a virtual time for the first detection of an obstacle is assumed in terms of *Time To Collision* (t_{TTC}) which is further considered as $t_{\mathrm{TTC_{ini}}}$. The related longitudinal distance to the obstacle at the first detection event is

$$x^{\mathrm{Obj}}(k) = v_x(0|k) \cdot t_{\mathrm{TTC_{ini}}}. \tag{5.1}$$

Approach	ST-Planner
$\mathrm{a}_{\max}$ $[\mathrm{m/s^2}]$	[7.0 9.81]
$\kappa_{\max}$ $[1/\mathrm{m}]$	0.04
$\dot{a}_{x,\max}$ $[\mathrm{m/s^3}]$	20.00
$\dot{\delta}_{\max}$ $[^\circ/\mathrm{s}]$	9.00
$\mathrm{N+M}$	$20+20$

Table 5.2: Trajectory parameter set of ST-Planner. Variation of absolute acceleration limit $\mathrm{a}_{\max}$, limits for curvature $\kappa_{\max}$, longitudinal jerk $\dot{a}_{y,\max}$ and the steering rate $\dot{\delta}_{\max}$. $\mathrm{N+M}$ are the samples of the trajectory.

The simulation runs are performed on a personal computer with an Intel® core i5 processor. The trajectory planning approaches are implemented in Matlab® using the internal function *fmincon* with the solver option *Active-set* as provided by the optimization toolbox [70] to solve the optimization problem. *fmincon* uses the method of Sequential Quadratic Program to solve the nonlinear problem, whereas the Quadratic Program is solved iteratively. The Quadratic Program (QP) subproblem is solved using the active-set strategy. A detailed description of the solver principles are covered by the literature (see e.g. [21, 7, 10, 3]).

An example of the planned and executed trajectories is shown in Fig. 5.2 for the parameter set $\mathrm{a}_{\max} = 9.81\,\mathrm{m/s^2}$ and $v_x(0|k) = 70\,\mathrm{km/h}$. The left figure shows planned and executed trajectories in the x-y plane. The upper right figure shows planned and executed trajectories of the velocity and the lower right figure shows planned lateral and longitudinal acceleration trajectories over time. Both, x-y plane and velocity reveal little difference between the compared trajectories.

The simulation results are collected in Table 5.3, listing the time to last maneuver execution t_{TLME}, the passing time t_{P} and the maneuver duration

Approach	ST-Planner
$\bar{t}_{\mathrm{TLME}}$ [s]	0.69
$\bar{t}_{\mathrm{P}}$ [s]	1.30
$\bar{t}_{\mathrm{F}}$ [s]	2.35

Table 5.3: Simulation result of trajectories obtained by the ST-Planner with mean values of time to last maneuver execution $\bar{t}_{\mathrm{TLME}}$, passing time $\bar{t}_{\mathrm{P}}$ and maneuver duration $\bar{t}_{\mathrm{F}}$.

t_{F} for the four scenarios. The results of the data analysis are listed in Table 5.4 with the performance measure MAPE (see Section 4.4.1) for the area difference between the two trajectories. In addition, the MAPE for the deviations of longitudinal, lateral, and velocity trajectories can be retrieved. The planned and executed trajectories differ by less than $3\,\%$. The mean values of the lateral deviation ($2.02\,\%$) is smaller than the longitudinal deviation ($2.76\,\%$). Measured in terms of covered distance ($40\,\mathrm{m}$ in longitudinal direction and $2.30\,\mathrm{m}$ in lateral direction), the slightly higher deviation in longitudinal direction seems tolerable. The velocity has a deviation of $0.49\,\%$.

These simulations of characteristic scenarios show that the chosen concept and the implemented algorithm fulfill the described requirements for evasive trajectories. ST-Planner shows the potential of the presented optimal trajectories for collision avoidance to find last possible evasive maneuvers. The simulative evaluation of the ADAS shows good trajectory tracking performance. An overall deviation of less than 3 percent between planned and executed trajectories is achieved, even when the utilized maximum acceleration is close to the limit. The low tracking deviation corroborates the approach to provide dynamically feasible trajectories. This implies that the assumed limitations in scale and function are chosen appropriately for the given problem.The test was performed without the consideration of addi-

MAPE(Area) [%]	2.66
MAPE(s_x) [%]	2.76
MAPE(s_y) [%]	2.02
MAPE(v_x) [%]	0.49

Table 5.4: Evaluation of ST-Planner comparing planned and executed trajectories. Mean values of performance measures for the deviation of the X-Y Area, s_x, s_y, and v_x trajectories.

tional safety margins. For the subsequent vehicle implementation, longitudinal and lateral safety margins shall be applied. For longitudinal margin, a temporal margin of additional $100\,\mathrm{ms}$ shall be applied. This covers all computational and executional delays. For a longitudinal velocity of $20\,\mathrm{m/s}$ this adds $2\,\mathrm{m}$ safety margin. The obstacle's lateral expansion shall be considered by additional $10\,\mathrm{cm}$. This covers the imposed uncertainties within the object detection system. Assuming the safety margins are included, the total longitudinal deviation of $2.76\,\%$ would be $40\,\%$ below the safety margin and the lateral deviation of $2.02\,\%$ would be $54\,\%$ below the safety margin. To conclude from this, imposing the additional safety margin as proposed ensures collision free trajectories.

5.2 Comparison of Polynomial Trajectory Planner (P-Planner) with Single-Track Model Trajectory Planner (ST-Planner)

The preceding analysis of the ST-Planner has proven its potential for collision avoidance. In particular, the approach ensures dynamically feasible trajectories that can be utilized up to the dynamic limits. Additionally, the approach provides trajectories that enable an evasion at the latest possible moment. The following investigation shall verify the applicability of the proposed approximation of the dynamic model by parametric trajecto-

Approach	ST-Planner P-Planner
$x^{\mathrm{Obj}}(k)$ [m]	$v_x(0\|k) \cdot t_{\mathrm{TTC_{ini}}}$
$y^{\mathrm{Obj}}(k)$ [m]	0.50
$w^{\mathrm{Obj}}(k)$ [m]	2.00
$v_x(0\|k)$ [km/h]	70.00
$t_{\mathrm{TTC_{ini}}}$ [s]	2.00
$c_{0,\mathrm{L}}(k)$ [m]	5.00
$c_{0,\mathrm{R}}(k)$ [m]	-1.50

Table 5.5: Scene parameter set of ST-Planner and P-Planner. Obstacle's coordinates relative to the ego-vehicle with longitudinal and lateral coordinate, $x^{\mathrm{Obj}}(k)$ and $y^{\mathrm{Obj}}(k)$, and width of the obstacle $w^{\mathrm{Obj}}(k)$. Initial speed $v_x(0|k)$, first detection time of the obstacle $t_{\mathrm{TTC_{ini}}}$, and left and right lateral margin, $c_{0,\mathrm{L}}(k)$ and $c_{0,\mathrm{R}}(k)$.

ries. The characteristics of ST-Planner and P-Planner shall be analyzed and compared to determine if the considered polynomials deliver suitable trajectories.

Either approach is simulated for a specific test scenario to achieve optimal evasive trajectories executable at the latest possible moment. The test scenario is again defined as shown in Fig. 5.1. Table 5.5 lists the parameter set specifying the test scenario. The parameter set for the trajectory planners are listed in Table 5.6. The steering rate, $\dot{\delta}(i|k)$, is considered in the ST-Planner to constrain the steering actuator. Analog, the lateral jerk, $\dot{a}_y(i|k)$, is constrained in the P-Planner to realize steering actuator limitations. The limits are chosen according to prior vehicle studies (see Section 2.7) providing comparable and realistic limits for each approach.

The simulation results are shown in Fig. 5.3. The top plot shows the trajectories in the x-y plane of ST-Planner and P-Planner. The red circles highlight

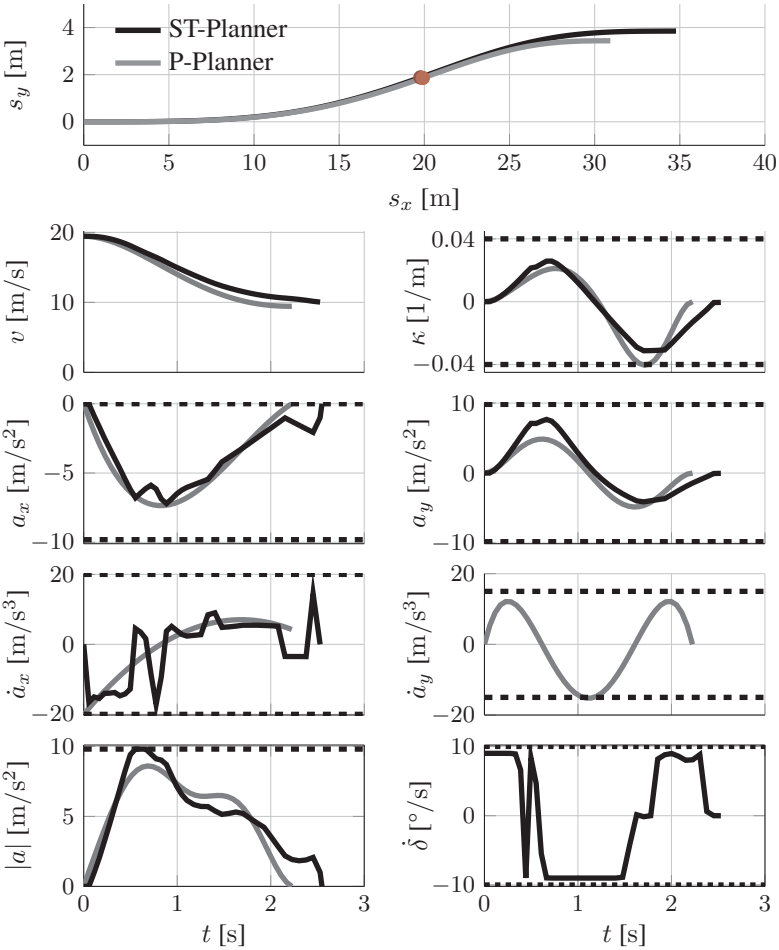

Figure 5.3: Comparison of ST-Planner and P-Planner trajectories. The upper plot shows trajectories of ST-Planner and P-Planner in the x-y plane with there corresponding spatiotemporal point at t_P in red. The left column shows (from top to bottom) the trajectories of both approaches over time for v, a_x, $\dot{a}_x$, and $|a|$. The right column shows (from top to bottom) the trajectories over time for κ and a_y for both approaches, $\dot{a}_y$ for the parametric trajectory, and $\dot{\delta}$ for the dynamic model-based trajectory.

Approach	ST-Planner	P-Planner
$\mathrm{a_{max}}$ $[\mathrm{m/s^2}]$	9.81	
$\kappa_{\max}$ $[1/\mathrm{m}]$	0.04	
$\dot{a}_{x,\max}$ $[\mathrm{m/s^3}]$	20.00	
$\dot{a}_{y,\max}$ $[\mathrm{m/s^3}]$		15.00
$\dot{\delta}_{\max}$ $[^\circ/\mathrm{s}]$	9.00	
$\mathrm{N+M}$	$20+20$	

Table 5.6: Trajectory parameter set of ST-Planner and P-Planner. Absolute acceleration limit $\mathrm{a_{max}}$. Limit for trajectory curvature $\kappa_{\max}$, longitudinal and lateral jerk, $\dot{a}_{x,\max}$ and $\dot{a}_{y,\max}$, and steering rate $\dot{\delta}_{\max}$. $\mathrm{N+M}$ are the trajectory samples.

the spatiotemporal point when the ego-vehicle passes the obstacle at t_P (relative to the vehicle's center of gravity). The left column of the figure shows (from top to bottom) the trajectories of velocity, longitudinal acceleration and jerk, and absolute acceleration for both approaches, respectively. The right column of the figure shows (from top to bottom) the trajectories of curvature and lateral acceleration for both approaches, lateral jerk for the polynomial trajectory and the steering rate of the trajectory associated to the ST-Planner. In addition to the trajectories, the corresponding limits according to Table 5.6 are plotted.

All trajectories lie within the given limits. For the trajectories of the P-Planner, the lower limit of the longitudinal jerk is reached right at the start of the maneuver. For the lateral jerk trajectory, the lower limit is reached at the moment of the passing time t_P. The curvature trajectory reaches the lower limit in the second half of the maneuver. Looking at the trajectories of the ST-Planner, lower longitudinal jerk and absolute acceleration limits are already reached during the first half of the maneuver. The steering rate trajectory is at the upper and lower limit during the maneuver.The trajectory

$\mathrm{MAPE}(\mathrm{Area}, t_\mathrm{P})[\%]$	1.01
$\mathrm{MAPE}(\mathrm{Area}, t_\mathrm{F})[\%]$	12.65
$\mathrm{MAPE}(s_x, t_\mathrm{P})[\%]$	2.04
$\mathrm{MAPE}(s_x, t_\mathrm{F})[\%]$	1.00
$\mathrm{MAPE}(s_y, t_\mathrm{P})[\%]$	1.45
$\mathrm{MAPE}(s_y, t_\mathrm{F})[\%]$	6.26
$\mathrm{MAPE}(v_x, t_\mathrm{P})[\%]$	3.05
$\mathrm{MAPE}(v_x, t_\mathrm{F})[\%]$	7.41

Table 5.7: Comparison of trajectories generated with ST-Planner and P-Planner. Performance measures for two temporal intervals, $[0,\ t_\mathrm{P}]$ and $[t_\mathrm{P},\ t_\mathrm{F}]$, comparing relative deviation of the X-Y area, s_x, s_y, and v_x trajectories.

shapes of both approaches are very close. Hardly any difference is observable for the trajectories shown in x-y plane from the start of the maneuver until the object is passed. With respect to lateral acceleration trajectories, maximum and minimum levels are achieved at the same time. The maximum acceleration levels differ significantly, where the ST-Planner has the highest lateral acceleration levels.

Table 5.8 lists time to last maneuver execution t_TLME, passing time t_P, and maneuver duration t_F for ST-Planner and P-Planner, revealing little difference in t_TLME and small difference in t_P and t_F. The values for t_TLME only differ by $13\,\mathrm{ms}$.

The trajectories are further assessed by the performance measures MAPE (see Section 4.4.1). The trajectories are subdivided into two temporal intervals, $[0,\ t_\mathrm{P}]$ and $[t_\mathrm{P},\ t_\mathrm{F}]$, for better analyses and distinction of different effects. The results are listed in Table 5.7. The first interval $[0, t_\mathrm{P}]$ shows small deviations except for the longitudinal trajectories in magni-

Approach	ST-Planner	P-Planner
t_{TLME} [s]	0.95	0.93
t_{P} [s]	1.05	1.20
t_{F} [s]	2.53	2.20

Table 5.8: Simulation result of ST-Planner and P-Planner. Compared values are time to last maneuver execution t_{TLME}, passing time t_{P}, and maneuver duration t_{F}.

tudes of the performance measure. The $\mathrm{MAPE}(\cdot, t_{\mathrm{P}})$ values in a range of $[1.08\,\% \ldots 3.05\,\%]$ (see Table 5.7). The second interval shows higher variations with $\mathrm{MAPE}(\cdot, t_{\mathrm{F}})$ values are in a range of $[1.02\,\% \ldots 12.65\,\%]$. A reasonable explanation for the deviation in the second interval can be given by a discussion of the constraints. In the first interval, trajectories have equal and "fixed" constraints where the vertices of the two opponents meet at passing time t_{P} (see Section 3.5.1). Whereas in the second interval, the end conditions are unbounded except for the lateral position, which shall stay within the drivable corridor. This extra degree of freedom is likely to be the reason for the differences at the maneuver end for these two different approaches.

Both evasive trajectories appear to reach the limits in at least one measure, which indicates that the last-possible evasive trajectories are found by both approaches. The achieved time to last maneuver execution t_{TLME} values are nearly equal (see Table 5.8) for both planners. Overall, it is shown that the approximation of the trajectories of the ST-Planner by a polynomial function of degree 7 for the lateral trajectories and a polynomial function of degree 5 for the longitudinal trajectories lead to acceptable results. The investigation confirmed the compliance with constraints and requirements together with the dynamical integrity of the parametric trajectories.

5.3 Comparison of reduced Polynomial Trajectory Planner (rP-Planner) and Single-Track Model Trajectory Planner (ST-Planner)

The prior comparison of P-Planner with ST-Planner has confirmed the proposed parametric trajectories to be sufficient to provide dynamically feasible collision avoidance trajectories. In this section, rP-Planner shall be compared with ST-Planner to investigate the behavior of both approaches with regards to their capabilities to handle various traffic situations. Further, specific temporal characteristics of the last-possible evasive maneuver shall be evaluated and compared. Besides the comparison of the two planning approaches, the computational efficiency of the rP-Planner shall be verified together with the clarification whether the proposed approach enables trajectory planning in real time.

The approaches are examined by simulation of different test scenarios according to Fig. 5.1. The approaches are again simulated for different scene and trajectory parameters. The scene parameters are listed in Table 5.9. Initial velocity, $v_x(0|k)$, lateral position of the obstacle, $y^{\mathrm{Obj}}(k)$, and left road boundary, $c_{0,\mathrm{L}}(k)$, are varied. The left road boundary is varied depending on the variation of the obstacle's lateral position according to Eq. (5.2) to ensure a sufficient maneuver corridor to pass for the evasive maneuver.

$$\hat{c}_{0,\mathrm{L}}(k)(y^{\mathrm{Obj}}(k)) = \sum_{i=0}^{\mathrm{N}_c} \left(y^{\mathrm{Obj}}(k) + 0.5w^{\mathrm{Obj}}(k) + w + \epsilon\right) + \left(\frac{c_{0,\mathrm{L,max}} - \left(y^{\mathrm{Obj}}(k) + 0.5w^{\mathrm{Obj}}(k) + w + \epsilon\right)}{\mathrm{N}_c}\right) i \quad (5.2)$$

with the amount of desired measures N_c, the width of the ego-vehicle w, the lateral safety margin ϵ, and the maximum of the varied road boundary

Approach	ST-Planner rP-Planner
$x^{\mathrm{Obj}}(k)$ [m]	$v_x(0\|k) \cdot t_{\mathrm{TTC_{ini}}}$
$y^{\mathrm{Obj}}(k)$ [m]	[-0.5 0.0 0.5]
$w^{\mathrm{Obj}}(k)$ [m]	2.00
$v_x(0\|k)$ [km/h]	[40.0 50.0 60.0 70.0]
$t_{\mathrm{TTC_{ini}}}$ [s]	2.00
$c_{0,\mathrm{L}}(k)$ [m]	$\hat{c}_{0,\mathrm{L}}(k)(y^{\mathrm{Obj}}(k))$
$c_{0,\mathrm{R}}(k)$ [m]	-1.50
No. of variations	108

Table 5.9: Scene parameter set of ST-Planner and rP-Planner. Obstacle's coordinate relative to the ego-vehicle with longitudinal coordinates $x^{\mathrm{Obj}}(k)$, variation of lateral coordinate $y^{\mathrm{Obj}}(k)$, and width of the obstacle $w^{\mathrm{Obj}}(k)$. Variation of initial speed $v_x(0|k)$, first detection time of the obstacle $t_{\mathrm{TTC_{ini}}}$, left lateral margin depending on the obstacles lateral coordinate , $c_{0,\mathrm{L}}(k)$, and right lateral margin, $c_{0,\mathrm{R}}(k)$.

$c_{0,\mathrm{L,max}}$. In the presented case, $\mathrm{N}_c = 2$, $w = 2.00\,\mathrm{m}$, $\epsilon = 0.10\,\mathrm{m}$, and $c_{0,\mathrm{L,max}} = 6\,\mathrm{m}$. The time for the first detection of an obstacle, $t_{\mathrm{TTC_{ini}}}$, is again considered with the related longitudinal distance to the obstacle at the first detection event according to Eq. (5.1). The trajectory parameter set is listed in Table 5.10 with variations in the absolute acceleration limits.

In contrast to ST-Planner and P-Planner, the simulation of rP-Planner is already performed on a dSPACE MicroAutoBox II of type 1401/1511/1512 [15] which is the target hardware for the subsequent vehicle test implementation. It shall facilitate realistic and reliable insights to the real-time capabilities. The approach is implemented in Matlab/Simulink® using the Nlopt optimization package [32]. The *COBYLA* [53] algorithm is used to solve the nonlinear optimization problem.

Approach	ST-Planner	rP-Planner
$\mathrm{a}_{\max}$ $[\mathrm{m/s^2}]$	[7.50 8.655 9.81]	
$\kappa_{\max}$ $[1/\mathrm{m}]$	0.04	
$\dot{a}_{x,\max}$ $[\mathrm{m/s^3}]$	20.00	
$\dot{a}_{y,\max}$ $[\mathrm{m/s^3}]$		15.00
$\dot{\delta}_{\max}$ $[^\circ/\mathrm{s}]$	9	
$\mathrm{N+M}$	$20+20$	
H		5

Table 5.10: Trajectory parameter set for ST-Planner and rP-Planner. Variation of the absolute acceleration limit $\mathrm{a}_{\max}$. Limits for curvature $\kappa_{\max}$, longitudinal and lateral jerk, $\dot{a}_{x,\max}$ and $\dot{a}_{y,\max}$, and steering rate $\dot{\delta}_{\max}$. $\mathrm{N+M}$ and H are the number of samples used for the trajectory.

For the comparison of the approaches, only feasible solutions with $t_{\mathrm{TLME}} \geq 0$ are considered. For rP-Planner, 10 out of 108 test cases reveal an infeasible solution whereas ST-Planner succeeds to find a feasible solution in all 108 test cases. These 10 infeasible cases are removed from the sample set to ensure reliable comparison. Further analyses yield the cause for the 10

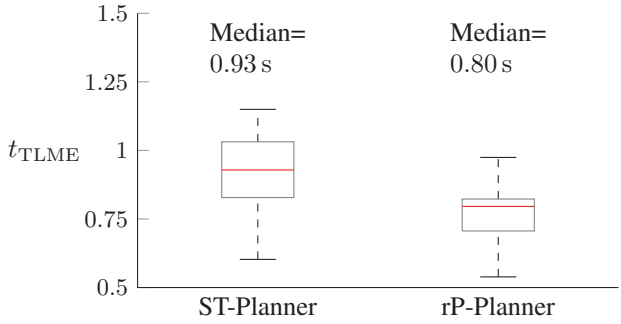

Figure 5.4: Simulation results of ST-Planner and rP-Planner comparing the time to last maneuver execution t_{TLME}.

Approach	ST-Planner	rP-Planner
$\bar{t}_{\mathrm{TLME}}$ [s]	0.93	0.80
$\bar{t}_{\mathrm{P}}$ [s]	0.95	1.13
$\bar{t}_{\mathrm{F}}$ [s]	2.19	3.13

Table 5.11: Simulation results for ST-Planner and rP-Planner, comparing mean values of the time to last maneuver execution t_{TLME}, passing time t_{P} and maneuver duration t_{F}.

infeasible cases, originating from a too narrow lateral distance between the obstacle and the road boundary.

The simulation results are shown in Fig. 5.4. All values of time to last maneuver execution, t_{TLME}, for ST-Planner and P-Planner are collected in the corresponding box plots. Table 5.11 shows the achieved medians values of the trajectories' time to last maneuver execution $\bar{t}_{\mathrm{TLME}}$, passing time $\bar{t}_{\mathrm{P}}$, and maneuver duration $\bar{t}_{\mathrm{F}}$ for the set of feasible solutions. The characteristic median values differ significantly between both approaches. The $\bar{t}_{\mathrm{TLME}}$ of ST-Planner is higher with a value of $\bar{t}_{\mathrm{TLME}} = 0.93\,\mathrm{s}$ compared to the rP-Planner with $\bar{t}_{\mathrm{TLME}} = 0.80\,\mathrm{s}$, which is a total difference of $0.13\,\mathrm{s}$. This indicates that the trajectories generated with ST-Planner enable an execution of a latest possible evasive maneuver in average $0.13\,\mathrm{s}$ later than the trajectories generated by the rP-Planner. Passing time $\bar{t}_{\mathrm{P}}$ and maneuver duration $\bar{t}_{\mathrm{F}}$ are reached earlier for the trajectories of ST-Planner.

Both planning approaches show the potential of handling variations in the scenery. Overall, ST-Planner is more robust in scene variations, whereas rP-Planner sometimes finds an infeasible solution. ST-Planner outperforms rP-Planner in its temporal behavior. In average, the model-based planning approach finds last-possible trajectories that can be executed at a later moment than the parametric trajectories. However, good results are achieved

Approach	rP-Planner
$\mathrm{a}_{\max}$ $[\mathrm{m/s^2}]$	9.81
$\kappa_{\max}$ $[1/\mathrm{m}]$	0.04
$\dot{a}_{x,\max}$ $[\mathrm{m/s^3}]$	20.00
$\dot{a}_{y,\max}$ $[\mathrm{m/s^3}]$	15.00
H	5

Table 5.12: Trajectory parameter set of rP-Planner. Limits for absolute acceleration $\mathrm{a}_{\max}$, curvature $\kappa_{\max}$, longitudinal and lateral jerk, $\dot{a}_{x,\max}$ and $\dot{a}_{y,\max}$. H is the amount of trajectory samples.

with rP-Planner, though a reduced scenery set can be covered. This significant difference in the temporal behavior of rP-Planner owes to the trajectory approximation and the inclusion of the heuristic sampling approach, which on the other hand offers a reduced computational complexity.

Consideration of the average worst-case execution time for computing a single trajectory, ST-Planner terminates after $10.00\,\mathrm{s}$, whereas the implementation of rP-Planner has a worst-case execution time of less than $50\,\mathrm{ms}$.The potential of an efficient implementation and the real-time capabilities of the proposed approach is verified with the achieved low average worst-case execution time.

5.4 Risk indication capabilities

As described in the previous section, rP-Planner shows good potential to fulfill the functional requirements for a collision avoidance trajectory planner while being efficient for a potential integration in an in-vehicle application. In this section the thread assessment capabilities of the trajectory planning approach are investigated and shown exemplarily for the rP-Planner. The same test scenarios as before will be applied with different parameters being

Approach	rP-Planner
$x^{\mathrm{Obj}}(k)$ [m]	$v_x(0\|k) \cdot t_{\mathrm{TTC_{ini}}}$
$y^{\mathrm{Obj}}(k)$ [m]	0.00
$w^{\mathrm{Obj}}(k)$ [m]	2.00
$v_x(0\|k)$ [km/h]	70.00
$t_{\mathrm{TTC_{ini}}}$ [s]	$[2 \ldots 0]$
$c_{0,\mathrm{L}}(k)$ [m]	5.00
$c_{0,\mathrm{R}}(k)$ [m]	-1.50

Table 5.13: Scene parameter set of rP-Planner. Initial speed, $v_x(0|k)$, and lateral object position, $y^{\mathrm{Obj}}(k)$, varied longitudinal object position, $x^{\mathrm{Obj}}(k)$, and the corresponding initial time to collision. $t_{\mathrm{TTC_{ini}}}$, left and right lateral margin, $c_{0,\mathrm{L}}(k)$ and $c_{0,\mathrm{R}}(k)$.

permuted. The scene and trajectory parameter sets are listed in Table 5.12 and Table 5.13, respectively.

An imminent collision shall be simulated where no action is taken to avoid the collision of the ego-vehicle with the obstacle ahead. To simulate the continuing rapprochement of the ego-vehicle towards the obstacle, the virtual time for the first detection of an obstacle $t_{\mathrm{TTC_{ini}}}$ is varied in descending order. The collision event emerges when $t_{\mathrm{TTC_{ini}}}$ reaches zero.

The simulation results are shown in Fig. 5.5. The upper plot shows the descending time to collision t_{TTC} and the lower one shows the time to last maneuver execution t_{TLME} of the successively planned trajectory. The vertical dotted line indicates the time when the time to last maneuver execution t_{TLME} drops below zero.

At the start of the simulation ($t_{\mathrm{TTC_{ini}}} = 2.00\,\mathrm{s}$), the situation is uncritical and a collision avoidance trajectory is successfully found with a sufficient

time until the maneuver has to be executed ($t_{\mathrm{TLME}} = 0.93\,\mathrm{s}$). While the time to collision, t_{TTC}, decreases monotonically and, hence, the longitudinal distance to the obstacle decreases, the situation becomes more and more critical since t_{TLME} decreases. At $t = 2.00\,\mathrm{s}$, the value of the time to last maneuver execution changes its sign from positive to negative with a corresponding time to collision of $t_{\mathrm{TTC}} = 1.00\,\mathrm{s}$. When this moment has been reached, no further collision avoidance trajectory can be found.

The proposed approaches provide trajectories that enable a latest possible evasive maneuver strategy for a set of given constraints while indicating situations when no collision-free trajectories can be found. The risk criteria supported by the approaches contributes to system design for decision-making modules.

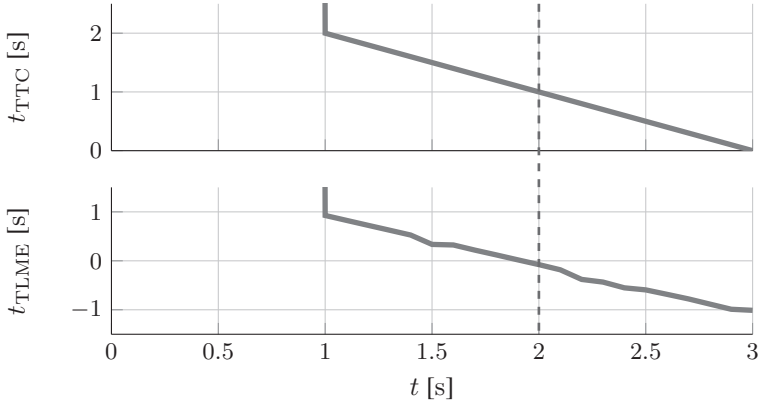

Figure 5.5: Simulation results generated with rP-Planner illustrating the risk assessment capabilities of the proposed approaches. The upper plot shows the descending t_{TTC} and the lower plot shows the t_{TLME} of the successively planned trajectory

6 Vehicle Test Results

In the previous chapter, the trajectory planning approaches were analyzed using a simulation environment for characteristic scenarios. The evaluation supports the assumption, that the rP-Planner is suitable fo a real-time application while providing trajectories with high quality, which are close to optimal trajectories achieved with the Single-Track Model Trajectory Planner (ST-Planner). In this chapter, the implementation of the reduced Polynomial Trajectory Planner (rP-Planner) in the test vehicle shall be described and the performance of the approach in real test scenarios shall be investigated. The achieved simulation results with regard to the last possible

Figure 6.1: Automated collision avoidance maneuver performed in a test vehicle

maneuver execution time shall be verified. The system is tested in the traffic scenarios described in Section 4.4.2, with a maximum speed of $70\,\mathrm{km/h}$ and a limited lateral maneuver space typical for city traffic. Fig. 6.1 shows the test vehicle performing an evasive maneuver for a scenario defined in Use case 3 (4.4.2).

6.1 Experimental setup

This section describes the hardware and software implementation utilized in the test vehicle.

6.1.1 Hardware setup

As integration vehicle, a model-year 2014 Opel Insignia 5-door sedan is used with a 2.0L ECOTEC direct injection turbo engine, 6-Speed automatic transmission, and all-wheel-drive.

An overview of the hardware implementation is given in Fig. 6.2.
A dSPACE® MicroAutoBox II of type 1401/1511/1512 [15] is used as Electronic Control Unit (ECU), hosting the collision avoidance system. For all other required components, series and near-production hardware is used. The on-board steering and braking systems are triggered via Controller Area Network (CAN).

A near-production object sensor system is used to observe the environment. A combination of camera and radar system is used to observe the area ahead of the ego-vehicle. At the rear corners of the ego-vehicle, two radar sensors are mounted to observe both rearward and side traffic area. The object sensor system provides fused environment information, which is transfered to the MicroAutoBox via Ethernet using a UDP/IP protocol. The provided environment information comprises object information, in-

cluding the object dimensions, position, and velocity, each relative to the ego-vehicle. Detected objects are classified, where the system distinguishes between vehicles, pedestrians, and bicycles. In addition, drivable area and lane markings are provided.

Real-time kinematic information of the ego-vehicle, position, orientation, and motion, are provided by a six degree of freedom Inertial Measurement Unit (IMU) aided GPS. All relevant vehicle states are provided to the system via CAN.

6.1.2 Software Setup

The collision avoidance system is implemented in Matlab®/Simulink® using the dSPACE® Real-Time Interface (RTI) library accessing the MicroAutoBox II. Fig. 6.3 illustrates the algorithmic structure of the system.

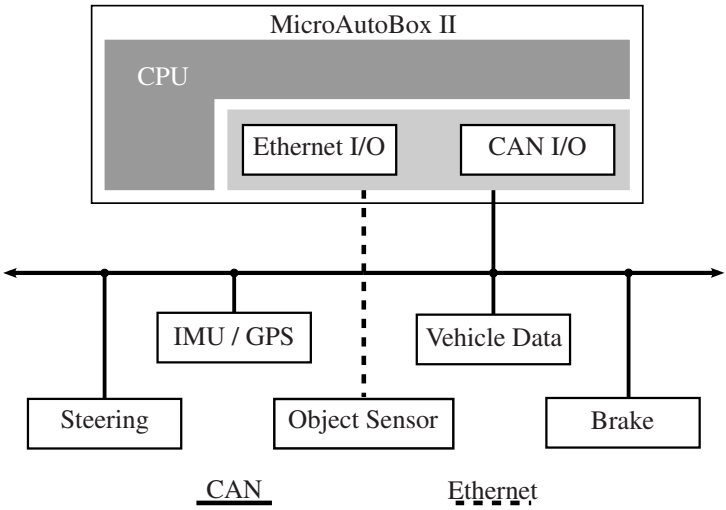

Figure 6.2: Hardware structure for vehicle tests

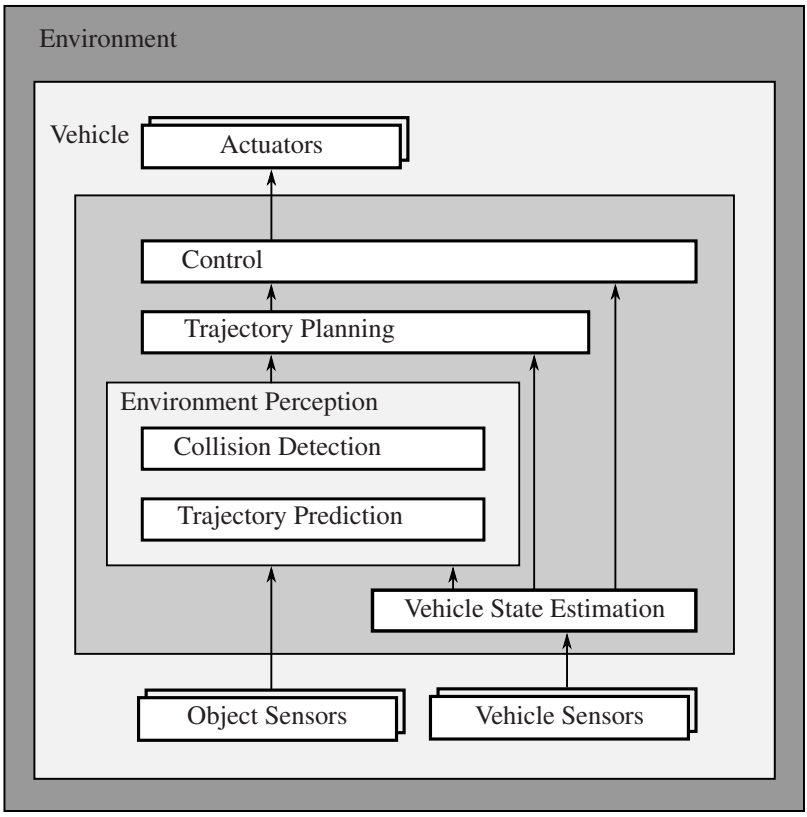

Figure 6.3: Software structure of the Advanced Driver Assistance System (ADAS)

The vehicle state estimation [72, 58], predicts the current vehicle states on the basis of the vehicle sensors and provides the information to the environmental model, the trajectory planner, and the control module. The environment perception model collects object sensor information and generates a model of the environment for the current scenery. Trajectories of moving objects and of the ego-vehicle are predicted in the trajectory prediction module. The predicted trajectories are placed into a grid map together

with stationary obstacles and road-boundaries [12]. The ego-vehicle trajectory is permanently analyzed for a possible collision ahead with either the road boundary or any objects, moving or stationary. If an imminent collision with an object is predicted, position and width of the object of interest are sent to the trajectory planner. A detailed description of the environment perception module can be found in [55].

With the information of environment perception and vehicle states estimation, the trajectory planner searches for the latest possible evasive trajectory. The evaluated trajectory including the estimated time to last maneuver execution t_{TLME} is sent to the control module, which triggers the vehicle's steering and brake actuators. For lateral control, a Model Predictive Control (MPC) is applied, similar to [14]. The longitudinal trajectory is controlled by the on-board brake control module.

6.2 Test setup

The collision avoidance system is tested in a prototypical implementation under realistic conditions. The goal is to evaluate the proposed collision avoidance system for characteristic traffic scenarios that can typically occur within urban areas. The main focus is on sceneries where a suddenly appearing obstacle enters the driving lane of the ego-vehicle. Those scenarios are selected with a short temporal distance between ego-vehicle and obstacle, so that a braking maneuver would no longer avoid the collision. The constellation of the traffic participants for the considered characteristic use cases is described in Section 4.4.2. The collision avoidance system is tested for these scenarios.

The parameter set of the trajectory planner is listed in Table 6.1. The parameters are equal to those considered for the simulative tests of the rP-Planner in Section 5.3. Except for lateral margins which are bounded,

Approach	rP-Planner
$\mathrm{a}_{\max}$ [$\mathrm{m/s^2}$]	9.81
$\kappa_{\max}$ [$1/\mathrm{m}$]	0.04
$\dot{a}_{x,\max}$ [$\mathrm{m/s^3}$]	20.00
$\dot{a}_{y,\max}$ [$\mathrm{m/s^3}$]	15.00
$c_{0,\mathrm{L}}(k)_{\max}$ [m]	4.50
$c_{0,\mathrm{R}}(k)_{\min}$ [m]	-4.50
H	5

Table 6.1: Trajectory Parameter set of rP-Planner. Limits of absolute acceleration $\mathrm{a}_{\max}$, curvature $\kappa_{\max}$, longitudinal and lateral jerk, $\dot{a}_{x,\max}$, and $\dot{a}_{y,\max}$. Limits of the lateral road margins, $c_{0,\mathrm{L}}(k)_{\max}$ and $c_{0,\mathrm{R}}(k)_{\max}$. H is the amount of trajectory samples.

covering the case where no margin is detected by the environment perception system.

6.3 Performance results

Four snapshots of relevant maneuver events are listed in the analysis plot, see Fig. 6.4 for example.

From top to bottom, the first row shows the non-critical situation. The second row shows the event when the critical object is detected for the first time. The third row shows the event when the latest possible evasive trajectory is executed. The forth row shows the end of the maneuver. Each event corresponds to the scenery image in the left column. The scenery image is augmented by the following Information:

- Detected critical objects are overlaid with a red bounding box.
- Detected non-critical objects are overlaid with a green bounding box.

- Left and right road boundaries are marked as blue lines.
- The current time stamp is shown in the lower-left corner of the scenery image.

In the right column, the corresponding result of the trajectory planning algorithm, comprising the trajectory, t_{TLME}, and the related t_{TTC} , is given. The trajectories for each event are illustrated in the x-y plane. The plots contain the planned trajectory, the determined road boundaries, $c_{0,j}(k)$, and the predicted location and width of the obstacle. The inherent criticality of t_{TLME} has a color coding to highlight criticality. When the imminent collision is avoidable, t_{TLME} is greater zero and, hence, colored green. When the imminent collision is unavoidable, t_{TLME} is less than or equal to zero and, hence, colored red.

Besides the event-based analysis of the use cases, the temporal chronology of t_{TTC} and t_{TLME} for each use case is additionally analyzed (see Fig. 6.5 as example). The upper plot shows the t_{TTC} over time whereas the lower plot shows the successively calculated t_{TLME}. The vertical dotted lines indicate the corresponding events.

For the time period between start of the evasive maneuver and maneuver end, the executed trajectory is illustrated. The upper plot shows the executed trajectory in the x-y plane. The trajectory with the corresponding ego-vehicle shape and additionally, road boundary and obstacle are shown. On the left side, from top to bottom, velocity, longitudinal acceleration, and jerk over time are shown. On the right, curvature, lateral acceleration, and jerk over time are shown. The corresponding constraints, as listed in Table 6.1, are given as dotted black lines.

A detailed description of the use case analysis is given exemplary for use case one.

Use case 1

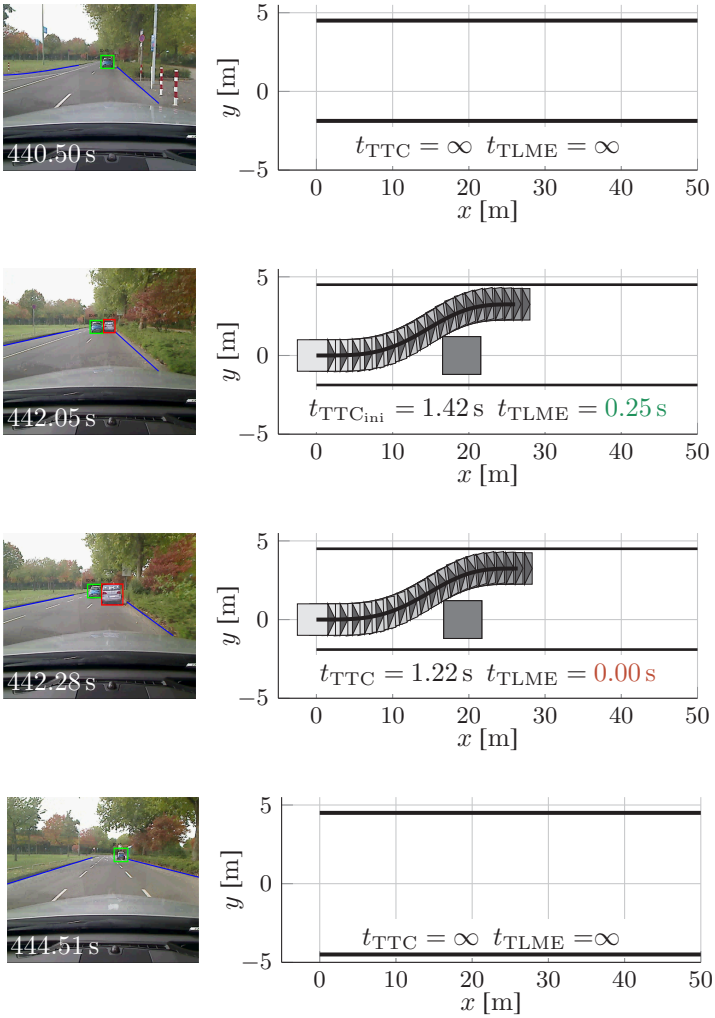

Figure 6.4: Relevant scenery events of use case 1. Left column shows the scenery image from the on-board perspective out of the ego-vehicle with overlays, right column shows the corresponding results of the trajectory planner.

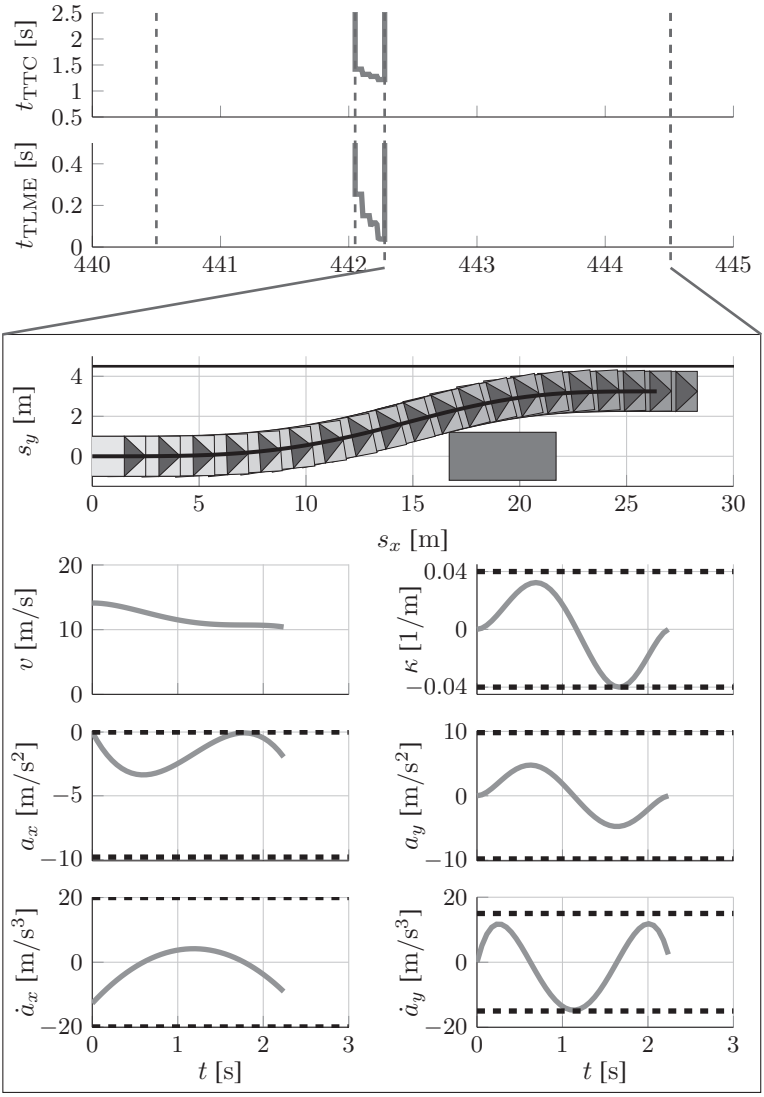

Figure 6.5: Temporal chronology of t_{TTC} and t_{TLME} and corresponding executed trajectory with relevant measures for use case 1.

Use case 2

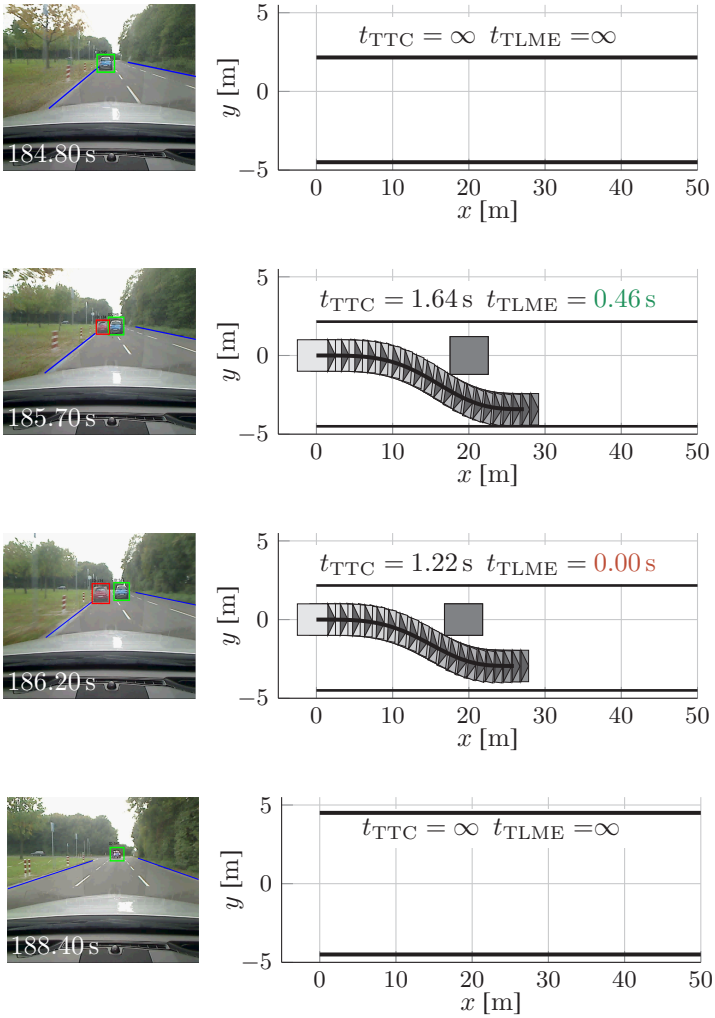

Figure 6.6: Relevant scenery events of use case 2. Left column shows the scenery image from the on-board perspective out of the ego-vehicle with overlays, right column shows the corresponding results of the trajectory planner.

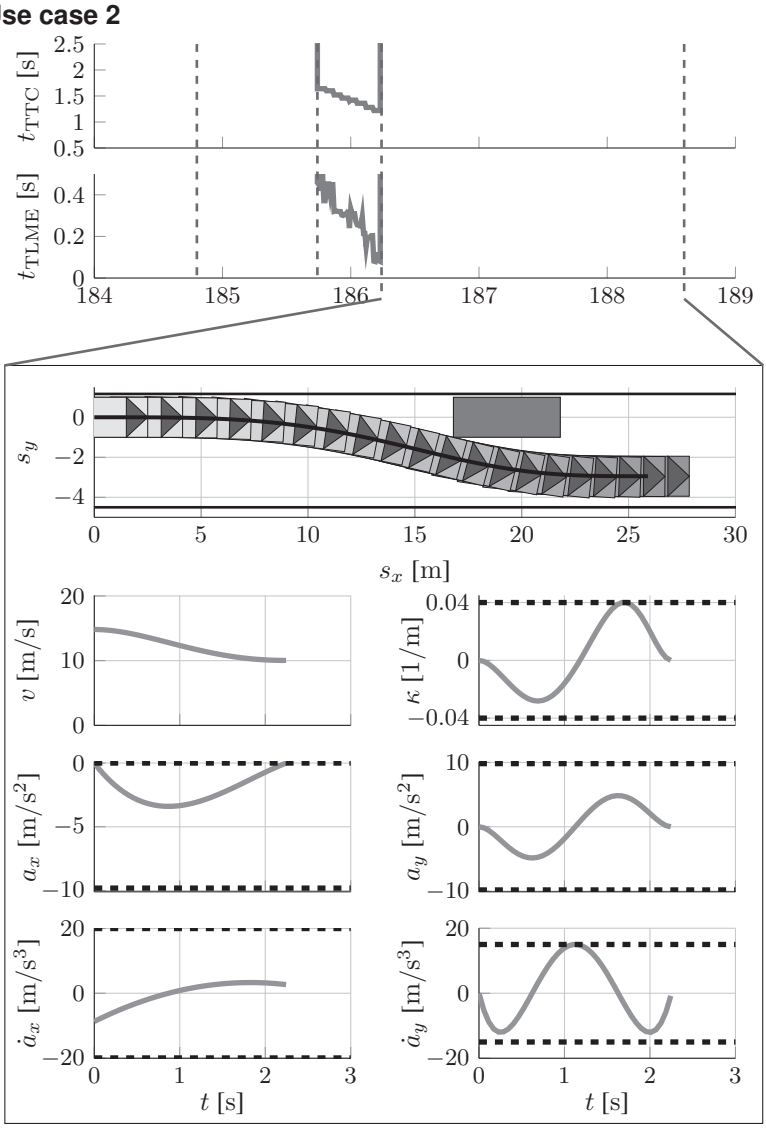

Figure 6.7: Temporal chronology of t_{TTC} and t_{TLME} and corresponding executed trajectory with relevant measures for use case 2.

Use case 3

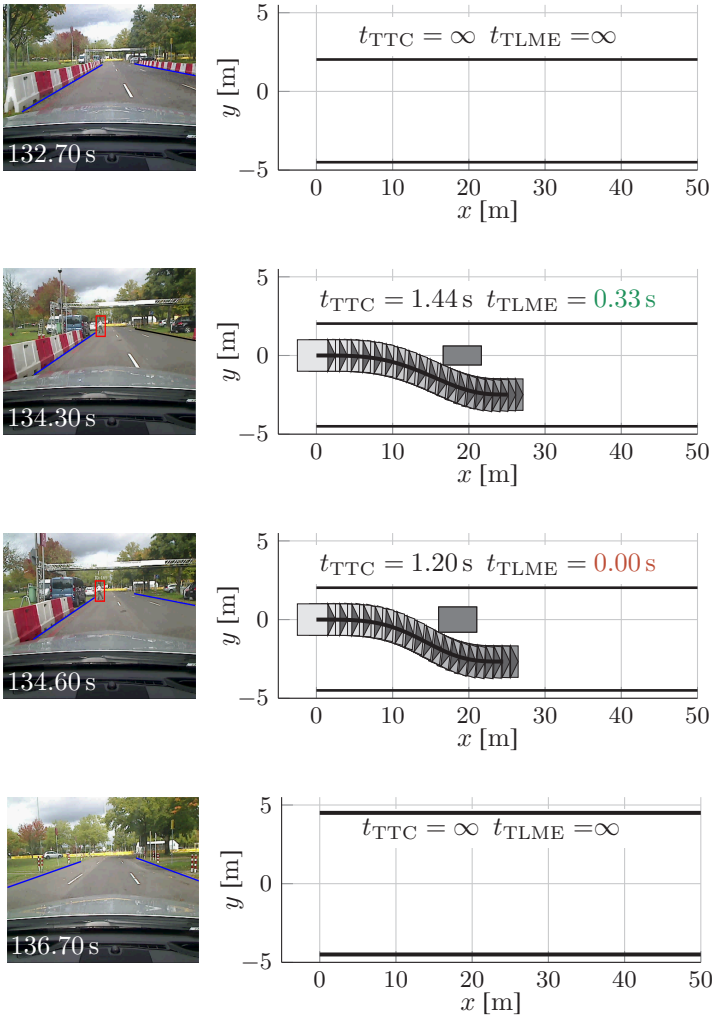

Figure 6.8: Relevant scenery events of use case 3. Left column shows the scenery image from the on-board perspective out of the ego-vehicle with overlays, right column shows the corresponding results of the trajectory planner.

Use case 3

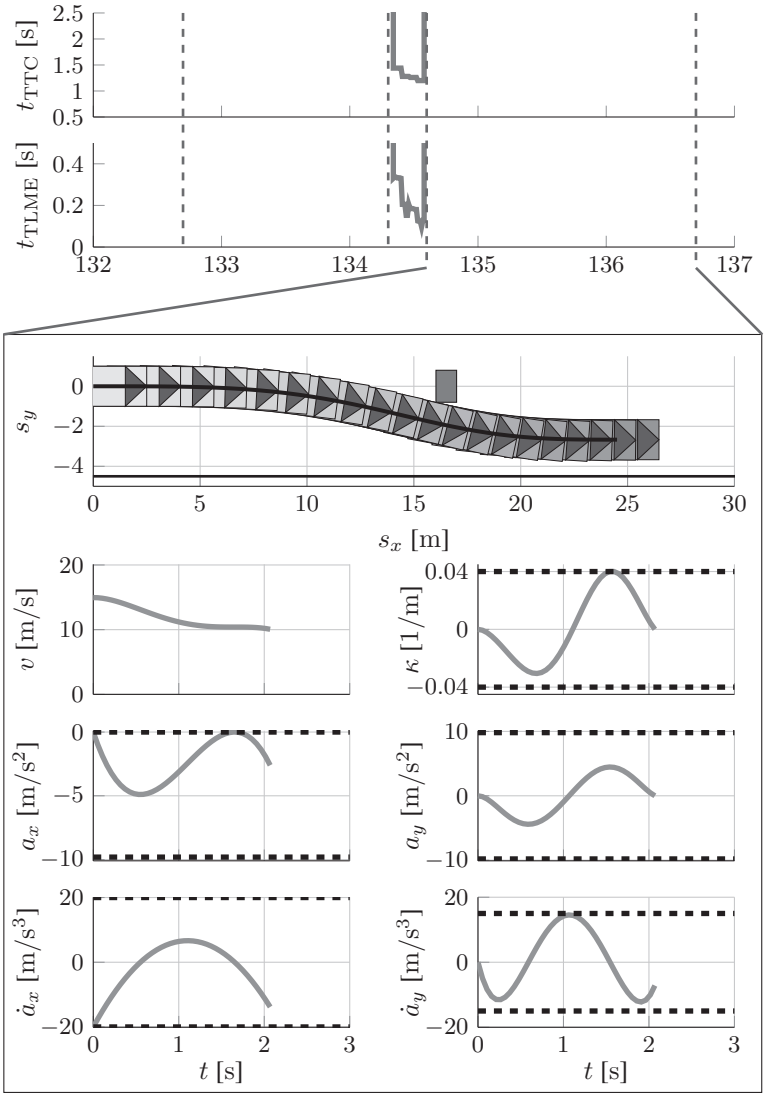

Figure 6.9: Temporal chronology of t_{TTC} and t_{TLME} and corresponding executed trajectory with relevant measures for use case 3.

Use case 1

The events of the scenery are depicted in Fig. 6.4, the chronology of t_{TTC}, t_{TLME}, and the executed latest possible trajectory are illustrated in Fig. 6.5. Next, the relevant events of the scenery are described in detail:

440.50 s The ego-vehicle follows a leading vehicle with a speed of $15\,\mathrm{m/s}$ while keeping a constant distance to it. Road boundaries are detected. The vehicle ahead is classified as an uncritical object, hence, marked with a green bounding box. No evasive trajectory is planned, t_{TTC} and t_{TLME} are infinite indicating an uncritical situation.

442.05 s The leading vehicle suddenly evades an obstacle by moving to the left. The critical object is detected ahead and marked with a red bounding box. An evasive trajectory is found for the actual situation. The found trajectory intends an evasion to the left to avoid the imminent collision with the obstacle. The actual t_{TLME} is greater than zero with $t_{\mathrm{TLME}} = 0.25\,\mathrm{s}$, thus, colored green. The corresponding time to collision is $t_{\mathrm{TTC}} = 1.42\,\mathrm{s}$. On the basis of the evaluated t_{TLME} for the actual event, an execution of the planned trajectory is postponed and the situation is further observed.

442.28 s The leading vehicle has successfully evaded the obstacle. The ego-vehicle's distance to the obstacle has decreased further. The situation is re-evaluated and the collision avoidance trajectory is re-planned. The actual t_{TLME} equals zero, which demands an imminent execution of the maneuver. The corresponding time to collision is $t_{\mathrm{TTC}} = 1.22\,\mathrm{s}$. The planned trajectory is released to the control unit and the collision avoidance maneuver is executed.

444.51 s The collision has been avoided. No further critical object is detected in the driving path, indicated by t_{TTC} and t_{TLME} being infinite.

The two subsequent use cases are analyzed in an analogous way. Test results for use cases 2 and 3 with the events of the scenery are illustrated in Fig. 6.6 and Fig. 6.8, the chronology of t_{TTC}, t_{TLME}, and the executed latest possible trajectory are illustrated in Fig. 6.7 and Fig. 6.9 for use case 2 and 3, respectively.

The temporal behavior of the use cases shall be considered jointly. With the first detection of the critical obstacle, t_{TTC} and t_{TLME} start to decrease monotonously until t_{TLME} is zero. The time between the first detection of the critical obstacle to the execution of the latest possible evasive trajectory is noticeably small for the considered use cases with a typical duration below $500\,\mathrm{ms}$. For the period between maneuver execution and maneuver end, t_{TTC} and t_{TLME} remain infinite.

All planned and executed trajectories stay within the constraint set. The limits of steering actuator (lateral jerk) and curvature are reached for all test cases. The lateral jerk limits are reached in the middle of the trajectory. The curvature limits are reached after the obstacle is evaded. The maximum reached acceleration levels are below limits within a typical range of $5\,\mathrm{m/s^2}$ to $7\,\mathrm{m/s^2}$.

6.4 Robustness results

The executed vehicle test demonstrates the successful integration of the proposed trajectory planning approach in an ADAS for collision avoidance. The approach's applicability and robustness towards the handling of changing conditions could be verified. The vehicle test corroborates successful collision avoidance in all test cases while complying with constraints and satisfying all given requirements. The following paragraph shall verify the simulative results of the parameter study of Section 5.3 with focus on the time to last maneuver execution, t_{TLME}.

Approach	rP-Planner
$x^{\mathrm{Obj}}(k)$ [m]	$v_x(0\|k) \cdot t_{\mathrm{TTC_{ini}}}$
$y^{\mathrm{Obj}}(k)$ [m]	0.50
$w^{\mathrm{Obj}}(k)$ [m]	2.00
$v_x(0\|k)$ [km/h]	[50 70]
$t_{\mathrm{TTC_{ini}}}$ [s]	2.00
$c_{0,\mathrm{L}}(k)$ [m]	5.00
$c_{0,\mathrm{R}}(k)$ [m]	-1.50

Table 6.2: Scene parameter set of rP-Planner planner for in vehicle test. The obstacle's coordinates relative to the ego-vehicle with longitudinal distance $x^{\mathrm{Obj}}(k)$, lateral coordinate $y^{\mathrm{Obj}}(k)$, and width of the obstacle $w^{\mathrm{Obj}}(k)$. Variation of initial speed $v_x(0|k)$. First detection time of the obstacle $t_{\mathrm{TTC_{ini}}}$, and left and right lateral margin, $c_{0,\mathrm{L}}(k)$ and $c_{0,\mathrm{R}}(k)$.

The verification run is performed by vehicle tests of the ADAS for collision avoidance discussed in the previous section. The vehicle tests are executed on a proving ground, where the previously simulated traffic scenario is recreated. The ego-vehicle is traveling towards a stationary obsta-

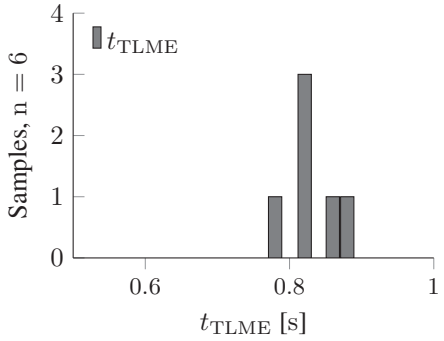

Figure 6.10: Test results of $\mathrm{n} = 6$ collision avoidance maneuvers, evaluating the time to last maneuver execution t_{TLME} of the rP-Planner.

Approach	rP-Planner
$\mathrm{a_{max}}$ $[\mathrm{m/s^2}]$	9.81
$\kappa_{\max}$ $[1/\mathrm{m}]$	0.04
$\dot{a}_{x,\max}$ $[\mathrm{m/s^3}]$	20.00
$\dot{a}_{y,\max}$ $[\mathrm{m/s^3}]$	15.00
H	5

Table 6.3: Trajectory parameter set of rP-Planner for vehicle test. Limits for absolute acceleration $\mathrm{a_{max}}$, curvature $\kappa_{\max}$, and longitudinal and lateral jerk, $\dot{a}_{x,\max}$ and $\dot{a}_{y,\max}$, respectively. H is the number of samples used for optimization.

cle, the drivable area is bounded with a left margin of $4.50\,\mathrm{m}$ and a right margin of $-1.50\,\mathrm{m}$. The parameter set defining the scenery is collected in Table 6.2. With this scenario, only evasive maneuvers to the left are feasible. The initial velocity of the vehicle, $v_x(0|k)$, is varied within a range of $[50\,\mathrm{km/h} \ldots 70\,\mathrm{km/h}]$. The parameters of the trajectory planner are as provided in Table 6.3. Discarding the influence of the object sensor system with regard to first object detections, the virtual first detection of an obstacle is again assumed to be at $t_{\mathrm{TTC_{ini}}} = 2.00\,\mathrm{s}$. This provides a baseline for the comparison of the time to last maneuver execution, which will be calculated relative to this virtual first object detection time.

Six test runs are considered for the evaluation of t_{TLME}. In all test rides, a collision of the ego-vehicle with the obstacle is successfully avoided. The time to last maneuver execution, t_{TLME}, of the vehicle is shown in Fig. 6.10. The median of the time to last maneuver execution, $\tilde{t}_{\mathrm{TLME}}$, for the test drives is $\tilde{t}_{\mathrm{TLME}} = 0.82\,\mathrm{s}$. The simulation results of the time to last maneuver execution $\tilde{t}_{\mathrm{TLME}}$ of Section 5.3 was $\tilde{t}_{\mathrm{TLME}} = 0.80\,\mathrm{s}$. The vehicle test discussed here could verify the consistency of the rP-Planner with the simulation results.

6.5 Summary

The planning approach was successfully integrated into a comprehensive ADAS for collision avoidance in urban traffic situations. The tested characteristic use cases proved that the planning approach delivers trajectories for the latest point in time that are dynamically feasible. The robustness of the proposed method against changing conditions in the environment was successfully verified in the vehicle test. During the test runs and beyond, all planned and executed trajectories stayed within the constraint set. The constraining borderline of the steering actuator and the curvature were reached for all test cases. The constraining borderline of the curvature was reached when the ego-vehicle was turning back after the obstacle has been evaded. These results, utilizing the proposed rP-Planner, are an indication that the latest possible evasive maneuvers is found.

Moreover, it could be verified that the last maneuver execution time of the in-vehicle test are consistent with the simulation results received by the rP-Planner. Also test in bad weather conditions lead to reasonable results, which confirms the robustness of the method. The on-board actuators could be identified as limiting factors during the vehicle test, especially within the typical velocity range of urban areas and in narrow roads. The actuator limits were reached right before the acceleration limit. Also the limited lateral maneuver space, typical in urban areas, influenced the accessibility of the maximum acceleration. For the characteristic use cases, a rapid change of direction seems to be more crucial than reaching the maximum acceleration. This is further supported by the use case investigation where the maximum steering jerk was always reached in the middle of the trajectory, which is exactly the counter steering point.

7 Conclusion and Outlook

Conclusion

A comprehensive trajectory planning method as functional component of an Advanced Driver Assistance System (ADAS) for automated collision avoidance systems in urban traffic was developed. Urban traffic presents challenging environment conditions, like narrow roads or vehicles parking aside the road, and as such demand special considerations to plan collision avoidance trajectories. To solve the trajectory planning problem for these situations the principle of optimization was considered.

Three optimal trajectory planners were covered in this work. The kinematic and dynamic characteristic of the underlying vehicle dynamics were considered in the trajectories including the physical limits of the brake and steering actuators. In the trajectory design the available maneuver space and arbitrary objects were considered in order to be robust against use case variations, e.g., evasion to the left or to the right, available maneuver space, or object width. The first approach, a model-based trajectory planner, could be successfully applied to find optimal, dynamically feasible trajectories for the given set of constraints and boundary conditions. The second approach approximates the dynamic model by polynomial trajectories with a marginal performance reduction. The third approach, extending the parametric trajectories with a heuristic sampling strategy, and as a result opens up the potential for real-time implementation.

The objective to implement an integrated risk assessment mechanism prior to maneuver initiation could be achieved. Each situation is assessed and the optimal moment for the execution of the latest possible collision-free evasive trajectory is successively evaluated. Moreover, the mechanism is capable of indicating situations where no collision-free trajectories are feasible. This mechanism benefits from the chosen cost functional leading to a risk criteria that may serve as input to a decision logic.

The developed approaches were assessed and compared in a simulative environment. It was verified that all approaches provide collision avoidance trajectories that are dynamically feasible and enable an intervention at the latest possible moment. The trajectory approximation by polynomials provide reliable results with marginal degradation in performance. To evaluate system performance and real-time capabilities of the developed approaches, the reduced Polynomial Trajectory Planner was integrated into a comprehensive Advanced Driver Assistance System for collision avoidance. This ADAS was successfully demonstrated on a prototypical implementation in an experimental vehicle. The robustness towards changing conditions and the practicality of the proposed approach could be successfully verified in the demonstration.

Outlook

As one results of the vehicle test, the actuators reveal to be the decisive limitation factor for automated evasive maneuvers. To broaden the potential of automated collision avoidance and further gain the coverable use cases the investigation in improved actuator concepts appears most promising. However the approaches presented in this work were designed such that they can cope with any kind of actuator limits. The proposed trajectory planning approaches imply more versatility than the application of automated braking only. The presented optimization problem is capable of achieving any kind

of lane change maneuvers. The maneuver characteristics are prescribed by the set of constraints and the corresponding limitations. Modifying the limitations enables further options in the design of characteristic maneuvers. For example, comfortable lane-change maneuvers can be generated by lowering the maximum levels of the dynamic constraints. Adjusting the constraints to application specific requirements opens even more versatile maneuver possibilities.

The greatest challenge in trajectory planning is to achieve the given real-time requirements, especially when a nonlinear optimization problem is to be solved. One solution to resolve this issue was successfully developed and verified in this work. In order to enable more complex trajectory planners further development and investigations in nonlinear solvers and there implementation on production-type Electronic Control Units (ECUs) is required. Investigation in the field of parallel computing or computing on a graphic chip will even provide more computational efficiency to solve nonlinear optimization problems.

The relevance of automated collision systems will continuously increase, considering the ongoing developments in the field of automated driving. The approach presented here contributes to these upcoming developments and presents an scalable solution for systems of varying complexity.

Bibliography

[1] S. Albers, D. Klapper, U. Konradt, A. Walter, and J. Wolf, Eds., *Methodik der empirischen Forschung*. Gabler, 2009.

[2] S. J. Anderson, "Constraint-based navigation for safe, shared control of ground vehicles," Ph.D. dissertation, Massachusetts Institute of Technology, 2013.

[3] A. Antoniou and L. Wu-Sheng, *Practical Optimization Algorithms and Engineering Applications*, 1, Ed. Springer, 2007.

[4] T. Arens, F. Hettlich, C. Karpfinger, U. Kockelkorn, K. Lichtenegger, and H. Stachel, *Mathematik*. Springer Spektrum, 2015.

[5] E. Bauer, F. Lotz, M. Pfromm, and M. Schreier, "PRORETA 3: An Integrated Approach to Collision Avoidance and Vehicle Automation," *at – Automatisierungstechnik*, Dec. 2012.

[6] M. S. Bazaraa, H. D. Sherali, and C. M. Shetty, *Nonlinear Programming: Theory and Algorithms*, 3rd ed. John Wiley & Sons, Inc., 2005.

[7] J. Betts, *Practical Methods for Optimal Control and Estimation Using Nonlinear Programming*, 2nd ed. Society for Industrial and Applied Mathematics, 2010.

[8] L. Biagiotti and C. Melchiorri, *Trajectory Planning for Automatic Machines and Robots*. Springer-Verlag Berlin Heidelberg, 2008.

[9] F. Bonarens, J. Ferdinand, G. Schmidt, and B. Yi, "Forschungsprojekt UR:BAN – Kognitive Assistenz: Schlussbericht zum Teilprojekt: Projektsäule UR-BAN-KA: Kollisionsvermeidung durch Ausweichen und Bremsen: Laufzeit: 01.04.2012–31.03.2016," 2016.

[10] F. Borrelli, *Constrained Optimal Control of Linear and Hybrid Systems*. Springer-Verlag Berlin Heidelberg, 2003.

[11] M. E. Bouzouraa, "Belegungskartenbasierte Umfeldwahrnehmung in Kombination mit objektbasierten Ansätzen fü Fahrerassistenzsysteme," Ph.D. dissertation, Technische Universität München, 2011.

[12] W. Burgard and M. Hebert, "World Modeling," in *Handbook of Robotics*. Springer-Verlag, 2008, ch. 36, pp. 853–869.

[13] W. Chee, M. Tomizuka, S. Patwardhan, and W.-B. Zhang, "Experimental study of lane change manoeuvre for AHS applications," in *American Control Conference*, vol. 1, Jun. 1995, pp. 139–143.

[14] M. Choi and S. Choi, "Model Predictive Control for Vehicle Yaw Stability With Practical Concerns," *IEEE Transactions on Vehicular Technology*, vol. 63, no. 8, pp. 3539–3548, 2014.

[15] dSPACE GmbH, "MircoAutoBox II Product Information," 2014.

[16] M. Durali, G. Javid, and A. Kasaiezadeh, "Collision avoidance maneuver for an autonomous vehicle," in *Proc. of the IEEE International Workshop on Advanced Motion Control (AMC)*, 2006, pp. 249–254.

[17] J. Ferdinand and B. Yi, "Trajectory Planning for Collision Avoidance in Urban Areas," in *Proc. of the IEEE Intelligent Vehicles Symposium (IV)*, 2016.

[18] J. Ferdinand and B. Yi, "Trajektorienplanung zur Kollisionsvermeidung im urbanen Raum," in *32. VDI/VW – Gemeinschaftstagung "Fahrerassistenzsysteme und automatisiertes Fahren"*, 2016.

[19] D. Ferguson, T. Howard, and M. Likhachev, "Motion planning in urban environments: Part I," in *Proc. of the IEEE/RSJ International Conference on Intelligent Robots and Systems (IROS)*, 2008, pp. 1063–1069.

[20] R. Findeisen, L. Imsland, F. Allgower, and B. A. Foss, "State and output feedback nonlinear model predictive control: An overview," *European journal of control*, vol. 9, no. 2, pp. 190–206, 2003.

[21] R. Fletcher, *Practical Methods of Optimization*. John Wiley & Sons, 1987, vol. 2.

[22] A. Gern, U. Franke, and P. Levi, "Advanced lane recognition-fusing vision and radar," in *Proc. of the IEEE Intelligent Vehicles Symposium (IV)*, 2000, pp. 45–51.

[23] J. Hillenbrand, A. Spieker, and K. Kroschel, "A Multilevel Collision Mitigation Approach – Its Situation Assessment, Decision Making, and Performance Tradeoffs," *IEEE Transactions on Intelligent Transportation Systems*, pp. 528–540, 2006.

[24] T. M. Howard, "Adaptive Model Predictive Motion planning for navigation in complex environments," Ph.D. dissertation, Carnegie Mellon University, 2009.

[25] T. M. Howard, C. J. Green, and A. Kelly, "Receding Horizon Model-Predictive Control for Mobile Robot Navigation of Intricate Paths," Robotics Institute, Carnegie Mellon University, Tech. Rep., 2009.

[26] T. M. Howard and A. Kelly, "Trajectory generation on rough terrain considering actuator dynamics," in *Field and Service Robotics*. Springer, 2006, pp. 479–490.

[27] T. M. Howard and A. Kelly, "Optimal rough terrain trajectory generation for wheeled mobile robots," *International Journal of Robotics Research (IJRR)*, vol. 26, no. 2, pp. 141–166, 2007.

[28] K. Iagnemma, S. J. Anderson, S. C. Peters, and T. E. Pilutti, "An optimal-control-based framework for trajectory planning, threat assessment, and semi-autonomous control of passenger vehicles in hazard avoidance scenarios," *Int. J. Vehicle Autonomous Systems*, vol. 8, pp. 190–216, 2010.

[29] R. Isermann, Ed., *Fahrdynamik-Regelung*. Vieweg + Teubner, 2006.

[30] R. Isermann, E. Bender, R. Bruder, M. Darms, M. Schorn, U. Stählin, and H. Winner, "Antikollisionssystem PRORETA – Integrierte Lösung für ein unfallvermeidendes Fahrzeug," in *Handbuch Fahrerassistenzsysteme*, H. Winner, S. Hakuli, and G. Wolf, Eds. Vieweg & Teubner, 2009, vol. 1, ch. 41, pp. 632–645.

[31] J. Ji, A. Khajepour, W. W. Melek, and Y. Huang, "Path Planning and Tracking for Vehicle Collision Avoidance Based on Model Predictive Control With Multiconstraints," *IEEE Transactions on Vehicular Technology*, vol. 66, no. 2, pp. 952–964, Feb. 2017.

[32] S. G. Johnson, "The NLopt nonlinear-optimization package," Feb. 2014. http://ab-initio.mit.edu/nlopt [Online. Accessed: 10.02.2014]

[33] N. Kaempchen, B. Schiele, and K. Dietmayer, "Situation Assessment of an Autonomous Emergency Brake for Arbitrary Vehicle-to-Vehicle Collision Scenarios," *IEEE Transactions on Intelligent Transportation Systems*, vol. 10, no. 4, pp. 678–687, 2009.

[34] W. Kamm, "Die Entwicklung des Kraftfahrzeugs," *Deutsches Museum. Abhandlungen und Berichte. VDI-Verlag*, 1937.

[35] C. Keller, T. Dang, H. Fritz, A. Joos, C. Rabe, and D. Gavrila, "Active Pedestrian Safety by Automatic Braking and Evasive Steering," *IEEE Transactions on Intelligent Transportation Systems*, vol. 12, no. 4, pp. 1292–1304, 2011.

[36] A. Kelly and B. Nagy, “Reactive nonholonomic trajectory generation via parametric optimal control,” *International Journal of Robotics Research (IJRR)*, vol. 22, no. 7-8, pp. 583–601, 2003.

[37] L. König, “Ein virtueller TestfaTest für den querdynamischen Grenzbereich,” Ph.D. dissertation, Universität Stuttgart, 2009.

[38] B. Kouvaritakis and M. Cannon, *Model Predictive Control: Classical, Robust and Stochastic*, M. J. Grimble and M. A. Johnson, Eds. Springer, 2015.

[39] J.-C. Latombe, *Robot motion planning*. Springer Science & Business Media, 1991.

[40] S. M. LaValle, *Planning Algorithms*. Cambridge University Press, 2004.

[41] M. Maurer and C. Stiller, *Fahrerassistenzsysteme mit maschieneller Wahrnehmung*. Springer, 2005.

[42] U. Meis and S. Robert, “Radar image acquisition and interpretation for automotive applications,” in *Proc. of the IEEE Intelligent Vehicles Symposium (IV)*, Jun. 2003, pp. 328–332.

[43] H. F. Meyer, “Echtzeitoptimierung für Ausweichtrajektorien mittels der Sensitivitätsanalyse eines parametergestörten nichtlinearen Optimierungsproblems,” Ph.D. dissertation, Universität Bremen, 2016.

[44] M. C. L. Min Gyu Park, “Artificial Potential Field Based Path Planning for Mobile Robot Using a Virtual Obstacle Concept,” in *Proc. of the IEEE/ASME International Conference on Advanced Intelligent Mechatronics (AIM)*, vol. 2, Jul. 2003, pp. 735–740.

[45] M. Mitschke and H. Wallentowitz, *Dynamik der Kraftfahrzeuge*. Springer Vieweg, 2014.

[46] N. Moshchuk, S.-K. Chen, C. Zagorski, and A. Chatterjee, “Path Planning for Collision Avoidance maneuver,” in *Proc. of the ASME International Mechanical Engineering Congress and Exposition (IMECE)*, 2013.

[47] B. Nagy and A. Kelly, “Trajectory generation for car-like robots using cubic curvature polynomials,” *Field and Service Robots*, vol. 11, p. 6, 2001.

[48] J. Nocedal and S. J. Wright, *Numerical Optimization*, P. Glynn and S. M. Robinson, Eds. Springer, 2006.

[49] L. Papula, *Mathematische Formelsammlung Für Ingenieure und Naturwissenschaftler*. Vieweg & Teubner, 2006.

[50] M. G. Park, J. H. Jeon, and M. C. Lee, “Obstacle avoidance for mobile robots using artificial potential field approach with simulated annealing,” in *Proc. of the IEEE International Symposium on Industrial Electronics (ISIE)*, vol. 3. IEEE, 2001, pp. 1530–1535.

[51] M. Pivtoraiko, R. A. Knepper, and A. Kelly, “Optimal, smooth, nonholonomic mobile robot motion planning in state lattices,” Robotics Institute, Carnegie Mellon University, Tech. Rep., 2007.

[52] A. Polychronopoulos, M. Tsogas, A. Amditis, U. Scheunert, L. Andreone, and F. Tango, “Dynamic situation and threat assessment for collision warning systems: the EUCLIDE approach,” in *Proc. of the IEEE Intelligent Vehicles Symposium (IV)*, Jun. 2004, pp. 636–641.

[53] M. J. D. Powell, “Direct search algorithms for optimization calculations,” *Acta Numerica*, vol. Acta Numerica 7, pp. 287–336, 1998.

[54] M. M. Rahman, L. Bobadilla, and B. Rapp, “Sampling-Based Planning Algorithms for Multi-Objective Missions,” in *Proc. of the IEEE International Conference on Automation Science and Engineering (CASE)*, 2016.

[55] C. Schirm, “Situations- und Kollisionserkennung im urban Straßenumfeld,” Master’s thesis, Hochschule Koblenz, 2015, supervised Masters Thesis at Adam Opel AG by Jens Ferdinand.

[56] C. Schmidt, F. Oechsle, and W. Branz, “Research on trajectory planning in emergency situations with multiple objects,” in *Proc. of the IEEE Conference on Intelligent Transportation Systems (ITSC)*, 2006, pp. 988–992.

[57] C. Schmidt, “Fahrstrategien zur Unfallvermeidung im Straßenverkehr für Einzel-und Mehrobjektszenarien,” Ph.D. dissertation, Karlsruhe Institute of Technology (KIT), 2014.

[58] M. Schorn, “Quer- und Längsregelung eines Personenkraftwagens für ein Fahrerassistenzsystem zur Unfallvermeidung,” Ph.D. dissertation, TU Darmstadt, 2007.

[59] D. Schramm, M. Hiller, and R. Bardini, “Single Track Models,” in *Vehicle Dynamics Modeling and Simulation*. Springer, 2014, ch. 10, pp. 223–244.

[60] Z. Shiller and S. Sundar, “Optimal Emergency Maneuvers Of Automated Vehicles,” Institute of Transportation Studies, UC Berkeley, Tech. Rep., Jan. 1996.

[61] Z. Shiller and S. Sunder, “Emergency maneuvers for AHS vehicles,” *Emergency*, vol. 951, p. 893, 1996.

[62] N. Simm, J. Firl, and T. Schramm, “Forschungsprojekt Aktiv-AS: adaptive und kooperative Technologien für den intelligenten Verkehr – Assistenzsysteme, aktive Sicherheit; Schlussbericht zu den Teilprojekten: AGB – Aktive Gefahrenbremsung, FAS – Fahrsicherheit und Aufmerksamkeit; Laufzeit: 01.09.2006 – 31.12.2010,” 2011.

[63] N. Simm and N. Wagner, “Forschungsinitiative INVENT: intelligenter Verkehr und nutzergerechte Technik; Schlussbericht; Beitrag

des Zuwendungsempfängers: Adam Opel GmbH zu den Teilprojekten: STA – Stauassistent, FUE – Fahrumgebungserfassung; Laufzeit: 1.06.2001 – 30.09.2005," 2005.

[64] K. M. Sledge, N. H.; Marshek, "Comparison of Ideal Vehicle Lane-Change Trajectories," in *Research into Vehicle Dynamics and Simulation*, 1997.

[65] D. Soudbakhsh, A. Eskandarian, and D. Chichka, "Vehicle steering maneuvers with direct trajectory optimization," in *Proc. of the IEEE Intelligent Vehicles Symposium (IV)*, 2010, pp. 449–453.

[66] D. Soudbakhsh, A. Eskandarian, and J. Moreau, "An emergency evasive maneuver algorithm for vehicles," in *Proc. of the IEEE Conference on Intelligent Transportation Systems (ITSC)*, 2011, pp. 973–978.

[67] B. Southall and C. J. Taylor, "Stochastic road shape estimation," in *IEEE International Conference on Computer Vision (ICCV)*, vol. 1, 2001, pp. 205–212.

[68] Statistisches Bundesamt Wiesbaden, "Verkehrsunfälle Fachserie 8 Reihe 7 - 2014," 2016.

[69] A. Takahashi, T. Hongo, Y. Ninomiya, and G. Sugimoto, "Local Path Planning And Motion Control For Agv In Positioning," in *Proc. of the IEEE/RSJ International Conference on Intelligent Robots and Systems (IROS)*, 1989, pp. 392–397.

[70] The MathWorks, Inc., "Optimization Toolbox ™ User's Guide," 2012.

[71] E. Velenis, "Analysis and Control of High-Speed Wheeled Vehicles," Ph.D. dissertation, Georgia Institute of Technology, 2006.

[72] A. Von Vietinghoff, "Nichtlineare Regelung von Kraftfahrzeugen in querdynamisch kritischen Fahrsituationen," Ph.D. dissertation, Karlsruhe Institute of Technology (KIT), 2008.

[73] E. W. Weisstein, “Euler Forward Method,” From MathWorld – A Wolfram Web Resource, Apr. 2016. http://mathworld.wolfram.com/EulerForwardMethod.html [Online. Accessed: 21.04.2016]

[74] E. W. Weisstein, “Point-Line Distance–3-Dimensional,” From MathWorld – A Wolfram Web Resource, Apr. 2016. http://mathworld.wolfram.com/Point-LineDistance3-Dimensional.html [Online. Accessed: 12.04.2016]

[75] M. Werling, “Ein neues Konzept für die Trajektoriengenerierung und -stabilisierung in zeitkritischen Verkehrsszenarien,” Ph.D. dissertation, Karlsruhe Institute of Technology (KIT), 2011.

[76] M. Werling, P. Reinisch, and K. Gresser, “Kombinierte Brems-Ausweich-Assistenz mittels nichtlinearer modellprädiktiver Trajektorienplanung für den aktiven Fußgängerschutz,” in *8. Workshop Fahrerassistenzsysteme (FAS)*, 2012, pp. 77–86.

[77] M. Werling, J. Ziegler, S. Kammel, and S. Thrun, “Optimal trajectory generation for dynamic street scenarios in a Frenét Frame,” in *Proc. of the IEEE International Conference on Robotics and Automation (ICRA)*, 2010, pp. 987–993.

[78] H. Winner, “Frontalkollisionsschutzsysteme,” in *Handbuch Fahrerassistenzsysteme*, ser. ATZ/MTZ-Fachbuch, H. Winner, S. Hakuli, and G. Wolf, Eds. Vieweg & Teubner, 2009, vol. 1, ch. 33, pp. 522–540.

[79] H. Winner, S. Hakuli, F. Lotz, and C. Singer, Eds., *Handbuch Fahrerassistenzsysteme*. Vieweg & Teubner, 2015.

[80] H. Winner, S. Hakuli, and G. Wolf, Eds., *Handbuch Fahrerassistenzsysteme*. Vieweg & Teubner, 2009.

[81] J. Ziegler, P. Bender, T. Dang, and C. Stiller, “Trajectory planning for Bertha; A local, continuous method,” in *Proc. of the IEEE Intelligent Vehicles Symposium (IV)*, Jun. 2014, pp. 450–457.

[82] J. Ziegler, “Optimale Bahn- und Trajektorienplanung für Automobile,” Ph.D. dissertation, Karlsruhe Institute of Technology (KIT), 2015.

[83] J. Ziegler and C. Stiller, “Spatiotemporal state lattices for fast trajectory planning in dynamic on-road driving scenarios,” in *Proc. of the IEEE/RSJ International Conference on Intelligent Robots and Systems (IROS)*, 2009, pp. 1879–1884.

[84] A. Zomotor, *Fahrwerktechnik: Fahrverhalten*, 2nd ed. Vogel Buchverlag, 1991.

Own Publications and Supervised Student Projects

[85] F. Bonarens, J. Ferdinand, G. Schmidt, and B. Yi, “Forschungsprojekt UR:BAN – Kognitive Assistenz: Schlussbericht zum Teilprojekt: Projektsäule UR-BAN-KA: Kollisionsvermeidung durch Ausweichen und Bremsen: Laufzeit: 01.04.2012–31.03.2016,” 2016.

[86] J. Ferdinand and F. Bonarens, “Driver assistance system and methods for collision avoidance,” Jun. 29 2017, uS Patent App. 15/383,789.

[87] J. Ferdinand and F. Bonarens, “Fahrerassistenzsystem und Verfahren zur Kollisionsvermeidung,” Jun. 22 2017, dE Patent App. DE201,510,016,531.

[88] J. Ferdinand and F. Bonarens, “Method to determine an evasion trajectory for a vehicle,” Jun. 29 2017, uS Patent App. 15/383,799.

[89] J. Ferdinand and F. Bonarens, “Verfahren zum Finden einer Ausweichtrajektorie für ein Fahrzeug,” Jun. 22 2017, dE Patent App. DE201,510,016,544.

[90] J. Ferdinand and B. Yi, “Trajectory Planning for Collision Avoidance in Urban Areas,” in *Proc. of the IEEE Intelligent Vehicles Symposium (IV)*, 2016.

[91] J. Ferdinand and B. Yi, “Trajektorienplanung zur Kollisionsvermeidung im urbanen Raum,” in *32. VDI/VW – Gemeinschaftstagung "Fahrerassistenzsysteme und automatisiertes Fahren"*, 2016.

[92] C. Schirm, “Situations- und Kollisionserkennung im urban Straßenumfeld,” Master’s thesis, Hochschule Koblenz, 2015, supervised Masters Thesis at Adam Opel AG by Jens Ferdinand.

[93] B. Yi, J. Ferdinand, N. Simm, and F. Bonarens, “Application of Local Linear Steering Models with Model Predictive Control for Collision Avoidance Maneuvers,” in *Proc. IFAC Symposium on Intelligent Autonomous Vehicles (IAV)*, 2016.

[94] B. Yi, J. Ferdinand, and H. Wu, “Robuste Fahrdynamikregelung zur Kollisionsvermeidung,” in *Proc. of the 6th GMM-Fachtagung Automotive meets Electronics (AME)*, 2015.

[95] B. Yi, S. Gottschling, J. Ferdinand, N. Simm, F. Bonarens, and C. Stiller, “Real Time Integrated Control and Trajectory Planning with MPC for Critical Maneuvers,” in *Proc. of the IEEE Intelligent Vehicles Symposium (IV)*, 2016.